

**GEOCHEMICAL CHARACTERISTICS OF
PACIFIC SEAMOUNT
FERROMANGANESE CRUSTS: EVIDENCE
FOR THEIR GENESIS**

A THESIS SUBMITTED TO THE GRADUATE DIVISION OF THE
UNIVERSITY OF HAWAII IN PARTIAL FULFILLMENT OF THE
REQUIREMENTS FOR THE DEGREE OF

MASTER OF SCIENCE

IN
GEOLOGY AND GEOPHYSICS

MAY 1995

By

Xi Yuan Wen

Thesis Committee:
Eric H. DeCarlo, Chairperson
Craig Glenn
Yuan Hui Li

We certify that we have read this thesis and that, in our opinion, it is satisfactory in scope and quality as a thesis for the degree of master of science in Geology and Geophysics

Telu:

Thank you very much
for your teaching and help!

Luqman ☺

312971995

monobuku

THESIS COMMITTEE


Chairperson

Greg R. Glenn

Yuan-Hsin Li

ACKNOWLEDGMENTS

It is difficult to put into words my gratitude to Eric H. DeCarlo, my thesis advisor. His valuable guidance, persistent encouragement, financial support and constructive comments at each step in the preparation of this research have been significant in my learning of surface chemistry, analytical chemistry and REE geochemistry. I would also like to thank my committee members Yuan (Telu) H. Li and Craig Glenn. Telu Li taught me geochemical method and helped me to formulate many ideas outlined in this thesis. Craig Glenn provided helpful and important suggestions and the use of his lab.

I would like to take this opportunity to thank the people outside my committee who have assisted in various aspects of this thesis. My sincere thanks to Brain Popp for the use of the sampling instrument. My sincere thanks also goes to Fred MacKenzie for teaching me the the fine points of oceanic carbon system. I wish to thank James Cowen for providing biostratigraphic dating results and his suggestions. The opportunities to discuss with Denys VonderHaar, Gary McMurtry, Mimi Bertram and Jinchun Yuan were invaluable and helpful. I would also like to thank our working group, Wayne Shibata, Mark Irving and Haisheng Li for their discussions and suggestions. Chuck Fraley provided helpful assistance on ICP/OES analysis. I am grateful to John Wiltshire for his help in overcoming a difficult financial situation. My parents and my brother provided me with an education and encouragement. Most of all, I must acknowledge the tremendous amount of encouragement and love which my wife, Xue (Kathy) Hu has provided over the past years.

ABSTRACT

The millimeter scale compositional variability of Fe-Mn oxide crusts from a seamount near Phoenix Islands in Kiribati, and another near Hawaii was investigated using a variety of techniques. This study is designed to evaluate how the changes in the mineralogy, internal structure, and chemical composition of crusts relate to their growth history, and elucidate the changes in oceanic water chemistry which the crusts experienced. The XRD mineralogy indicated that while vernadite is the principal mineral phase, variations in other mineral constituents highly correlate with the chemical composition of the crusts. Four types of internal structure were observed by reflected light microscopy: columnar, botryoidal, mottled, and compact. Thirty seven major and minor constituents, and the rare earth elements (REE) were analyzed by ICP/AES and ICP/MS in sub-samples picked at approximately 2mm intervals throughout the crust sequences. These data were supplemented by semi-quantitative electron microprobe profiles acquired at 0.5mm intervals on the same samples.

Enrichment factors show that the elements Y, REEs, Ir, Pt, Pb, Bi, Cu, Co, Mn, Fe, Ni, Zn, Ti are highly enriched in the crusts relative to seawater and pelagic clay. A strong correlation between $1/K_d$ ($\log C_{sw}/C_{mn}$) and the mean residence time (τ) of elements in seawater was also observed. These findings may suggest that the chemistry of seawater and the geochemistry of crusts regulate each other. Principal component factor analysis indicates that the chemical composition of crusts in general can be partitioned among four major genetic groups. These are inferred to represent a hydrogenetic group (Mn, Ni, Co, Zn, Cu, Ce, CeAN), a biogenetic group (Ba, Zn, Cu, Pt, Fe, CeAN), a detrital group (Si, Al, Fe) and a carbonate fluorapatite group (Ca, P, REEs). The hydrogenetic and detrital groups display the expected strong inverse correlation, whereas the biogenetic elements exhibit environment dependence. The geochemistry of the crusts is highly dependent on conditions in the local environment and on the local seawater chemistry rather than on basin-wide oceanic conditions. Paleotracks are proposed for these crusts based upon the results of factor scores. These, aided by REE and biostratigraphic data (Cowen et al., 1993), are used to reconstruct the growth history of the crusts and the possible environmental records of ocean.

TABLE OF CONTENTS

| | <u>Page</u> |
|--|-------------|
| ACKNOWLEDGMENTS..... | iii |
| ABSTRACT..... | iv |
| LIST OF TABLES..... | vii |
| LIST OF FIGURES..... | viii |
| Chapter 1. Introduction..... | 1 |
| 1.1 Background..... | 1 |
| 1.2 Surface Chemistry of Metal Oxides..... | 5 |
| 1.3 Objectives of this Study..... | 7 |
| Chapter 2. Methodology..... | 10 |
| Chapter 3. Internal Structure and Mineralogy Study..... | 14 |
| 3.1 Characteristics of Internal Structures..... | 14 |
| 3.2 XRD Mineralogy | 16 |
| 3.3 Internal Structures and Chemical Compositions..... | 18 |
| Chapter 4. Geochemistry of Ferromanganese Crust..... | 23 |
| 4.1 Enrichment Factors..... | 23 |
| 4.2 Geochemistry of Major Elements..... | 37 |
| 4.3 Geochemistry of Minor Elements..... | 41 |
| 4.4 Geochemistry of Rare Earth Elements (REE)..... | 48 |
| Chapter 5. The Factor Analysis Approach..... | 54 |
| 5.1 Utility of Factor Analysis in Ferromanganese Crust Studies..... | 54 |
| 5.2 Brief Introduction to Factor Analysis..... | 54 |
| 5.3 Factor Loadings..... | 55 |

| | | |
|------------|--|-----|
| 5.4 | Factor Scores..... | 65 |
| Chapter 6. | Genesis and Paleooceanographic Implications..... | 72 |
| 6.1 | Genesis of Ferromanganese Crusts..... | 72 |
| 6.2 | Chemical Stratigraphy..... | 74 |
| 6.3 | Rare Earth Elements as Paleoindicators..... | 86 |
| Chapter 7. | Conclusions..... | 94 |
| 7.1 | Future Research..... | 95 |
| Appendix A | | 98 |
| Appendix B | | 104 |
| Appendix C | | 119 |
| References | | 123 |

LIST OF TABLES

| | <u>Page</u> |
|----------------|-------------|
| Table 4.1..... | 24 |
| Table 4.2..... | 25 |
| Table 4.3..... | 26 |
| Table 4.4..... | 28 |
| Table 4.5..... | 30 |
| Table 4.6..... | 31 |
| Table 6.1..... | 76 |
| Table 6.2..... | 77 |

LIST OF FIGURES

| | <u>Page</u> |
|------------------|-------------|
| Figure 2.1..... | 10 |
| Figure 3.1..... | 15 |
| Figure 3.2..... | 17 |
| Figure 3.3..... | 20 |
| Figure 3.4..... | 21 |
| Figure 4.1..... | 33 |
| Figure 4.2..... | 35 |
| Figure 4.3..... | 36 |
| Figure 4.4..... | 38 |
| Figure 4.5..... | 40 |
| Figure 4.6..... | 41 |
| Figure 4.7..... | 43 |
| Figure 4.8..... | 44 |
| Figure 4.9..... | 45 |
| Figure 4.10..... | 46 |
| Figure 4.11..... | 47 |
| Figure 4.12..... | 48 |
| Figure 4.13..... | 50 |
| Figure 4.14..... | 52 |
| Figure 5.1..... | 56 |
| Figure 5.2..... | 57 |
| Figure 5.3..... | 59 |
| Figure 5.4..... | 60 |

| | |
|------------------|----|
| Figure 5.5..... | 62 |
| Figure 5.6..... | 63 |
| Figure 5.7..... | 67 |
| Figure 5.8..... | 68 |
| Figure 5.9..... | 69 |
| Figure 5.10..... | 70 |
| Figure 6.1..... | 73 |
| Figure 6.2..... | 79 |
| Figure 6.3..... | 80 |
| Figure 6.4..... | 81 |
| Figure 6.5..... | 82 |
| Figure 6.6..... | 83 |
| Figure 6.7..... | 84 |
| Figure 6.8..... | 85 |
| Figure 6.9..... | 88 |
| Figure 6.10..... | 89 |
| Figure 6.11..... | 90 |
| Figure 6.12..... | 92 |
| Figure 6.13..... | 93 |

CHAPTER 1

INTRODUCTION

1.1 Background

Seamount ferromanganese crusts are considered as potential mineral resources and have been studied extensively over the past thirty years. Recent studies (DeCarlo, 1991; Hein et al., 1992; McMurtry et al., 1994) indicate that Fe-Mn crusts are important not only as mineral resources but also as potential paleoceanographic records. Because the geochemistry of a given crust is mainly related to the chemistry of the seawater in which it accreted, the geochemical signature and elemental distributions through the crust can be used to infer the temporal changes in oceanic chemistry during the growth of the crust in the oceans.

The oceans comprise the world's biggest steady state reservoir; hence it is believed that geological and geochemical processes occurring in the ocean and on the oceanic floor ultimately control the distribution of elements in this reservoir. In the ocean, most of the elements are mainly derived from riverine inputs, atmospheric inputs, tectonic activity and hydrothermal activity inputs, and anthropogenic inputs. The main removal processes for most elements are via sedimentary deposition and burial, and hydrothermal interactions with deep sea basalts on the ocean floor (Whitfield and Turner 1987). The controlling mechanisms for the enrichment of elements in sediments on the oceanic floors involve mainly chemical and physical interactions between dissolved elements and particles falling through the water column (Goldberg, 1954; Krauskopf, 1956; Balistrieri et al., 1981; Li, 1981; Bruland, 1983; Halbach and Puteanus, 1984;

Whitfield and Turner, 1987; DeCarlo et al., 1987a, b; DeCarlo, 1991; Li, 1991). These particles can be either detrital, biogenic, or authigenic materials.

Studies of elemental distribution between seawater and sediments (pelagic clays, ferromanganese oxides and biogenic sediments) reveal that the most important removal mechanism for most of the trace elements from the ocean is through an interaction with the surfaces of hydrous oxides of manganese and iron, and clay minerals (Li, 1981, 1991). A review of the oceanic chemistry literature (Broecker and Peng, 1982; Bruland, 1983; Whitfield and Turner, 1987; Elderfield, 1988; Li, 1991) indicates that most elements can be characterized as exhibiting either conservative, nutrient, scavenged type behaviors, or a mixture of thereof. Other than the control imposed on the composition of seawater by source materials, to a great extent, the formation and distribution of sediments in the ocean play an important role in determining the oceanic water composition (Li, 1991).

Ferromanganese oxides are highly enriched in scavenged type trace metals. The distributions of various scavenged elements in the ocean can be attributed to a significant extent to differences in the distribution of ferromanganese oxide deposits in the oceans, although other sediments are also important as sinks for certain elements.

Ferromanganese oxides are the principal mineral phases that result from the precipitation of Fe and Mn from seawater. Although Fe and Mn are the most abundant transition metals in the earth's crust, they are present in extremely low concentrations in seawater (Klinkhammer and Bender, 1980; Martin and Knauer 1985). Most scavenged type trace elements, such as the transition metals Co, Ni and Zn, and rare earth elements (REE) are absorbed by or coprecipitated with Fe-Mn oxides throughout the water column.

Ferromanganese oxides are minerals that have been extensively studied both in the field and through laboratory. In terms of their sedimentary abundance, ferromanganese oxides are the fourth largest sedimentary deposits after pelagic clay, carbonaceous, and siliceous sediments on the oceanic floors (Kennett, 1982). They have generated a lot of interest over the past three decades owing to their particular oceanographic features and their trace metal (Co, Ni, Cu, Pt) contents (Halbach et al., 1982; Li, 1982; Halbach and Puteanus, 1984; Von Stackelberg et al., 1984; Aplin et al., 1985; Halbach, 1986; Manheim, 1986; DeCarlo et al., 1987a, b; Kang, 1987; Hein et al., 1988; Manheim and Lane-Bostick, 1988; Le Suave et al., 1989; Hein et al., 1990; VonderHaar, 1990; DeCarlo 1991; DeCarlo and Fraley, 1992; DeCarlo and McMurtry, 1992; Hein et al., 1992; McMurtry et al., 1994). A large number of papers have reported general conditions conducive to the formation of ferromanganese crusts. A smaller number have interpreted geochemical variations within crusts in terms of their potential for elucidating paleoceanographic conditions. Although extensive efforts have been devoted to the bulk geochemistry of crusts, there is much less detailed work on describing the fine scale compositional variations and the interelement relationship within individual ferromanganese crusts or amongst crusts from different areas. This has somewhat hindered efforts to understand comprehensively the genesis of ferromanganese crusts in the Pacific ocean.

At the same time, a large number of laboratory experimental studies have been conducted to investigate interactions between dissolved elements and either manganese oxides or iron oxides (Murray, 1974, 1975a, b; Koeppenkastrop and DeCarlo, 1992; Koeppenkastrop et al., 1993; DeCarlo and Wen, unpublished results).

Geologically and geochemically, ferromanganese oxides can be divided into three types of deposit: diagenetic, hydrothermal and hydrogenetic (Halbach, 1986; DeCarlo et al., 1987a). Of these three, hydrogenetic deposits are by far the most important formation on seamounts in the central Pacific Ocean (VonderHaar, 1990). The major natural iron and manganese oxide phases in the ocean are goethite (αFeOOH), hydrous ferric oxide ($\text{Fe}(\text{OH})_3$), vernadite (δMnO_2), and todorokite

Recent improvements in dating methods for ferromanganese oxides (Janin, 1987, 1988; Manheim and Lane-Bostwick, 1988; Ingram et al., 1990; Hein et al., 1992; Cowen et al., 1993; Cowen and DeCarlo, unpublished data; McMurtry et al., 1994) have made it possible to correlate paleoceanographic records extant in ferromanganese oxides with large scale geological events. It is now widely accepted that hydrogenetic ferromanganese oxides (also called ferromanganese crusts) generally exhibit slower average growth rates (0.5-3 mm/Ma) than other marine Fe-Mn oxides .

Fe-Mn crusts should provide good geological and paleoceanographic records because a lack of post-depositional reworking of the deposits enhances the preservation of intact geological records. Halbach and Puteanus (1984), Halbach (1986) and DeCarlo et al. (1987a, b) demonstrated that elemental variations in the bulk metal composition of ferromanganese crusts are mainly related to differences in growth rates, water depths, carbonate compensation depth, bottom current activity and the depth of the oxygen minimum zone. More recent studies by Alvarez et al. (1990), DeCarlo (1991), Hein et al. (1992) and McMurtry et al. (1994) further provided evidence demonstrating that variations in the chemical composition and microstructure within ferromanganese crusts may reflect the

influence of prevailing environmental conditions at the time of formation of the deposit.

Although the studies referred to above are significant and provide new approaches to the study of ferromanganese crusts, there still remain many questions regarding the controlling mechanisms of elemental distributions in ferromanganese crusts. For example, during the formation of a ferromanganese crust, to what extent do elemental variations correlate with changes in growth rates and in internal structure? Is the growth rate a major factor in controlling the elemental distribution? Can we ascertain that post-depositional remobilization of elements has not occurred significantly after the formation of ferromanganese crusts? Do ferromanganese crusts record mainly conditions existing basin-wide in the ocean or in a more local environment? and how? Can we geologically and geochemically correlate and support the results of biostratigraphic dating (Janin, 1987; Cowen et al., 1993), a technique which appears to be one of the more reliable methods developed for dating ferromanganese crusts?

1.2 Surface chemistry of metal oxides

In order to answer some of the questions posed in the previous section, it is helpful to review the surface properties of hydrous manganese dioxide (vernadite), hydrous ferric oxide (HFO) and goethite, as well as the oceanic chemistry of the scavenged type elements. Studies of the surface properties of oxides and aluminosilicates (Murray, 1974; Stumm and Morgan, 1981; Balistrieri and Murray, 1981; Li, 1981, 1991), and experimental studies of transition metal (Co, Ni, Zn, Cu) and REE scavenging have revealed that vernadite and goethite or HFO have different surface properties with regard to uptake of elements from

seawater (Murray, 1974; Lee and Byrne, 1992, 1993; Koeppenkastrop et al., 1991; Koeppenkastrop and DeCarlo 1992; DeCarlo and Wen, unpublished results). Under typical conditions of the oceanic environment, the pH of zero point of charge (pH_{zpc}) for vernadite is 2.8, whereas for goethite and HFO, it is between 7.5 and 8.3 (Stumm and Morgan, 1981). Hence, vernadite is negatively charged in seawater, and can electrostatically attract positively charged ions in addition to forming surface chemical bonds. Goethite and HFO are only slightly charged or neutral in seawater pH, thus the adsorption of ions onto these phases proceeds mostly through chemical bond formation (Li, 1991).

Although electrostatic bond energies are small relative to chemical bond energies (Li, 1981) and experimental studies indicate that vernadite, goethite and HFO are almost equally effective in adsorbing cations from solution (Murray, 1974; Koeppenkastrop and DeCarlo, 1992; DeCarlo and Wen, unpublished results), their surface properties are not necessarily the same and they may interact differently with cations under oceanic water conditions. It is plausible to consider that upon initial approach of dissolved species toward a vernadite, goethite or HFO surface, the interaction energy is predominately electrostatic rather than chemical. Most trace elements are undersaturated in seawater, hence particles of vernadite, goethite and HFO effectively compete with each other to scavenge trace elements when these mineral phases precipitate in the marine environment. Owing to a greater excess of negatively charged (MeO^-) sites on the surface of vernadite relative to goethite or HFO, the difference in electrostatic force (better chance to interact initially with low valence cations) between these phases may be invoked to explain why many trace elements (Co, Ni, Pb) are associated with manganese oxides rather than with iron oxyhydroxides in ferromanganese crusts.

Because iron oxyhydroxide has a greater exchange capacity and neutral charge of surface relative to manganese oxide (Li, 1981), most higher valence cations which are highly hydrolyzed in seawater usually covary strongly with iron oxyhydroxides in ferromanganese crusts.

An important aspect of the partitioning of elements between ferromanganese crusts and seawater involves complexation with major species in seawater. For example, Cantrell and Byrne (1987) showed that carbonate accounts for most of the REE complexation in seawater, 86% of the total for the lightest rare earth, La, and 98% for the heaviest, Lu. Sorption studies of REE with Fe-Mn oxides (Koeppenkastrop et al., 1991; Koeppenkastrop and DeCarlo, 1992; Koeppenkastrop and DeCarlo, 1993; DeCarlo and Wen, unpublished results) revealed that fractionation of REEs during uptake from solution by particles is regulated by a competition between solution and surface complexation (OH^- , SO_4^{2-} and CO_3^{2-} complexes). Thus, the incorporation of REE into ferromanganese crusts through geologic time should be strongly influenced by variations in the concentration of complexing agents, particularly carbonate ion in seawater. A corollary of this hypothesis is that fractionation patterns of REE within ferromanganese crusts may be used to elucidate CO_3^{2-} concentrations in the oceans during the time periods in which the crusts accreted.

1.3 Objectives of this study

Initially, this study was designed to enhance understanding of the geochemical processes involved in ferromanganese crust formation. Subsequently, it was modified to acquire geochemical data that could be used to link the geochemical signatures of ferromanganese crust to ancient oceanic water

chemistry. Geochemical data were then used to reconstruct the growth history of the crusts and the paleochemistry of seawater during the formation of the ferromanganese crust.

Two crusts were chosen from two areas in the central Pacific ocean, one from McKean Seamount (6RD08-08, 4°S, 170°W), in the Phoenix Islands, Kiribati (DeCarlo et al; 1987b), and the other from the Musicians Seamount (RD50S1B 26°N, 160°W), in the Hawaiian Archipelago (DeCarlo et. al., 1987a). Both of these seamounts are Cretaceous in age (VonderHaar, 1990; Yan and Kroenke, 1993). The crust from McKean Seamount is the main subject of this study, with the crust from the Musicians Seamount used primarily on a comparative basis. The latter crust has been the subject of detailed chronological studies (VonderHaar, 1990; McMurtry et al., 1994), although only slightly more than one half of the stratigraphic sequence has been dated reliably (Cowen et al., 1993). Bulk data for ferromanganese crusts from the Marshall islands (Hein et al. 1988), and high resolution (<1mm scale) data obtained from a single rapidly accreting ferromanganese crust from Horizon Guyot (Hein et al., 1992) were also selected to examine interelement relationships in crusts. Previous results of factor analysis on bulk-sample data in crusts from the Hawaiian Archipelago (DeCarlo et al., 1987a; DeCarlo and McMurtry, 1992) were also compared to those from this study.

The objectives of this study are 1) to propose chemical paleotricks of the ferromanganese crusts; 2) to demonstrate the internal consistency between biostratigraphic dating results and interpretation of elemental variations that are used to infer paleoceanographic history; 3) to compare using factor analysis the interelement relationships in individual ferromanganese crusts with those obtained from a collection of bulk samples; 4) to elucidate the oceanic water conditions to which crusts were exposed, through observation and interpretation

of variations in the internal structure and the distribution and abundance of hydrogenetic elements; 5) to examine relationships between growth rates and elemental distributions; and 6) to establish that water column chemistry strongly influenced the growth of ferromanganese crusts.

CHAPTER 2

METHODOLOGY

The Fe-Mn crusts selected for this study were recovered at water depths of 2200 to 2500 meters from seamounts in two different areas of the central Pacific Ocean (Figure 2.1). Sampling was carried out by chain-bag dredging with

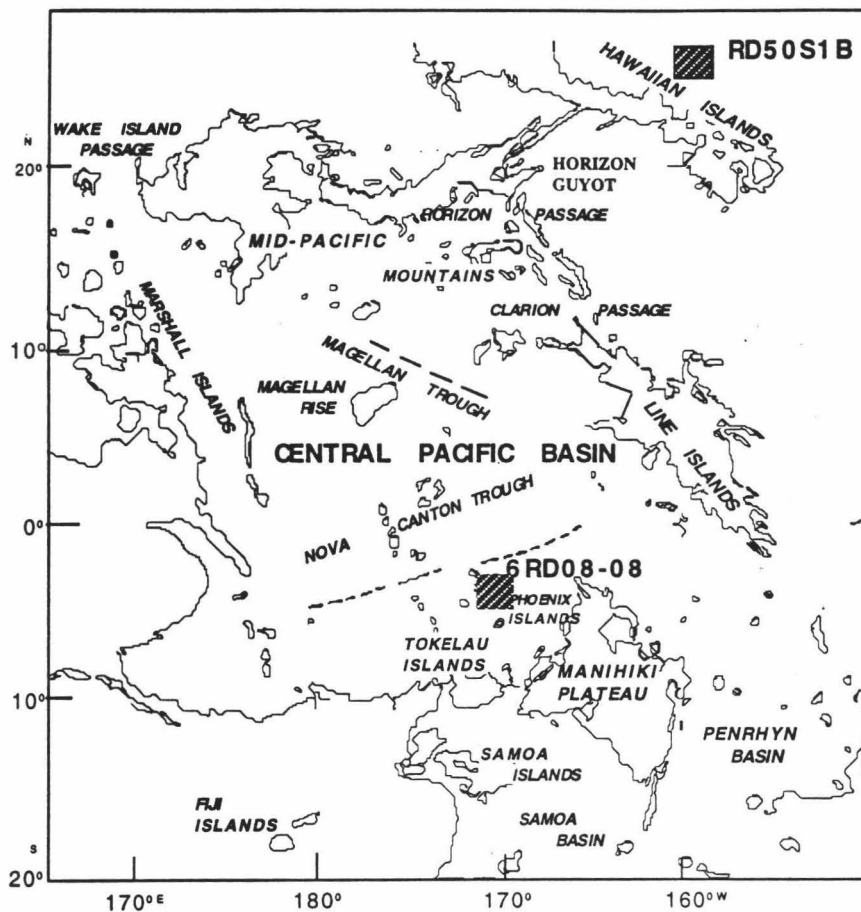


Figure 2.1 Ferromanganese crust sample location of Central Pacific Ocean. 6RD08-08 represents the crust from Mckean seamount, Phoenix Islands, Kiribati. RD50S1B represents the crust from Schumann seamount, Hawaii

guidance from 3.5 kHz echosounding and SeaMARC II sidescan acoustic imaging. Sample 6RD08-08 which consists of a maximum of 60 mm of Fe-Mn oxide underlain by 20 mm of carbonate fluorapatite was recovered from McKean seamount in the Phoenix islands, Kiribati, during the Moana Wave cruise 86-02 (DeCarlo et al., 1987b). Sample RD50S1B was recovered from the Musicians (Schumann) Seamount during the Kana Keoki cruise 84-08-24-02 (DeCarlo et al., 1987a). The latter crust consisted of a maximum thickness of 95 mm of Fe-Mn oxides surrounding a basaltic substrate. We report here only results from a 44 mm thick section taken from an area where the crust is about 65 mm thick. It is estimated that approximately two-thirds of its growth history are presented in this study.

Polished thin sections of each crust were examined by reflected light microscopy to identify internal structures and their morphologies. Observations were made on a 2 mm field of view. Seventeen major and minor elements (Na, Mg, Al, Si, S, P, K, Ca, Cl, Ti, V, Fe, Mn, Ni, Co, Cu, Zn) were determined in the thin sections using a JXA-8600 model electron microprobe at the Beijing Research Institute of Uranium Geology. The analyses were conducted at approximately 0.5 mm intervals using a 20 μm diameter electron beam. Comparisons of these data with ICP/OES (inductively coupled plasma / optical emission spectrometry) and ICP/MS (inductively coupled plasma/mass spectrometry) results confirm that the microprobe data are only semi-quantitative, these only suitable for the identification of trends and interelement relationships.

The mineralogy of the crusts was determined by X-ray powder diffractometry (XRD) using a Scintag PAD-V automatic diffractometer system equipped with a solid-state detector. Sub-samples of the crusts were taken at 2 to 3 mm intervals within each crust with a micro-auto drill operated under microscope control. Air-

dried powdered samples were tape-mounted and scanned at a rate of 2° $2\text{-}\theta$ per minute over the range of 2-70 degrees. Mineral identifications are based on peak positions and relative intensities as compared to those in the standard powder diffraction files (JCPDS)

Sub-samples of 9 - 15 mg were weighed on a micro-balance and transferred to 3 ml Teflon microwave digestion vessels. To each vessel was added 250 μl each of ultra-pure concentrated HNO_3 and HCl . The vessels were sealed and placed in a microwave oven and digested as described by DeCarlo (1991). After cooling, 100 μl of concentrated HF was added to each vessel to solubilize refractory aluminosilicates. Samples were quantitatively transferred to 8 ml bottles, and diluted with 0.5 M H_3BO_3 , and the exact final solution weight recorded.

Chemical analyses of sixteen major and minor elements (Al, Ca, Si, P, Ti, Cu, Ba, Mg, Co, Fe, Mn, Ni, Sr, Zn, V, Pb) of the crusts were performed by inductively coupled plasma optical emission spectrometry (ICP/OES), using a Leeman Labs Plasma Spec I high-resolution rapid-sequential echelle grating spectrometer. Standard analytical conditions using matrix-matched standards were employed. Precision was always better than $\pm 7\%$ of the reported value. Accuracy of the determinations was ascertained by simultaneous analysis of United State Geological Survey standard nodules A-1. If relative deviations greater than 5% of the recommended value were encountered the analyses were repeated.

Rare earth elements (REE) and other minor and trace elements were determined on a Perkin-Elmer SCIEX, Elan 5000 inductively coupled plasma/mass spectrometry (ICP/MS). Altogether twenty-two elements Cr, Y, Ba, La, Ce, Pr, Nd, Sm, Eu, Gd, Dy, Ho, Er, Tm, Yb, Ir, Pt, Au, Bi, Th, U, Pb were analyzed. Indium was added as an internal standard to dilutions of the original digestates. The calibration was conducted using a blank and six standards for each element over

the range 5-150 ppb. All samples were run in duplicates. Precision was 3% except for Ir and Pt where unoptimized conditions led to low count rates.

The Statview program on Macintosh-computers was used for factor analysis calculations. The following statistical information was extracted: means and standard deviations of variables (in the present case, the concentrations of various elements in a set of samples), correlation matrix, communalities, eigenvalues, factor loadings of orthogonal transformation solution-varimax, and factor scores. Any pair of elements in a coherent group should have a reasonably high (> 0.5) correlation coefficient in the correlation matrix. The results of any factor analysis should always be checked for consistency against other relevant information (Li, 1982). Interelement relationships are examined by R-mode factor analysis on three data sets (microprobe data, ICP/OES data and ICP/MS data) obtained from crusts RD50S1B and 6RD08-08, one data set for the crust from Horizon Guyot (Hein et al., 1992), and another bulk sample data set from the Marshall Islands (Hein et al., 1988).

CHAPTER 3

INTERNAL STRUCTURE AND MINERALOGY

It is generally accepted that the internal structure of ferromanganese crusts contains important information regarding crust formation. Thus, a complex internal structure may reflect a complex depositional history (Kang, 1987; Alvarez et al., 1990; Ingram et al., 1990). The influx of particles and bottom water currents are believed to be two major processes which control the transport of ferromanganese flocs required for the formation of a crust deposit. Bottom water currents exert a strong influence on Fe-Mn crusts, while a uniform internal structure may reflect steady continuous growth conditions under stable oceanic currents, a change in the internal structure may indicate a change in the water current conditions. These may possibly relate to global paleoceanographic events (DeCarlo, 1991; Hein et al., 1992; Wen and DeCarlo, 1994). Thus, observations of the microscale internal structure of crusts may be used to infer changes in environmental conditions that crusts experienced during their growth.

3.1 Characteristics of internal structures

The internal structure of Kiribati crust 6RD08-08 was examined in thin section by reflected light microscopy. Previous studies of crusts (Kang, 1987; Ingram et al., 1990), have identified four different types of internal structures which were also observed here.

The internal structures observed in Kiribati crust 6RD08-08 can be described as compact (massive), botryoidal, columnar, and mottled (Figure 3.1a, b, c, d). The compact structure (Figure 3.1a) is characterized by horizontal laminae, commonly

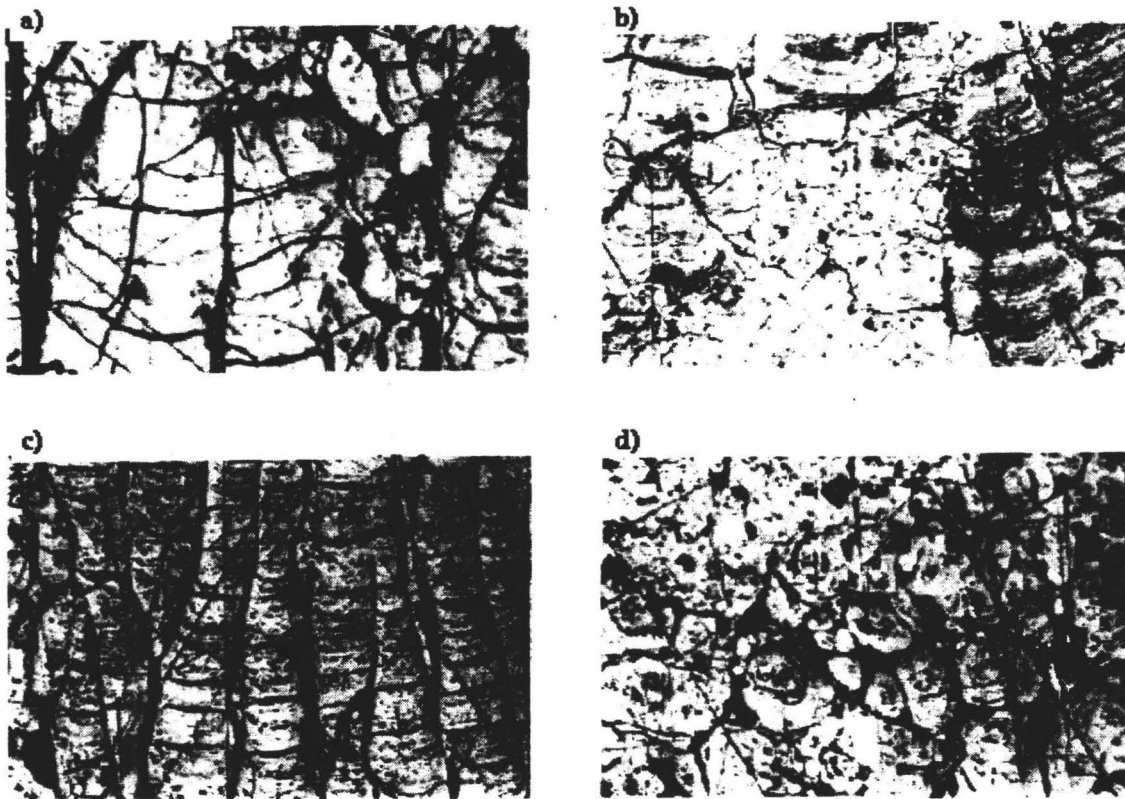


Figure 3.1 Characteristics of internal structure of crust 6RD08-08 from Kiribati in 2mm view. a) compact, b) botryoidal, c) columnar, d) Mottled

with low porosity and detrital content, and little complex internal structure. The botryoidal structure (Figure 3.1b) appears as a convex-up growth pattern of laminae commonly with higher porosity and little fine-grained detritus. In the columnar structure (Figure 3.1c), botryoids are separated by pore space filled with fine grained detritus (Alvarez et al., 1990). Finally the mottled structure (Figure 3.1d) represents botryoids that form separate concentrically laminated spheroids in a porous matrix of fine grained detritus. The latter have also been referred to as micronodules (VonderHaar, 1990).

The internal structure of Hawaii crust (RD50S1B) has been described thoroughly by VonderHaar (1990). In general, both crusts examined in this work exhibit very similar types of internal structures, although not in the same sequence of occurrence.

The features observed in crust 6RD08-08 are summarized in Figure 3.2. Examination of the internal structure profile (Figure 3.2) reveals that each type of internal structure appears several times at different intervals in crust 6RD08-08. For example, a compact structure was observed at the bottom (60 mm to 40 mm), middle (32 mm to 20 mm), and top (10 mm to top) of the crust. These variations may imply that the crust experienced similar water conditions (e.g., quiescent water flow) several times throughout geologic time.

3.2 XRD mineralogy

The mineralogy was studied at 2 mm intervals in crust 6RD08-08 from Kiribati and 2.5-3 mm intervals in crust RD50S1B from Hawaii. The mineralogy of crust RD50S1B has been described by DeCarlo (1991) and is quite similar to that

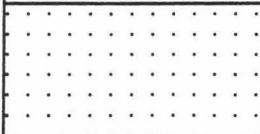




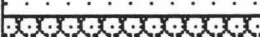

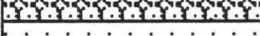
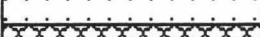

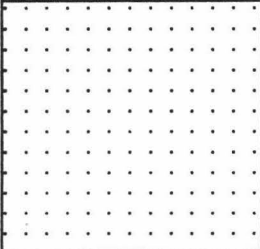
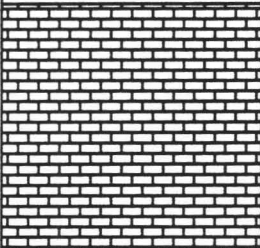
| | The profile of the internal structures of the crust | The characteristics of the internal structures of the crust 6RD08-08 | The mineral compositions of the crust 6RD08-08 by XRD |
|------|---|--|--|
| |  | compact | $\delta\text{MnO}_2 + \text{FeOOH} + \text{Quartz}$ |
| 12mm |  | columnar and botryoids | $\delta\text{MnO}_2 + \text{FeOOH} + \text{Quartz}$ |
| |  | compact and mottled | $\delta\text{MnO}_2 + \text{plag.} + \text{Quartz}$ |
| |  | dense columnar and botryoids | $\delta\text{MnO}_2 + \text{plag.} + \text{Quartz} + \text{Smecite}$ |
| 20mm |  | mottled with columnar | |
| |  | compact | $\delta\text{MnO}_2 + \text{plag.} + \text{Smecite}$ |
| |  | mottled | $\delta\text{MnO}_2 + \text{Plag.}$ |
| 30mm |  | mottled | $\delta\text{MnO}_2 + \text{CFA} + \text{FeOOH}$ |
| 32mm |  | compact | $\delta\text{MnO}_2 + \text{CFA} + \text{Plag.}$ |
| 40mm |  | very dense compact and botryoids | $\delta\text{MnO}_2 + \text{CFA} + \text{Quartz} + \text{Plag.}$ |
| 60mm |  | compact | $\text{CFA} + \delta\text{MnO}_2 + \text{Quartz} + \text{Plag.}$ |
| 80mm |  | CFA formation | Carbonate Fluorapatite |

Figure 3.2 Microscopy observation of the internal structures and X-ray diffraction mineralogy of ferromanganese crust from Kiribati (6RD08-08) in 2mm intervals

of crust 6RD08-08 (Figure 3-2). In both crusts, a typical pattern includes δMnO_2 (vernadite) as the dominant mineral phase with peaks at 2.43 Å and 1.41 Å (Burns and Burns, 1977; Ostwald, 1988). The presence of other minerals, such as goethite, francolite, carbonates, clays, quartz, and feldspar, influences the element composition of the crust but does not appear to correlate with changes in internal structure. No significant association between internal structure and mineralogy (Figure 3.2) was observed except for massive CFA underlying the Fe-Mn crust.

3.3 Internal structures and chemical compositions

It has been long accepted that the slower the accumulation rate (growth rate) is, the more the hydrogenetic group elements (Mn, Co, Ni) are enriched in ferromanganese crusts (Manheim and Lane-Bostwick, 1988). Heye (1978) suggested that compact and mottled structures be regarded as indicative of fast accumulation during an enhanced supply of iron and Al-Si detrital materials. Columnar and botryoidal structures were assumed to represent mainly direct precipitation from seawater (Friedrich and Schmitz-wiechowski, 1980). In addition, Hein et al. (1992) also suggest that botryoidal and columnar structures are representative of a relatively slow growth rate during a time of intensified deep water flow, whereas the compact and mottled structures are indicative of a relatively fast growth characteristic of more quiescent water conditions. Generally speaking, elemental distributions in crusts are influenced by supply and by chemical conditions existing in seawater.

A review of previous studies indicates there may be a relationship between chemical variations, growth rates, and internal structures. It is accepted that the growth rate is one of the more important factors in controlling the abundance of

elements in crusts, especially for hydrogenetic type elements (Manheim and Lane-Bostwick, 1988). However, if the sources of trace elements for different oceanic locations are variable, it will be more difficult to relate elemental abundances to growth rates.

It is reasonable to assume that the different internal structures of hydrogenetic crusts are more the result of physical phenomena (current activity) than of chemical phenomena. Although growth rates of crust are influenced by both types of processes, it is proposed that the physical signature is expressed more in the internal structures than on elemental distributions. Because no correlation was observed between mineralogy and internal structure, it is hypothesized that oceanic current activity is the most important factor in determining the internal structure of crusts.

To test the above hypothesis, the relationship between internal structure and chemical composition was examined. Electron microprobe data (Appendix A), collected at approximately 0.5 mm intervals of crust 6RD08-08, are plotted as a function of depth in Figures 3.3 and 3.4. These show an inverse relationship between Fe and Mn, a positive correlation between Mn/Fe and Ni (Figures 3.3a, b, c, d), and that Ca and P are relatively enriched in the bottom part of the crust (Figures 3.4a, b) correlating with the CFA identified by XRD. Figures 3.3 b and d show that Mn and Ni are relatively depleted at the bottom and top of the crust, whereas the detrital elements Al and Si are enriched in these parts of the crust (Figures 3.4 c, d).

An examination of both the internal structures and elemental variations in crust 6RD08-08 reveals that except for Al and Si most elements are not significantly correlated with changes in internal structures. These results

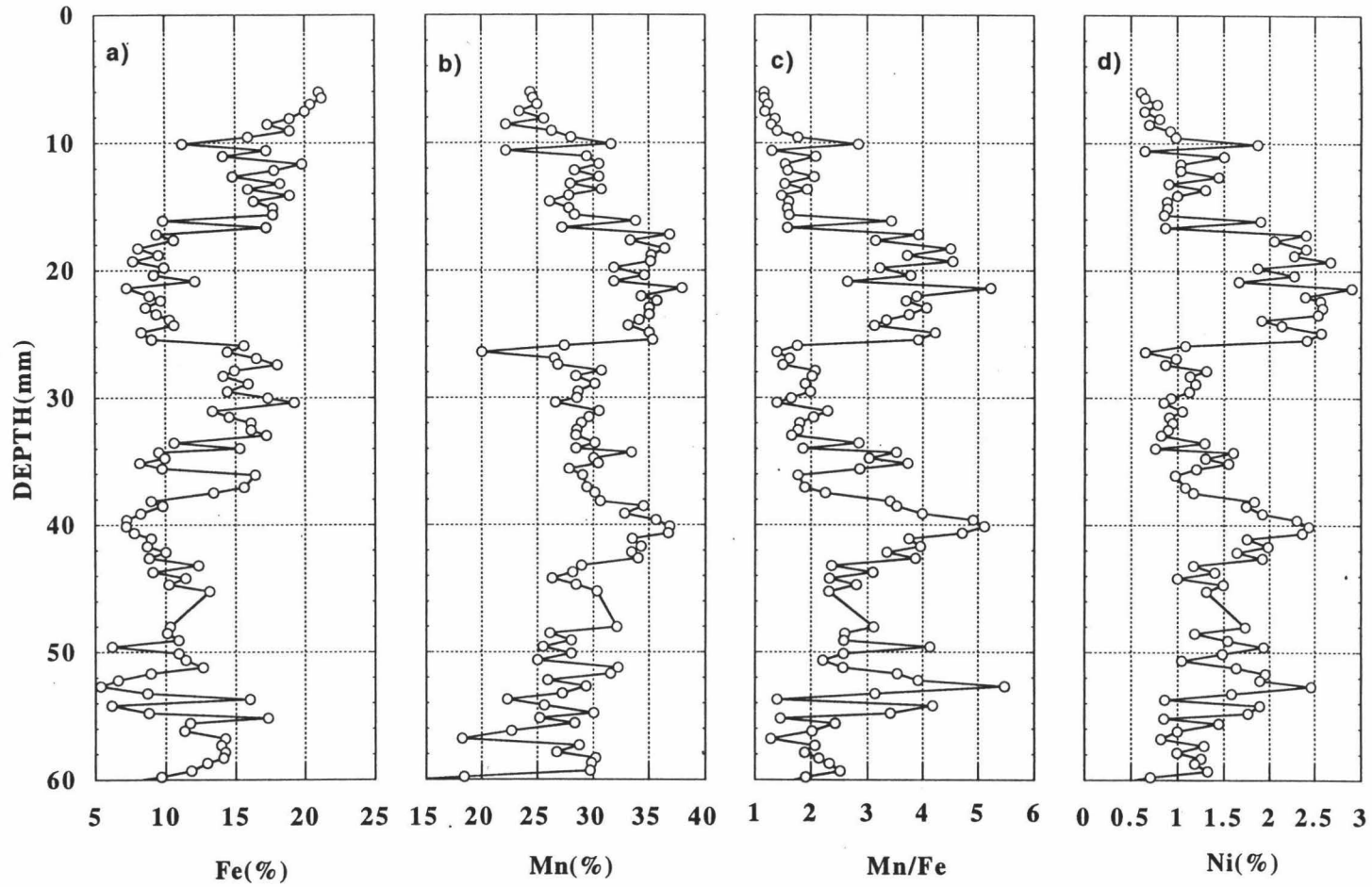


Figure 3.3. Semiquantitative microprobe data plot as a function of depth. a) Fe vs. depth b) Mn vs. depth c) Mn/Fe vs. depth d) Ni vs. depth

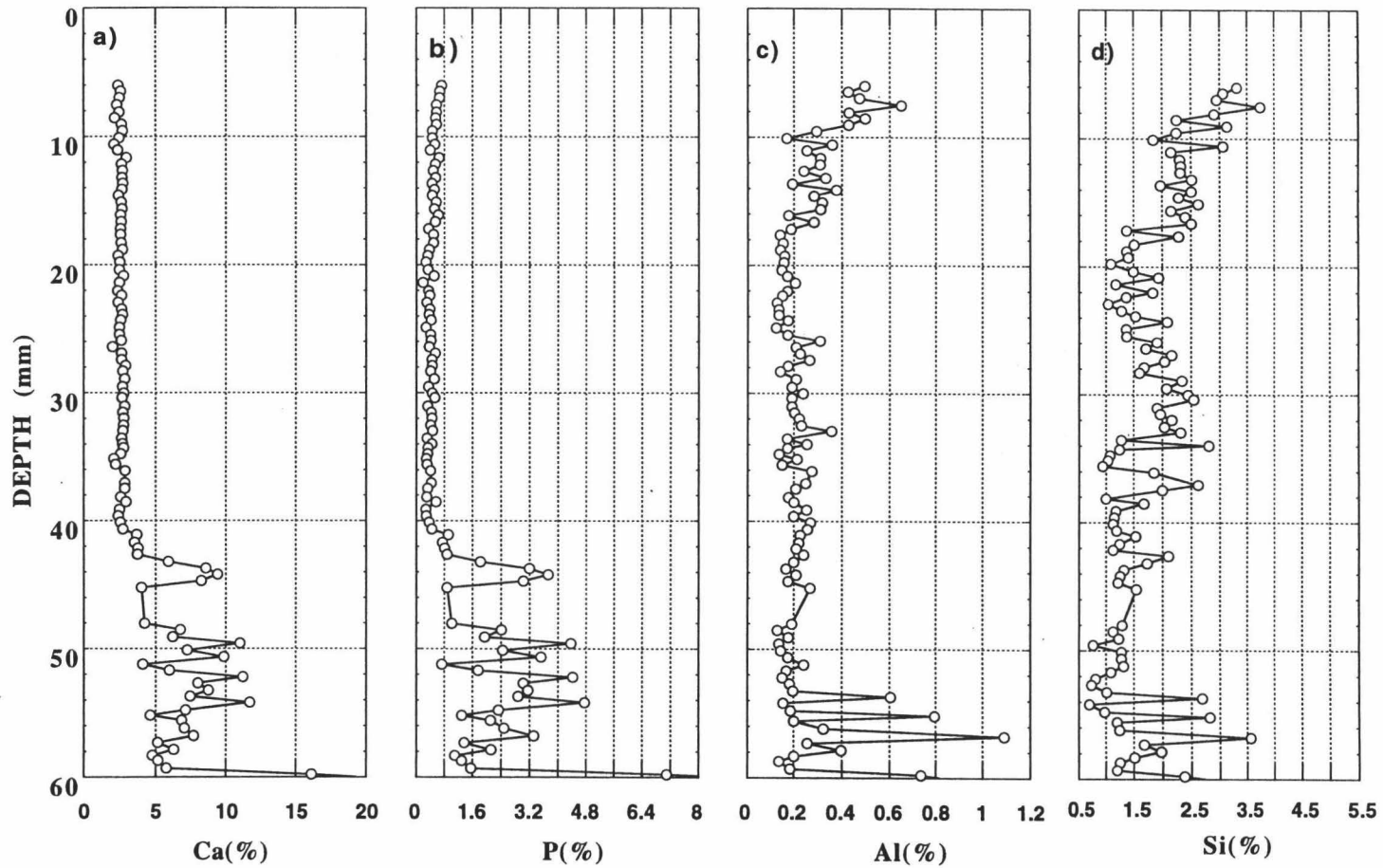


Figure 3.4 Semiquantitative microprobe data plot as a function of depth. a) Ca vs. depth b) P vs. depth c) Si vs. depth d) Al vs. depth

are consistent with the proposed hypothesis. Because the detrital elements Al and Si often occur in the form of insoluble matter derived from atmospheric transport of continental weathering products, they are incorporated within crusts after falling through the water column. Therefore, Si and Al are not as strongly influenced by water chemistry as are the other elements in crusts.

The lack of correlation between elemental distributions and internal structures in crusts may indicate that water current activity is not an important factor in controlling the elemental distributions in crust. This also suggest that the growth rate of crust may be not as important as previously thought in controlling the elemental distributions, rather the seawater chemistry and scavenging processes are the dominant factors

CHAPTER 4

GEOCHEMISTRY OF FERROMANGANESE CRUSTS

The abundance of major, minor, and trace elements, including rare earth elements (REE) in both crusts is presented on a mass basis (weight % or ppm) in Tables 4-1, 2, 3, 4, 5, 6. Ferromanganese crusts, in a manner similar to deep-sea nodules, act as sinks of "scavenged and nutrient type elements" and play an important role in influencing the composition of local seawater. Whenever Fe-Mn oxides precipitate or fall through the water column, they interact with dissolved species (Murray, 1974, 1975a, b; Li, 1982, 1991; Koeppenkastrop and DeCarlo, 1992; DeCarlo and McMurtry, 1992; Koeppenkastrop et al., 1993; DeCarlo and Wen, unpublished results). Elemental distributions between seawater and Fe-Mn oxides are also dependent on the chemistry of seawater. For example, the depth of the oxygen minimum zone, the calcite compensation depth, and the range of the lysocline and bio-productivity, all affect the abundance of dissolved species available for scavenging by Fe-Mn oxides (Halbach and Puteanus, 1984; Halbach, 1986; DeCarlo et al. 1987 a, b; DeCarlo 1991; Hein et al., 1992; McMurtry et al., 1994). The various approaches undertaken to elucidate the relationship between the composition of crusts and the conditions existing in seawater during crust growth are described below.

4.1 Enrichment factors

Enrichment ratio and enrichment factor calculations were applied to

Table 4.1 Major Elemental Abundance (weight percentage) of Crust 6RD08-08 from Kiribati.

| DEPTH (mm) | Mn(%) | Fe(%) | Al(%) | Si(%) | P(%) | Ca(%) | Mg(%) | Ti(%) | Fe/Mn | Si/Al | Ca/P |
|---------------|-------|-------|-------|-------|------|-------|-------|-------|-------|-------|-------|
| 4 | 19.72 | 12.88 | 0.2 | 3.33 | 0.29 | 1.95 | 0.71 | 0.66 | 0.65 | 16.65 | 6.72 |
| 6 | 19.29 | 12.21 | 0.49 | 3.85 | 0.41 | 1.85 | 0.65 | 0.67 | 0.63 | 7.86 | 4.51 |
| 8 | 19.74 | 10.66 | 0.24 | 2.07 | 0.18 | 1.81 | 0.78 | 0.69 | 0.54 | 8.63 | 10.06 |
| 10 | 17.32 | 12.57 | 0.4 | 3.06 | 0.28 | 1.72 | 0.67 | 0.73 | 0.73 | 7.65 | 6.14 |
| 12 | 18.91 | 11.49 | 0.23 | 1.87 | 0.23 | 1.9 | 0.71 | 0.73 | 0.61 | 8.13 | 8.26 |
| 14 | 18.9 | 11.68 | 0.28 | 2.48 | 0.25 | 1.84 | 0.74 | 0.78 | 0.62 | 8.86 | 7.36 |
| 16 | 16.96 | 12.8 | 0.78 | 3.71 | 0.48 | 0.99 | 0.72 | 0.52 | 0.75 | 4.76 | 2.06 |
| 18 | 21.06 | 10.92 | 0.36 | 2.63 | 0.25 | 1.83 | 0.76 | 0.86 | 0.52 | 7.31 | 7.32 |
| 20 | 22.82 | 10.24 | 0.18 | 2.07 | 0.23 | 1.9 | 0.8 | 0.81 | 0.45 | 11.5 | 8.26 |
| 22 | 22.48 | 11.45 | 0.25 | 1.82 | 0.28 | 1.97 | 0.86 | 0.8 | 0.51 | 7.28 | 7.04 |
| 24 | 22.47 | 10.89 | 0.22 | 1.76 | 0.3 | 1.99 | 0.83 | 0.81 | 0.48 | 8 | 6.63 |
| 26 | 22.49 | 9.84 | 0.11 | 1.52 | 0.26 | 1.97 | 0.83 | 0.81 | 0.44 | 13.82 | 7.58 |
| 28 | 22.39 | 11.09 | 0.09 | 1.83 | 0.24 | 2.08 | 0.77 | 0.84 | 0.5 | 20.33 | 8.67 |
| 30 | 23.91 | 9.77 | 0.05 | 1.41 | 0.23 | 2.01 | 0.86 | 0.09 | 0.41 | 28.2 | 8.74 |
| 32 | 22.32 | 10.49 | 0.16 | 1.47 | 0.23 | 1.97 | 0.81 | 1.07 | 0.47 | 9.19 | 8.57 |
| 34 | 18.21 | 10.56 | 0.18 | 2.21 | 0.34 | 1.74 | 0.72 | 1.03 | 0.58 | 12.28 | 5.12 |
| 36 | 20.35 | 11.98 | 0.24 | 1.55 | 0.32 | 2.01 | 0.78 | 1.23 | 0.59 | 6.46 | 6.28 |
| 38 | 20.98 | 11.68 | 0.17 | 1.33 | 0.28 | 2.17 | 0.81 | 1.27 | 0.56 | 7.82 | 7.75 |
| 40 | 23.84 | 7.2 | 0.01 | 0.82 | 0.27 | 2.04 | 0.89 | 0.91 | 0.3 | 82 | 7.56 |
| 42 | 23.47 | 7.6 | 0.13 | 1.38 | 0.63 | 3.31 | 1 | 0.92 | 0.32 | 10.62 | 5.25 |
| 44 | 19.86 | 9.65 | 0.13 | 1.58 | 1.59 | 5.94 | 0.75 | 1.04 | 0.49 | 12.15 | 3.74 |
| 48 | 18.92 | 8.53 | 0.2 | 1.68 | 2.44 | 8.77 | 0.72 | 0.71 | 0.45 | 8.4 | 3.59 |
| 50 | 16.46 | 8.68 | 0.31 | 1.58 | 3.24 | 10.3 | 0.67 | 0.7 | 0.53 | 5.1 | 3.18 |
| 52 | 17.96 | 7.53 | 0.24 | 1.78 | 2.59 | 9.65 | 0.74 | 0.6 | 0.42 | 7.42 | 3.73 |
| 54 | 17.09 | 8.31 | 0.25 | 1.55 | 2.99 | 11.1 | 0.67 | 0.71 | 0.49 | 6.2 | 3.71 |
| 58 | 17.71 | 7.06 | 0.1 | 0.97 | 1.77 | 8.05 | 0.63 | 0.78 | 0.4 | 9.7 | 4.55 |
| 60 | 17.71 | 7.06 | 0.1 | 0.97 | 1.77 | 1.81 | 0.63 | 0.78 | 0.4 | 9.7 | 1.02 |
| Average | 20.06 | 9.91 | 0.23 | 1.93 | 0.85 | 3.59 | 0.76 | 0.8 | 0.49 | 8.48 | 4.23 |

Table 4.2 Major Elemental Abundance (weight percentage) of Crust RD50S1B from Hawaii.

| DEPTH (mm) | Fe(%) | Mn(%) | Al(%) | Si(%) | P(%) | Ca(%) | Mg(%) | Ti(%) | Fe/Mn | Si/Al | Ca/P |
|---------------|-------|-------|-------|-------|------|-------|-------|-------|-------|-------|------|
| 3 | 13.95 | 17.21 | 1.28 | 6.29 | 0.33 | 1.75 | 1.05 | 1.05 | 0.81 | 4.91 | 5.3 |
| 5.5 | 16.09 | 18.74 | 0.61 | 4.99 | 0.34 | 2.07 | 0.91 | 1.04 | 0.86 | 8.18 | 6.09 |
| 8 | 15.36 | 19.41 | 0.29 | 4.29 | 0.3 | 2.07 | 0.85 | 1.05 | 0.79 | 14.79 | 6.9 |
| 10.5 | 15.88 | 21.9 | 0.43 | 5.24 | 0.34 | 2.4 | 0.93 | 1.21 | 0.73 | 12.19 | 7.06 |
| 13 | 15.46 | 18.87 | 0.48 | 4.55 | 0.29 | 2.1 | 0.87 | 1.22 | 0.82 | 9.48 | 7.24 |
| 15.5 | 15.08 | 13.91 | 2.09 | 11.11 | 0.33 | 2.09 | 0.85 | 1.1 | 1.08 | 5.32 | 6.33 |
| 18 | 16.1 | 15.08 | 1.89 | 9.35 | 0.52 | 2.69 | 0.89 | 1.51 | 1.07 | 4.95 | 5.17 |
| 20 | 13.38 | 14.69 | 2.06 | 8.49 | 0.54 | 2.46 | 0.91 | 1.02 | 0.91 | 4.12 | 4.56 |
| 22.5 | 13.27 | 13.11 | 2.25 | 8.76 | 2.03 | 5.93 | 0.91 | 1.1 | 1.01 | 3.89 | 2.92 |
| 25.5 | 16.82 | 12.19 | 2.85 | 11.07 | 0.78 | 2.98 | 1.04 | 0.96 | 1.38 | 3.88 | 3.82 |
| 28 | 19.13 | 11.03 | 3.21 | 12.62 | 0.9 | 3.04 | 0.95 | 0.64 | 1.73 | 3.93 | 3.38 |
| 31 | 17.37 | 17.61 | 1.39 | 6.36 | 0.41 | 2.22 | 0.98 | 0.81 | 0.99 | 4.58 | 5.41 |
| 33.5 | 17.11 | 17.96 | 0.98 | 5.62 | 0.26 | 2.06 | 0.86 | 0.82 | 0.95 | 5.73 | 7.92 |
| 36.5 | 15.02 | 21.07 | 0.66 | 4.42 | 0.28 | 2.41 | 0.89 | 0.76 | 0.71 | 6.7 | 8.61 |
| 39 | 15.68 | 20.09 | 0.74 | 4.83 | 0.28 | 2.25 | 0.91 | 0.89 | 0.78 | 6.53 | 8.04 |
| 44 | 17.88 | 18.42 | 1.07 | 5.61 | 0.39 | 2.21 | 0.91 | 0.99 | 0.97 | 5.24 | 5.67 |
| Average | 15.85 | 16.96 | 1.39 | 7.1 | 0.52 | 2.55 | 0.92 | 1.01 | 0.93 | 5.1 | 4.9 |

Table 4.3 Minor and Trace Elemental Abundance (ppm) of Crust 6RD08-08 from Kiribati.

| DEPTH (mm) | Co | Ni | Sr | Zn | Cu | Cr | Y | Ba |
|---------------|-------|------|------|-----|------|-----|------|------|
| 4 | 5897 | 4181 | 1339 | 600 | 353 | 3 | 153 | 1127 |
| 6 | 5680 | 3826 | 1294 | 475 | 365 | 4 | 137 | 1144 |
| 8 | 7062 | 5848 | 1404 | 600 | 548 | 7 | 105 | 1102 |
| 10 | 5454 | 3950 | 1171 | 581 | 511 | 16 | 118 | 1151 |
| 12 | 6001 | 4348 | 1237 | 513 | 614 | 4 | 118 | 1230 |
| 14 | 5822 | 5376 | 1106 | 555 | 654 | 7 | 110 | 1302 |
| 16 | 4617 | 3629 | 1113 | 599 | 594 | 17 | 149 | 1281 |
| 18 | 6018 | 5201 | 1272 | 721 | 706 | 5 | 99 | 1286 |
| 20 | 6837 | 6612 | 1294 | 792 | 803 | 3 | 91 | 1318 |
| 22 | 6077 | 5915 | 1350 | 774 | 791 | 3 | 81 | 1394 |
| 24 | 5263 | 6316 | 1337 | 779 | 837 | 3 | 84 | 1473 |
| 26 | 5904 | 6026 | 1393 | 801 | 880 | 1 | 74 | 1450 |
| 28 | 5997 | 5200 | 1410 | 745 | 834 | 2 | 75 | 1480 |
| 30 | 9489 | 5917 | 1293 | 802 | 930 | 0 | 62 | 1596 |
| 32 | 9636 | 5390 | 1383 | 820 | 973 | 0 | 58 | 1722 |
| 34 | 6375 | 4553 | 1200 | 669 | 976 | 2 | 58 | 1800 |
| 36 | 8377 | 3711 | 1452 | 701 | 925 | 0 | 65 | 1932 |
| 38 | 7408 | 4470 | 1477 | 726 | 974 | - | 53 | 1920 |
| 40 | 9230 | 7131 | 1131 | 779 | 1212 | - | 45 | 1773 |
| 42 | 10842 | 7471 | 1210 | 747 | 1329 | - | 127 | 1699 |
| 44 | 5855 | 4770 | 1401 | 707 | 1058 | - | 154 | 1755 |
| 48 | 3488 | 5354 | 1449 | 598 | 1093 | - | 179 | 1652 |
| 50 | 2903 | 4179 | 1400 | 548 | 881 | - | 289 | 1625 |
| 52 | 7060 | 5675 | 1457 | 718 | 1090 | - | 243 | 1613 |
| 54 | 2971 | 4329 | 1549 | 629 | 950 | - | 286 | 1619 |
| 58 | 10744 | 4617 | 1452 | 649 | 1016 | 257 | 104 | 1694 |
| 60 | 10744 | 4617 | 1452 | 649 | 1016 | - | 1070 | 1283 |
| Average | 6731 | 5133 | 1334 | 676 | 848 | 17 | 155 | 1497 |

Table 4.3 (Continued) Minor and Trace Elemental Abundance (ppm) of Crust 6RD08-08 from Kiribati.

| DEPTH (mm) | Ir | Pt | Au | Pb | Bi | Th | U | V |
|---------------|------|------|------|------|-------|------|------|-----|
| 4 | 0.09 | 0.27 | 0.94 | 1003 | 17.57 | 3.07 | 11.9 | 714 |
| 6 | 0.09 | 0.37 | 0.19 | 950 | 18.67 | 1.91 | 11.3 | 675 |
| 8 | 0.12 | 0.32 | 0.09 | 873 | 23.65 | 1.18 | 9.2 | 587 |
| 10 | 0.18 | 0.28 | 0.13 | 909 | 21.91 | 1.31 | 10.1 | 592 |
| 12 | 0.07 | 0.28 | 0.01 | 969 | 24.07 | 1.36 | 10.8 | 710 |
| 14 | 0.1 | 0.24 | 0 | 939 | 25.46 | 1.24 | 11 | 725 |
| 16 | 0.28 | 0.25 | 0.24 | 805 | 21.2 | 1.44 | 10.3 | 567 |
| 18 | 0.03 | 0.5 | - | 899 | 24.93 | 1.84 | 11.2 | 512 |
| 20 | 0 | 0.48 | - | 929 | 26.15 | 2 | 10.4 | 544 |
| 22 | 0.04 | 0.44 | - | 988 | 35.7 | 2.16 | 11.0 | 592 |
| 24 | 0.03 | 0.54 | - | 960 | 44.48 | 3.7 | 10.6 | 600 |
| 26 | 0.05 | 0.52 | - | 890 | 37.88 | 4.73 | 10.2 | 600 |
| 28 | 0 | 0.63 | - | 926 | 27.98 | 3.6 | 10.4 | 577 |
| 30 | 0 | 0.76 | - | 961 | 30.19 | 2.75 | 10.5 | 591 |
| 32 | 0.35 | 0.53 | 0.56 | 1025 | 33.16 | 4.01 | 11.7 | 615 |
| 34 | 0.27 | 0.55 | 0.56 | 1004 | 25.89 | 3.41 | 10.8 | 646 |
| 36 | 0.13 | 0.78 | 0.23 | 1081 | 28.7 | 4.14 | 13.5 | 701 |
| 38 | 0.09 | 0.71 | 0.19 | 985 | 27.6 | 3.03 | 13.6 | 721 |
| 40 | 0.06 | 0.72 | 0.26 | 753 | 28.9 | 2.5 | 9.6 | 632 |
| 42 | 0.07 | 0.52 | 0.12 | 709 | 29.6 | 2.07 | 9.2 | 594 |
| 44 | 0.1 | 0.68 | 0.16 | 876 | 27.4 | 3.11 | 12.7 | 632 |
| 48 | 0.11 | 0.51 | 0.1 | 833 | 34.1 | 2.55 | 10.1 | 551 |
| 50 | 0.13 | 0.4 | 0.1 | 809 | 32.4 | 3.16 | 10.3 | 510 |
| 52 | 4.53 | 0.74 | 6.06 | 726 | 28.7 | 3.23 | 9.1 | 553 |
| 54 | 0.09 | 0.59 | 0.47 | 706 | 28.3 | 3.34 | 9.68 | 483 |
| 58 | 1.41 | 0.94 | 0.21 | 806 | 42.7 | 2.97 | 9.84 | 492 |
| 60 | 0.16 | 0.52 | 0.07 | 307 | 18.2 | 1.51 | 7.52 | 492 |
| Average | 0.32 | 0.52 | 0.53 | 874 | 28.3 | 2.64 | 10.6 | 600 |

Table 4.4 Minor and Trace Elemental Abundance (ppm) of Crust RD50S1B from Hawaii.

| DEPTH (mm) | Co | Ni | Sr | Zn | Cu | Cr | Y | Ba |
|---------------|------|------|------|-----|------|-------|--------|------|
| 3 | 6598 | 4225 | 1161 | 646 | 1354 | 21.34 | 125.41 | 1605 |
| 5.5 | 4716 | 3097 | 1426 | 617 | 1243 | 0.81 | 135.77 | 1471 |
| 8 | 4278 | 3535 | 1468 | 630 | 1223 | - | 129.29 | 1760 |
| 10.5 | 5959 | 3833 | 1606 | 681 | 1351 | 0.71 | 104.2 | 1527 |
| 13 | 5824 | 2800 | 1499 | 625 | 1192 | - | 118.16 | 1678 |
| 15.5 | 4174 | 1906 | 1181 | 536 | 1022 | 8.35 | 118.92 | 1629 |
| 18 | 4401 | 2195 | 1313 | 636 | 1128 | 5.66 | 161.82 | 1872 |
| 20 | 4815 | 2514 | 1126 | 526 | 1143 | 9 | 215.32 | 1464 |
| 22.5 | 3875 | 2259 | 1270 | 542 | 1126 | 14.16 | 501.77 | 1501 |
| 25.5 | 2849 | 2180 | 1107 | 578 | 1433 | 10.53 | 268.77 | 1606 |
| 28 | 1674 | 2152 | 1075 | 602 | 1631 | 6.53 | 316.49 | 1804 |
| 31 | 3097 | 3014 | 1418 | 746 | 1773 | - | 146.34 | 2409 |
| 33.5 | 3302 | 3230 | 1410 | 704 | 1723 | - | 102.84 | 2300 |
| 36.5 | 3924 | 4005 | 1542 | 663 | 1752 | - | 90.75 | 2158 |
| 39 | 3944 | 3663 | 1482 | 680 | 1715 | - | 121.72 | 2322 |
| 44 | 3143 | 3414 | 1449 | 783 | 1896 | - | 141.9 | 2559 |
| Average | 4161 | 3001 | 1346 | 637 | 1419 | 8.57 | 174.97 | 1854 |

Table 4.4 (Continued) Minor and Trace Elemental Abundance (ppm) of Crust RD50S1B from Hawaii.

| DEPTH (mm) | Ir | Pt | Au | Pb | Bi | Th | U | V |
|---------------|------|------|------|------|-------|-------|-------|------|
| 3 | 2.56 | 0.43 | 0.18 | 1258 | 24.78 | 21.11 | 9.99 | 808 |
| 5.5 | 0.04 | 0.35 | - | 1155 | 25.5 | 11.22 | 12.01 | 708 |
| 8 | - | 0.23 | - | 1371 | 39.5 | 11.16 | 13 | 696 |
| 10.5 | - | 0.36 | - | 1025 | 43.23 | 12.04 | 11.34 | 733 |
| 13 | - | 0.38 | - | 1169 | 31.36 | 13.84 | 12.28 | 694 |
| 15.5 | 0.21 | 0.36 | - | 839 | 21.03 | 14.39 | 8.95 | 597 |
| 18 | - | 0.48 | - | 882 | 20.89 | 13.23 | 10.92 | 612 |
| 20 | 0.11 | 0.37 | - | 597 | 22.94 | 11.06 | 8.72 | 535 |
| 22.5 | - | 0.39 | - | 588 | 17.56 | 10.64 | 8.69 | 693 |
| 25.5 | - | 0.57 | - | 571 | 16.36 | 10.75 | 7.04 | 629 |
| 28 | - | 0.49 | - | 494 | 17.94 | 6.91 | 4.88 | 679 |
| 31 | - | 0.97 | - | 692 | 47.46 | 3.86 | 7.48 | 1077 |
| 33.5 | - | 0.78 | - | 726 | 45.85 | 4.07 | 7.98 | 853 |
| 36.5 | - | 1.12 | - | 667 | 37.15 | 3.58 | 7.91 | 904 |
| 39 | - | 0.83 | - | 836 | 37.85 | 4.6 | 8.45 | 870 |
| 44 | - | 0.69 | - | 995 | 31.73 | 6.23 | 8.11 | 1301 |
| Average | 0.73 | 0.55 | 0.18 | 867 | 30.07 | 9.92 | 9.23 | 774 |

Table 4.5 Rare Earth Elemental (REE) Abundance (ppm) of Crust 6RD08-08 from Kiribati.

| DEPTH (mm) | La | Ce | Pr | Nd | Sm | Eu | Gd | Tb | Dy | Ho | Er | Tm | Yb | CeAN | (Sm/Yb) _N |
|---------------|-------|--------|-------|-------|------|------|-------|------|-------|------|------|------|------|------|----------------------|
| 4.0 | 191.9 | 444.0 | 29.8 | 130.1 | 23.3 | 6.3 | 34.2 | 5.5 | 31.4 | 7.6 | 23.4 | 3.6 | 23.6 | 1.25 | 0.54 |
| 6.0 | 159.0 | 397.8 | 22.0 | 96.2 | 17.6 | 4.8 | 25.5 | 4.0 | 26.2 | 6.5 | 20.1 | 3.0 | 20.5 | 1.41 | 0.47 |
| 8.0 | 115.8 | 326.7 | 14.8 | 63.6 | 11.5 | 3.1 | 18.6 | 2.8 | 18.9 | 4.8 | 15.6 | 2.5 | 16.1 | 1.63 | 0.39 |
| 10.0 | 121.0 | 343.0 | 14.8 | 66.6 | 11.6 | 3.1 | 18.7 | 2.9 | 20.3 | 5.2 | 16.5 | 2.7 | 17.5 | 1.66 | 0.36 |
| 12.0 | 133.0 | 419.5 | 17.1 | 75.2 | 13.1 | 3.8 | 21.0 | 3.2 | 21.2 | 5.5 | 17.5 | 2.7 | 18.3 | 1.82 | 0.39 |
| 14.0 | 118.4 | 413.9 | 15.3 | 66.7 | 12.1 | 3.2 | 19.2 | 3.0 | 20.1 | 5.2 | 17.1 | 2.6 | 16.9 | 2.01 | 0.39 |
| 16.0 | 139.9 | 475.1 | 19.4 | 84.8 | 15.1 | 4.2 | 23.9 | 3.6 | 23.8 | 6.0 | 18.4 | 2.8 | 18.3 | 1.91 | 0.45 |
| 18.0 | 126.8 | 581.4 | 18.2 | 75.7 | 14.2 | 3.7 | 22.2 | 3.3 | 20.0 | 5.0 | 15.9 | 2.5 | 16.7 | 2.54 | 0.46 |
| 20.0 | 125.7 | 564.2 | 19.4 | 82.4 | 15.2 | 3.9 | 22.5 | 3.3 | 19.8 | 4.8 | 15.4 | 2.4 | 15.2 | 2.42 | 0.55 |
| 22.0 | 127.0 | 644.3 | 20.7 | 85.1 | 16.7 | 4.3 | 23.3 | 3.5 | 20.4 | 4.8 | 14.8 | 2.3 | 14.9 | 2.68 | 0.61 |
| 24.0 | 144.5 | 685.3 | 23.7 | 98.1 | 18.6 | 4.7 | 26.1 | 3.9 | 22.7 | 5.2 | 15.5 | 2.4 | 15.5 | 2.50 | 0.65 |
| 26.0 | 143.3 | 711.3 | 24.9 | 100.9 | 19.6 | 4.8 | 25.7 | 3.9 | 22.3 | 4.9 | 14.7 | 2.2 | 14.1 | 2.56 | 0.76 |
| 28.0 | 156.4 | 781.1 | 27.7 | 112.1 | 21.7 | 5.3 | 30.3 | 4.3 | 23.4 | 5.2 | 14.7 | 2.2 | 14.6 | 2.55 | 0.81 |
| 30.0 | 144.2 | 834.2 | 25.5 | 101.8 | 20.1 | 5.0 | 26.3 | 3.9 | 21.2 | 4.6 | 13.3 | 2.1 | 12.8 | 2.95 | 0.85 |
| 32.0 | 155.3 | 906.2 | 28.8 | 110.2 | 21.1 | 5.3 | 28.2 | 3.9 | 22.7 | 4.7 | 13.6 | 2.1 | 12.8 | 2.92 | 0.89 |
| 34.0 | 145.4 | 782.0 | 27.2 | 107.1 | 20.7 | 4.8 | 27.2 | 3.9 | 21.6 | 4.5 | 13.2 | 1.9 | 12.0 | 2.68 | 0.94 |
| 36.0 | 170.9 | 987.4 | 31.4 | 122.5 | 23.3 | 5.7 | 31.5 | 4.4 | 23.8 | 4.9 | 14.3 | 2.1 | 13.7 | 2.90 | 0.92 |
| 38.0 | 145.8 | 913.5 | 26.5 | 102.2 | 19.4 | 4.6 | 26.2 | 3.8 | 20.4 | 4.3 | 12.9 | 2.0 | 12.3 | 3.17 | 0.86 |
| 40.0 | 89.7 | 763.1 | 17.1 | 67.1 | 13.2 | 3.3 | 18.7 | 2.6 | 14.4 | 3.1 | 8.8 | 1.4 | 9.1 | 4.21 | 0.79 |
| 42.0 | 130.8 | 646.0 | 22.0 | 91.6 | 17.8 | 4.6 | 26.0 | 3.9 | 23.5 | 5.5 | 17.1 | 2.5 | 15.5 | 2.58 | 0.62 |
| 44.0 | 175.1 | 909.9 | 25.9 | 105.4 | 18.5 | 4.8 | 31.2 | 4.5 | 27.2 | 6.7 | 20.6 | 3.2 | 20.7 | 2.85 | 0.49 |
| 48.0 | 139.8 | 920.4 | 19.4 | 80.1 | 14.3 | 4.0 | 25.9 | 3.5 | 21.7 | 5.7 | 17.3 | 2.7 | 17.9 | 3.69 | 0.43 |
| 50.0 | 206.2 | 870.8 | 30.5 | 130.3 | 23.8 | 6.7 | 40.1 | 5.7 | 35.2 | 8.9 | 27.6 | 4.0 | 25.7 | 2.32 | 0.50 |
| 52.0 | 176.6 | 843.7 | 22.0 | 92.2 | 16.5 | 4.6 | 29.5 | 4.1 | 27.2 | 7.1 | 23.8 | 3.6 | 23.4 | 2.78 | 0.38 |
| 54.0 | 202.2 | 925.6 | 26.5 | 110.3 | 20.4 | 5.6 | 34.5 | 4.8 | 30.6 | 8.2 | 27.0 | 4.1 | 27.2 | 2.62 | 0.41 |
| 58.0 | 125.8 | 1099.9 | 16.0 | 66.0 | 11.8 | 3.0 | 22.2 | 2.6 | 16.2 | 3.9 | 12.1 | 1.9 | 12.6 | 5.06 | 0.51 |
| 60.0 | 660.9 | 467.7 | 112.3 | 481.6 | 94.2 | 24.6 | 128.8 | 19.6 | 121.5 | 29.7 | 86.4 | 12.0 | 73.4 | 0.37 | 0.70 |
| Average | 155.4 | 606.1 | 24.1 | 101.0 | 18.9 | 5.0 | 28.1 | 4.2 | 25.2 | 6.1 | 18.7 | 2.8 | 18.1 | 2.52 | 0.60 |

Table 4.6 Rare Earth Elemental (REE) Abundance (ppm) of Crust RD50S1B from Hawaii.

| DEPTH (mm) | La | Ce | Pr | Nd | Sm | Eu | Gd | Tb | Dy | Ho | Er | Tm | Yb | CeAN | (Sm/Yb) _N |
|---------------|-----|------|------|-----|------|------|------|------|------|------|------|-----|------|------|----------------------|
| 3 | 215 | 915 | 48.9 | 199 | 43.5 | 10.4 | 52.3 | 7.8 | 41.2 | 8.2 | 22.1 | 3.2 | 20.5 | 1.94 | 1.16 |
| 5.5 | 281 | 840 | 69.9 | 280 | 60.8 | 14.6 | 66.4 | 10.3 | 52.6 | 10.2 | 27.8 | 4 | 25.8 | 1.3 | 1.28 |
| 8 | 300 | 1090 | 75.4 | 298 | 63 | 15.2 | 69.4 | 10.6 | 53 | 10.3 | 26.9 | 4.1 | 25.6 | 1.58 | 1.34 |
| 10.5 | 252 | 1115 | 63.1 | 245 | 53 | 12.6 | 59.5 | 8.9 | 44.6 | 8.5 | 23.8 | 3.5 | 22.9 | 1.93 | 1.26 |
| 13 | 284 | 1185 | 67.7 | 267 | 56.7 | 13.5 | 62.3 | 9.5 | 47.7 | 9.4 | 25.4 | 3.8 | 24 | 1.86 | 1.29 |
| 15.5 | 228 | 1030 | 55.4 | 219 | 48.2 | 11.8 | 56.9 | 8.2 | 41.4 | 8.3 | 22.7 | 3.3 | 20.4 | 1.99 | 1.28 |
| 18 | 270 | 1178 | 66 | 264 | 57.8 | 14 | 66.7 | 9.8 | 50.4 | 9.9 | 28 | 3.9 | 24.9 | 1.92 | 1.26 |
| 20 | 262 | 1030 | 68.4 | 286 | 62.5 | 15.4 | 73 | 10.8 | 55.3 | 11.3 | 30.5 | 4.3 | 26.8 | 1.67 | 1.27 |
| 22.5 | 424 | 989 | 111 | 486 | 108 | 27.3 | 122 | 18.2 | 98.8 | 20.4 | 54.7 | 7.4 | 45 | 0.99 | 1.3 |
| 25.5 | 287 | 963 | 74.2 | 310 | 68.6 | 16.9 | 79.7 | 11.9 | 60.6 | 12.5 | 32.8 | 4.5 | 27.8 | 1.44 | 1.34 |
| 28 | 344 | 828 | 89.2 | 388 | 82.5 | 20.5 | 92.4 | 13.6 | 71.4 | 14.2 | 37.8 | 5 | 29.7 | 1.03 | 1.51 |
| 31 | 267 | 1162 | 56.7 | 232 | 46.5 | 11.3 | 56.8 | 8.1 | 41.9 | 8.8 | 23.7 | 3.4 | 21.2 | 2.05 | 1.19 |
| 33.5 | 248 | 1063 | 48 | 193 | 38.1 | 9 | 47.3 | 6.6 | 33.7 | 7 | 20 | 2.9 | 19 | 2.11 | 1.09 |
| 36.5 | 226 | 1162 | 43.3 | 170 | 32.8 | 7.8 | 42.8 | 5.9 | 30.7 | 6.2 | 17.8 | 2.7 | 16.4 | 2.54 | 1.09 |
| 39 | 268 | 1220 | 53.3 | 212 | 41.3 | 10 | 52.9 | 7.5 | 38.3 | 7.7 | 21.3 | 3.1 | 20.4 | 2.21 | 1.1 |
| 44 | 288 | 1277 | 59 | 234 | 46.7 | 11.2 | 57.8 | 8.1 | 41.3 | 8.5 | 23.5 | 3.5 | 20.4 | 2.13 | 1.24 |
| Average | 278 | 1065 | 65.6 | 268 | 56.8 | 13.8 | 66.1 | 9.7 | 50.2 | 10.1 | 27.4 | 3.9 | 24.4 | 1.79 | 1.25 |

CeAN defined as $2(Ce/Ce^*)/(La/La^*+Pr/Pr^*)$, $(Sm/Yb)_N$ defined as $(Sm/Sm^*)/(Yb/Yb^*)$ where * indicates shale value

explain and accentuate the differences in elemental distributions between ferromanganese crusts (C_{mn}) and reference material such as seawater (C_{sw}) and pelagic clay (C_{op}). The data for seawater and pelagic clay were obtained from the summary by Li (1991). The enrichment ratio is defined as elemental concentrations in crust divided by those in seawater. The patterns shown in Figure 4.1 reveal that: 1) in both crust 6RD08-08 and crust RD50S1B, most trace elements are highly concentrated, with Y, REEs, Pt, Pb, Bi, Th, Al, Cu, Co, Fe, Mn, Zn, and Ti exhibiting 10^6 - 10^9 enrichments over seawater; 2) there is a similarity in the enrichment of elements between the two crusts, except that the trivalent REE and the detrital elements Al and Si are relatively more concentrated in crust RD50S1B (from Hawaii) than in crust 6RD08-08 (from Kiribati); 3) a systematic decrease in enrichment is observed for trivalent REE as a function of increasing atomic number. This is consistent with a previous study of crusts from the Hawaiian Archipelago (DeCarlo and McMurtry, 1992).

The similarity in the average enrichment relative to seawater in both crusts suggests that the incorporation of trace elements in crusts occurs by similar mechanisms throughout the water column (DeCarlo and McMurtry, 1992). Slight differences in REEs, and Al and Si enrichments may be attributed to local differences in seawater chemistry or sources of supply. Such an interpretation would imply different wind patterns and water currents in the areas where the crusts accreted. The greater enrichment in crusts of light rare earth elements (LREE) La, Ce, Pr, Nd, Sm, Eu and Gd relative to heavy rare earth elements (HREE) Tb, Dy, Ho, Er, Tm and Yb is consistent with a greater ability of LREE to interact with the surface of Fe-Mn oxides than HREE owing to stronger complexation of HREE with carbonate in seawater (Cantrell and Byrne, 1987;

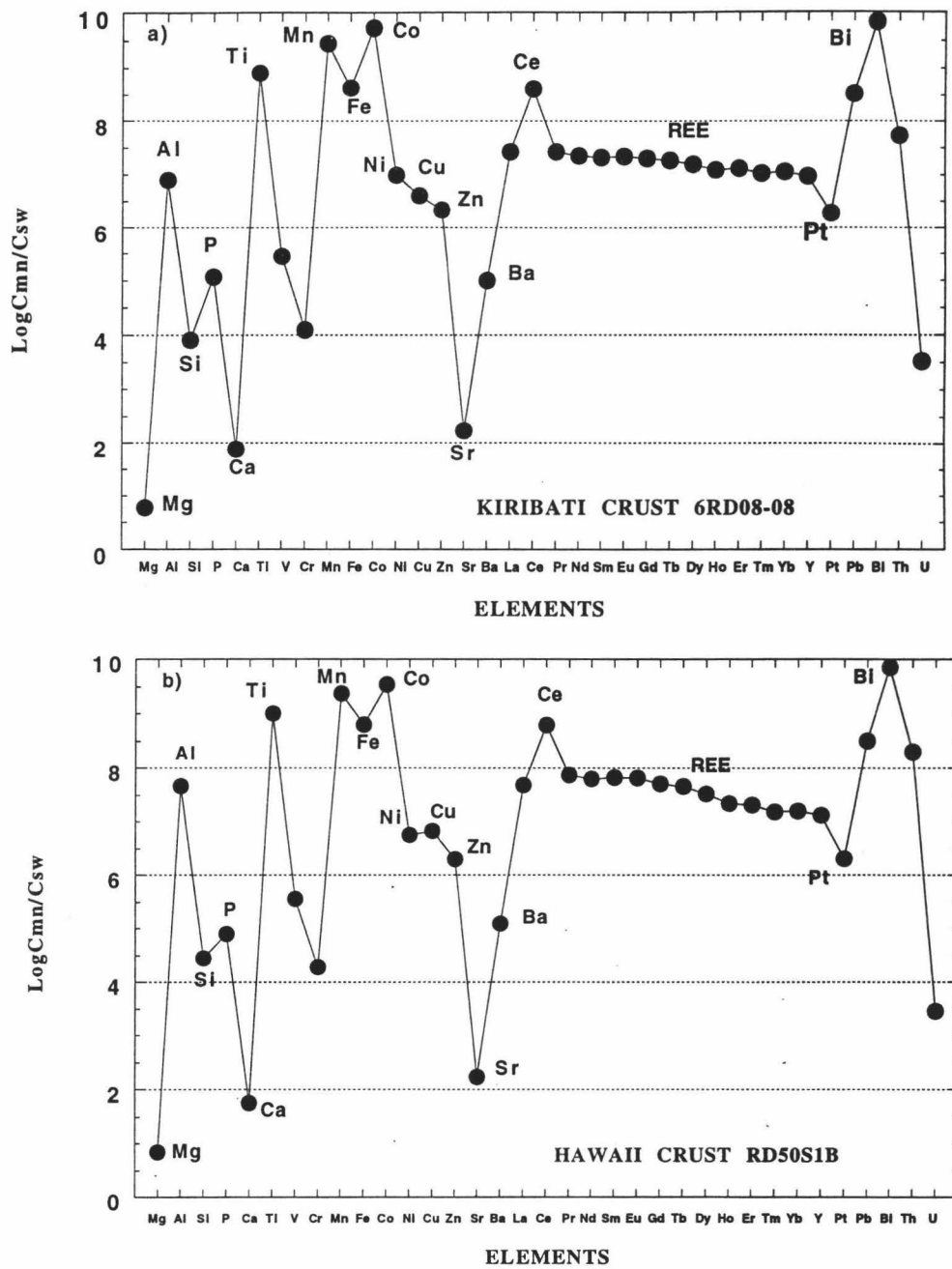


Figure 4.1 Enrichment analysis of C_{mn} and C_{sw} (Ferromanganese crust/ seawater), the data for crusts are the average of each crust and seawater data are obtained from Li (1991) a) Enrichment analysis for crust from Kiribati (6RD08-08) b) enrichment analysis for crust from Hawaii (RD50S1B).

Elderfield, 1988; Lee and Byrne, 1993, 1992; Koeppenkastrop et al., 1991; Koeppenkastrop and DeCarlo, 1992; Koeppenkastrop and DeCarlo, 1993; DeCarlo and Wen, unpublished results).

The enrichment factor, E_{Al}^i is defined here as the average ratio of the concentration of element i to the normalizing element Al (C^i/C^{Al}) in ferromanganese crust compared to this ratio in the reference material (Li, 1981). Figure 4.2 shows that the elements Y, REEs, Pb, P, Cu, Co, Mn, Ni, Sr, Zn, V, Th, Si, Mg are enriched in both crusts relative to pelagic clay, and Cr is depleted only in crust RD50S1B relative to pelagic clay. These results imply that the principal mineral phases in crusts, ferro-manganese oxide are more effectively scavenging elements like Co, Ni, Ce, Pt and REE (Li, 1982, 1991) than clay minerals.

Figure 4.2b shows that crust RD50S1B from Schumann Seamount has a less fractionated REE pattern than crust 6RD08-08 from Kiribati (Figure 4.2a), which exhibits a HREE enriched pattern ($LREE/HREE < 1$) relative to pelagic clay. This observation may suggest that differences exist in the seawater chemical environments experienced by the two crusts and that the source of REEs in the seawater to which crust RD50S1B was exposed was different from that of the crust 6RD08-08.

The crust to seawater (C_{mn}/C_{sw}) enrichment ratio is analogous to the partitioning coefficient (K_d) in the ferromanganese crust-seawater system. A relationship between the residence time (τ) of elements in seawater given by Whitfield and Turner (1987) and C_{sw}/C_{mn} ($1/K_d$) calculated here is shown in figure 4.3. The $\log C_{sw}/C_{mn}$ is highly correlated with $\log(\tau)$ ($r^2=0.913$ in crust RD50S1B, $r^2=0.876$ in crust 6RD08-08), i.e., elements that have a larger K_d exhibit a residence time that is generally less than the oceanic mixing time. An important implication of this observation is that the association of $1/K_d$ with

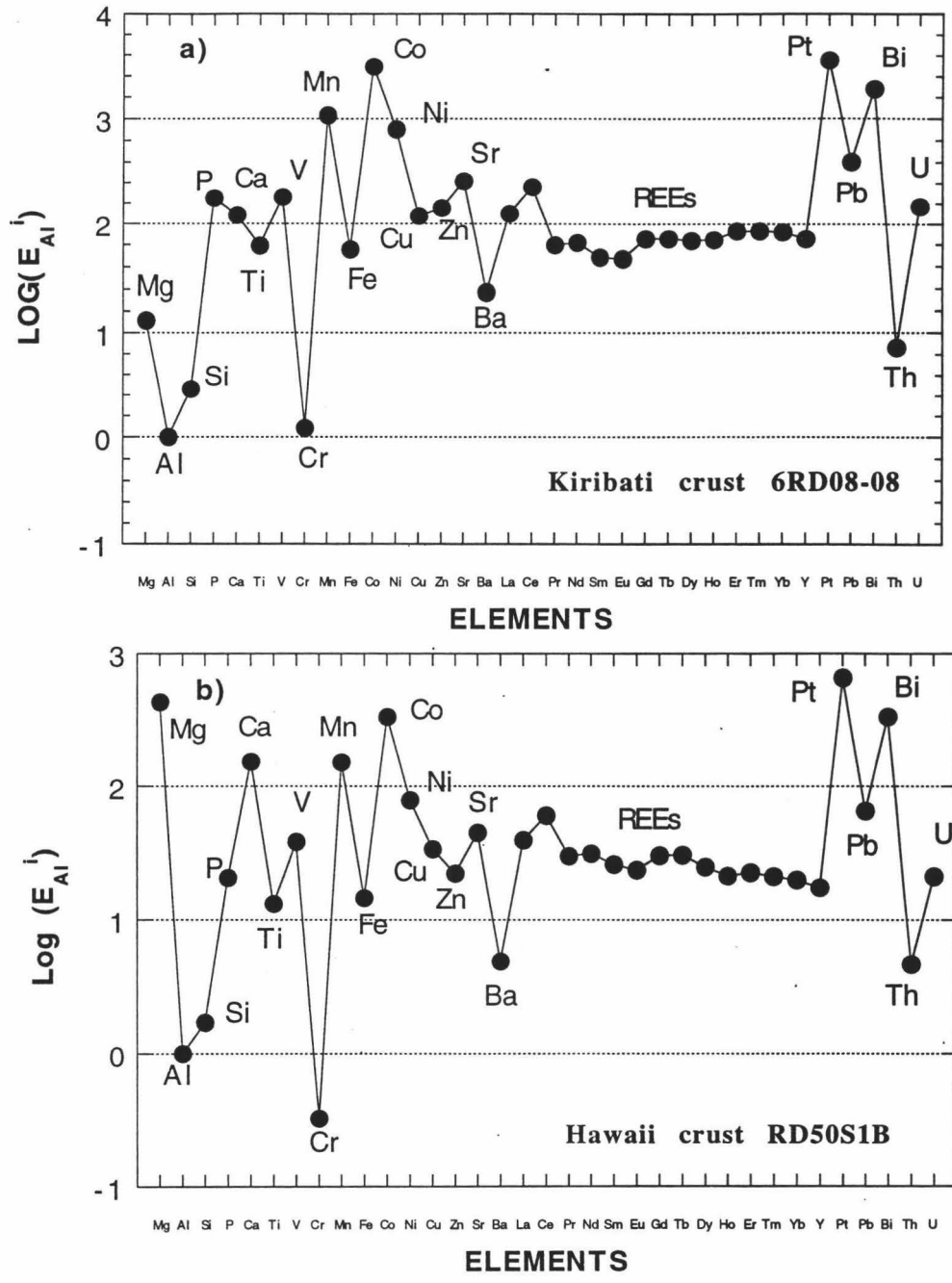


Figure 4.2 Enrichment factor of E_{Al}^i (ferromanganese crust / pelagic clay), the data for crusts are the average of each crust and pelagic clay data are obtained from Li (1991). a) Enrichment factor for crust 6RD08-08 from Kiribati. b) enrichment factor for crust RD50S1B from Hawaii

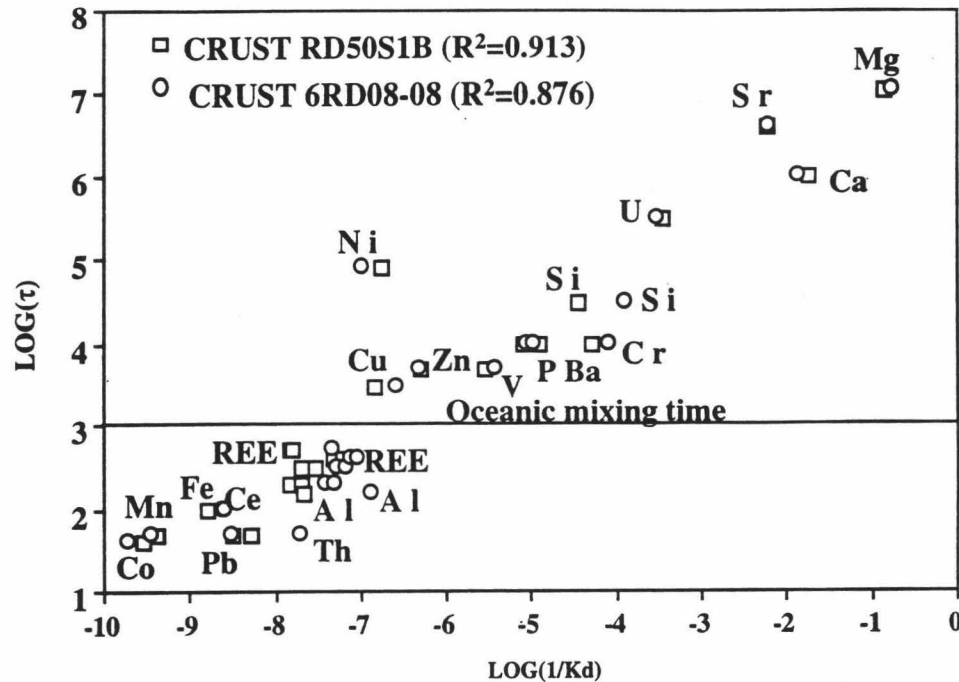


Figure 4.3 Relationship between the log of residence time (τ) of elements and log of the inverse distribution coefficient ($1/K_d$) between seawater and ferromanganese crust, squares represent the crust from Hawaii (RD50S1B) and circles represents the crust from Kiribati (6RD08-08). The residence time (τ) of elements is obtained from Whitfield and Turner (1987).

residence time (τ) provides further evidence as to how the chemistry of oceanic water and ferromanganese crusts are intimately related.

There are two possible reasons why an element would not fall on the line that defines the relationship between residence time (τ) and $1/K_d$. Either the residence time of the element or the chemical data are not reliable, or a catastrophic input of the given element to the system occurred. For example, Ni

does not fall on the line in Figure 4-3; suggesting the residence time for Ni may not be accurate.

4.2 Geochemistry of major elements

The studies by DeCarlo et al. (1987a, b), Kang (1987), Hein et al., (1988), VonderHaar (1990), DeCarlo (1991), DeCarlo and Fraley (1992), Hein et al. (1992) and this work all indicate that Mn-oxide (vernadite) and Fe-oxides (goethite and HFO) are the major mineral phases in ferromanganese crusts. Other common mineral phases, although less abundant, include aluminosilicates and francolite (carbonate-fluorapatite or CFA). Owing to the mineralogical control on composition, Mn, Fe, Al, Si, Ca and P are the major elemental components in crusts.

Scatter plots Fe vs. Mn are shown in Figure 4.4. A generally weak but inverse correlation between Fe and Mn is observed in crusts RD50S1B and 6RD08-08, if one excludes samples enriched in CFA mineral phase. Mn is considered to be of hydrogenetic origin and precipitates directly from seawater. Within the oxygen-minimum zone, seawater is usually enriched in soluble Mn^{2+} ; Mn^{2+} is diffusing out of this zone oxidized and precipitates as δMnO_2 (Mn^{4+}) (Martin and Knauer 1985; DeCarlo, 1987b; Hein et al., 1992). Although the element Fe can also undergo redox transformation in aqueous solution, it has a very different behavior as compared to Mn in crusts. Fe in ferromanganese crusts originates from multiple sources undergoing a variety of processes and often associated with several genetic elemental group (i.e., biogenetic and detrital inputs versus hydrogenetic input for Mn). Therefore, the abundance of Mn, Fe and the Mn/Fe ratio can be used to differentiate source materials. According to Figure 4.4 and

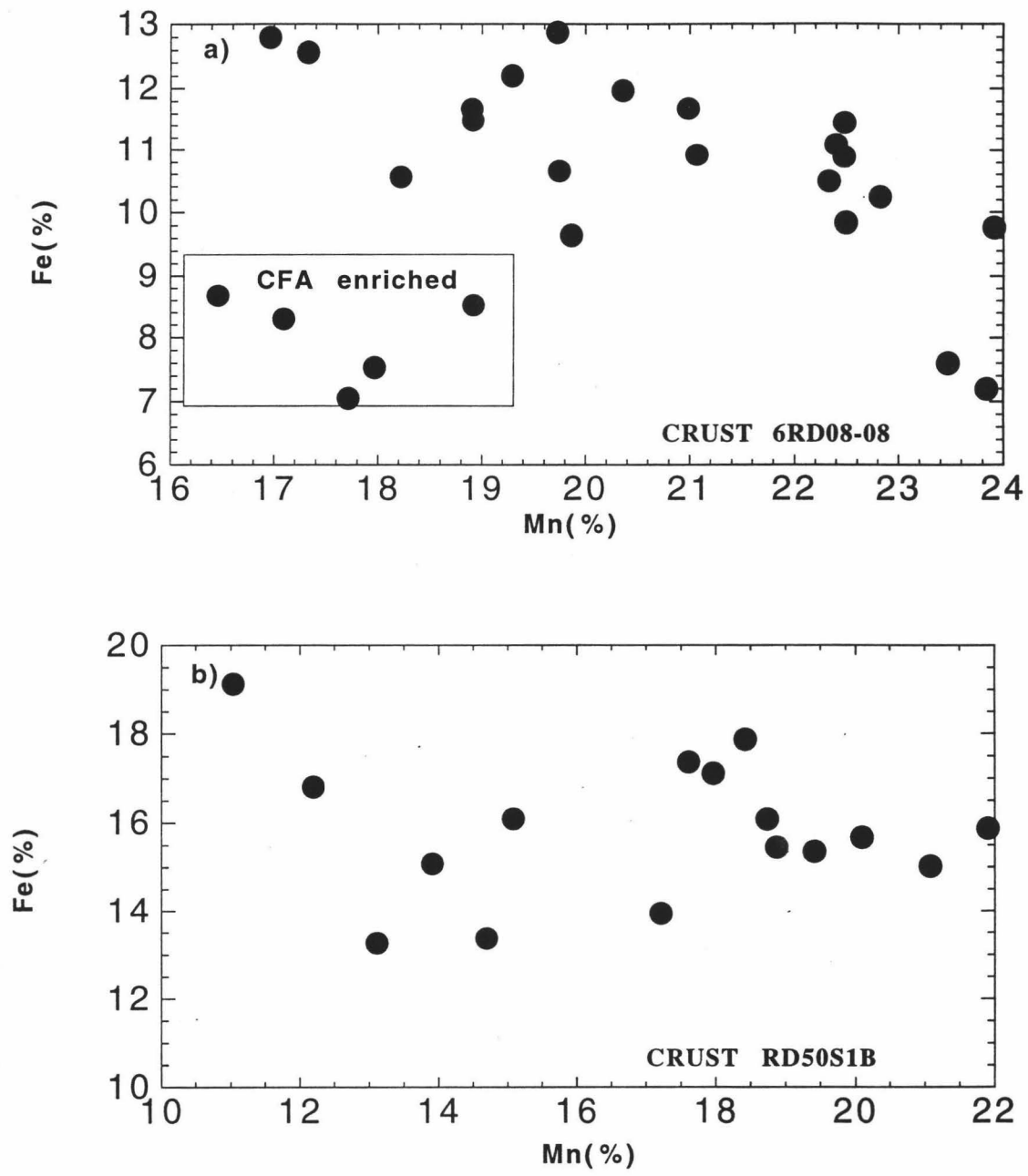


Figure 4.4 Fe vs. Mn. a) Crust 6RD08-08 from Kiribati. b) Crust RD50S1B from Hawaii

tables 4.1, 4.2, the concentration of Fe is higher in crust RD50S1B than in crust 6RD08-08 whereas the concentrations of Mn are similar. Therefore, the Mn/Fe ratios are lower in crust RD50S1B from Hawaii. It thus appears that crust 6RD08-08 is better "developed" than crust RD50S1B in terms of its hydrogenetic manganese oxide component (δMnO_2), and that there are more sources of Fe input to crust RD50S1B than to crust 6RD08-08.

A positive correlation is observed between Si and Al in both crusts (Figure 4.5). In general, Si and Al are associated with detrital mineral phases in crusts; however, Figure 4.5 shows that there is excess Si in both crusts relative to Al. This implies there is another source of Si to the crusts, possibly, a biogenetic input (amorphous opal). Interestingly, the slopes of the Si/Al lines in figure 4.5 (6.4-3.2) are consistent with Si/Al ratio in pelagic clays, although a wide range of ratios is observed for both crusts (Tables 4.1 and 4.2). The ratios of Si/Al in crusts 6RD08-08 and RD50S1B range from 4.76 to 28.2 and 3.88 to 14.79 respectively, and suggest a greater biogenetic input of Si crust 6RD08-08 relative to crust RD50S1B.

Because Ca and P are major components in the CFA phase in crusts, they exhibit a strong positive correlation (Figure 4.6). It should be noted that although the CFA phase exerts a major control on the distribution of Ca and P in crusts, there may be other important inputs of Ca based on the excess Ca observed relative to P in both crusts (Figure 4.6). Glenn and Arthur (1988) reported that the range of ratio Ca/P is from 3.6 to 2.37 in CFA of Phosphoria formation. For example, the slopes of Ca/P are between 3.4 in crust 6RD08-08 and 2.23 in crust RD50S1B (Figure 4.6), but most of the Ca/P ratios in both crusts are higher than that of CFA (Tables 4.1 and 4.2). The excess Ca is believed to be mostly derived from either carbonate minerals or detrital input to crusts.

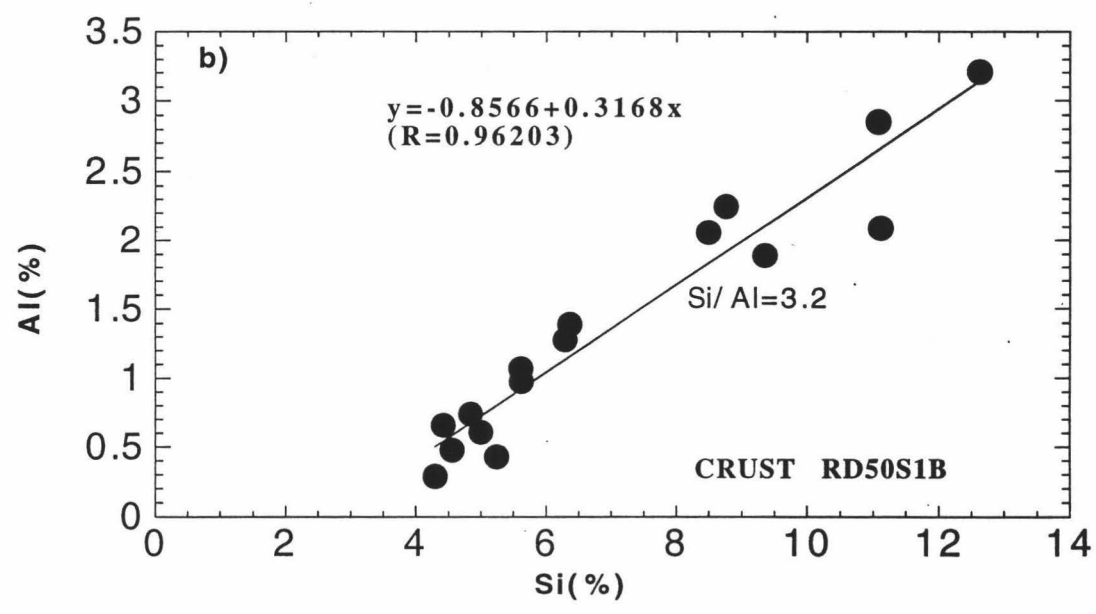
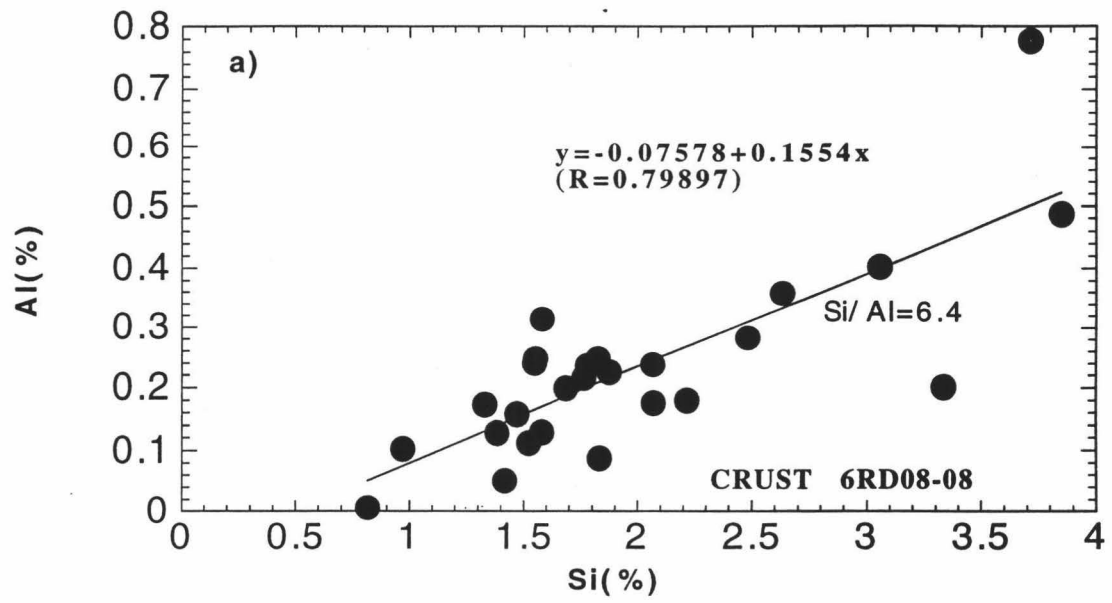


Figure 4.5 Si vs. Al. a) Crust 6RD08-08 from Kiribati. b) Crust RD50S1B from Hawaii

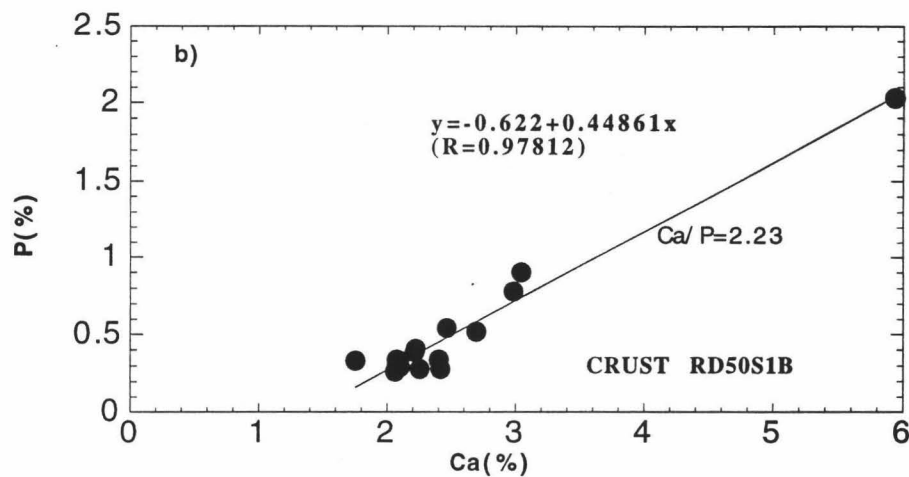
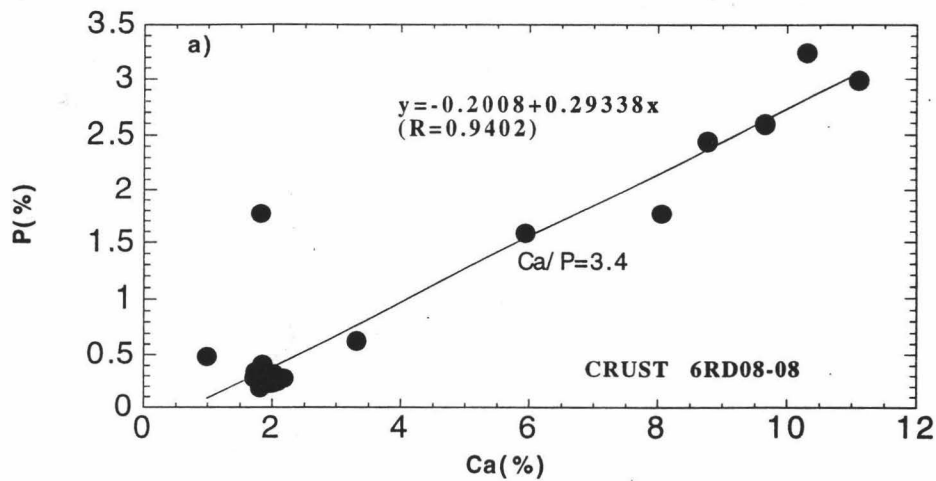


Figure 4.6 Ca vs. P. a) Crust 6RD08-08 from Kiribati. b) Crust RD50S1B from Hawaii

4.3 Geochemistry of minor elements

The elements Ba, Bi, Co, Cu, Mg, Ni, Pb, Ti, Sr, V and Zn are minor constituents (generally less than 1%) in crusts. A review of the oceanic trace element literature (Broecker and Peng, 1982; Bruland, 1983; Whitfield and Turner,

1987; Elderfield, 1988; Li, 1991) reveals that Ba, Cu, Ni and Zn are generally considered nutrient-type elements and their distribution in seawater is influenced by biological activity. The elements Bi, Co and Pb, on the other hand, are considered as scavenged type elements whose distribution is mainly controlled by interactions with solid phases. It can be noted from the plots of Co, Ni and Ba and versus Mn shown in Figures 4.7, 4.8 and 4.9 that Co and Ni correlate with Mn, while Ba, does not. There are two reasons why elements might be associated with the Mn oxide phase: either 1) they have a similar oceanic chemistry as Mn on the basis of their redox properties or genetic origin; or 2) the adsorption of these elements by manganese oxide phase is thermodynamically favored.

Several minor elements which do not display evidence for correlation with Mn are believed to be influenced by biogenetic factors. For example, no relationship exists between Ba and Mn in either crust (Figure 4.9), probably because Ba is controlled mainly by biological activity (Murray, 1978; Bertram and Cowen, 1994, Wen and DeCarlo 1994), whereas Mn is mainly of hydrogenetic origin. In addition, there are strong correlations observed between Ba and the elements Cu and Pt (Figures 4.10 and 4.11). The correlations between Ba, Cu and Pt suggest that Cu and Pt may also be biologically related in ferromanganese crusts. In some cases, these elements exhibit a much stronger covariance with Fe than Mn, such as the relationship between Fe and Cu shown in Figure 4.12. In crust RD50S1B (Schumann Seamount) significant amounts of Fe are biologically related (Figure 4.12b), whereas in crust 6RD08-08 (Kiribati) Fe is mainly detrital (Figure 4.12a) and an inverse relationship is observed between Cu and Fe. It should be pointed out that the "genetic" terms used above are inferred to represent predominant inputs of the various elements. However any given element is not necessarily

only from one origin. For example, Fe can be detrital or biogenetic (see discussions of factor analysis below).

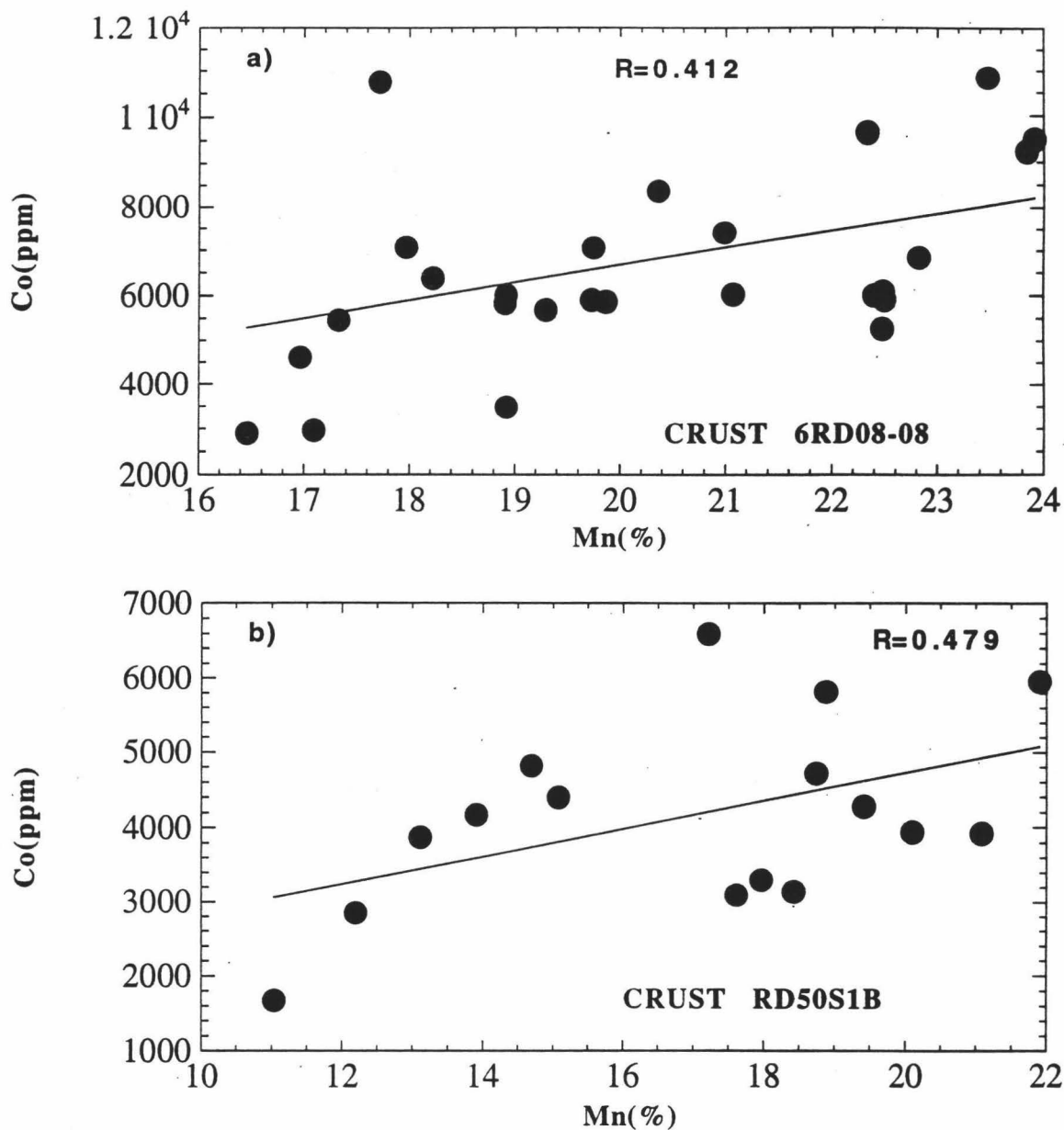


Figure 4.7 Co vs. Mn a) Crust 6RD08-08 from Kiribati. b) Crust RD50S1B from Hawaii

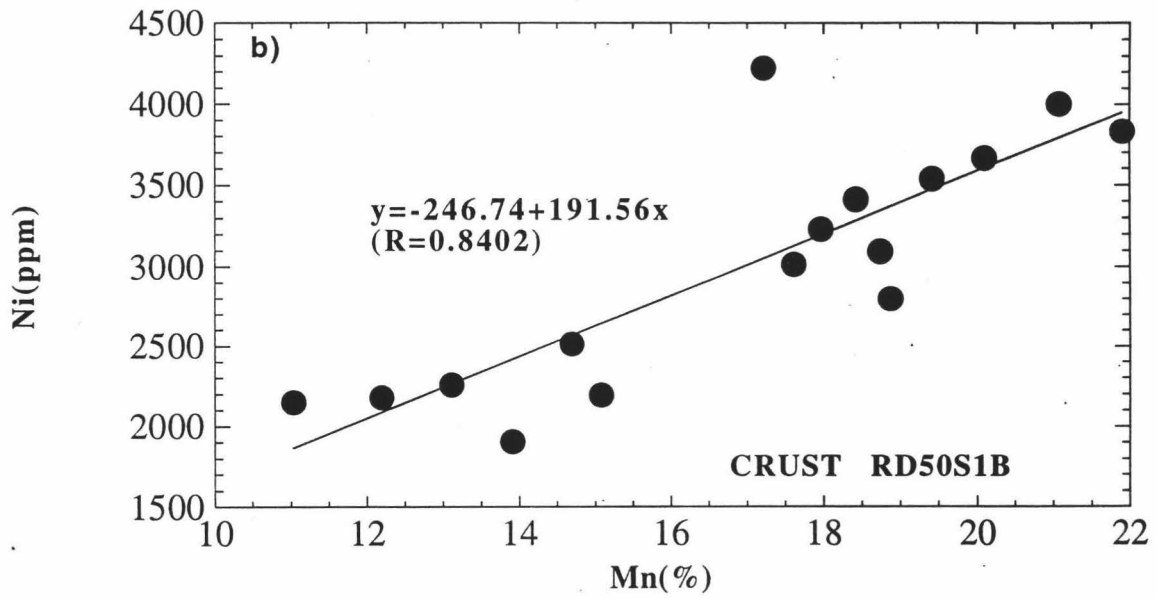
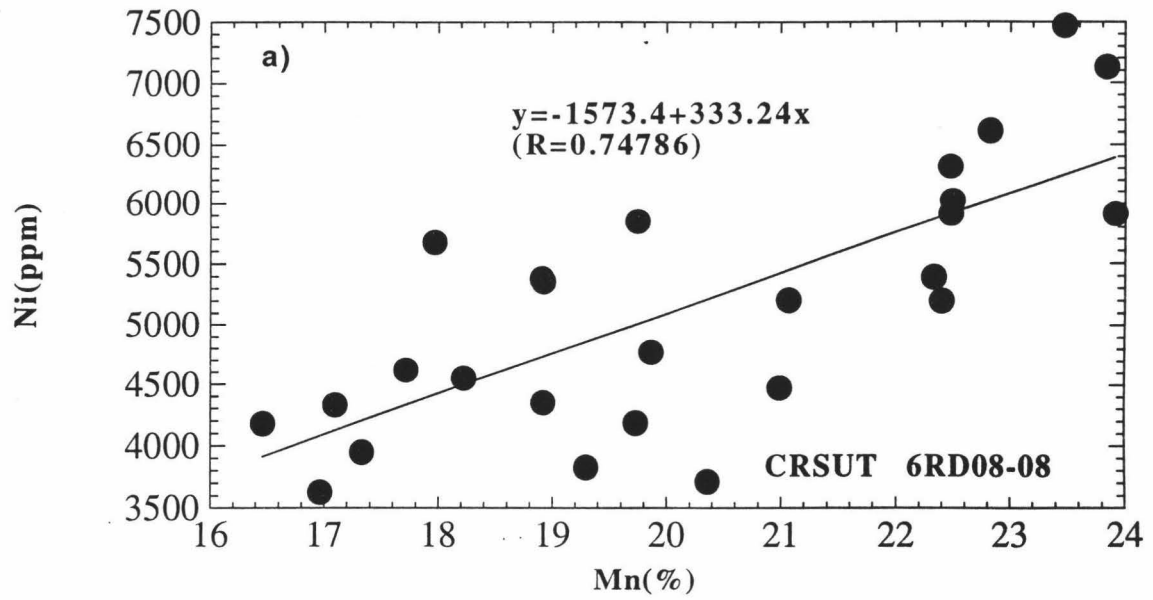


Figure 4.8 Ni vs. Mn. a) Crust 6RD08-08 from Kiribati. b) Crust RD50S1B from Hawaii

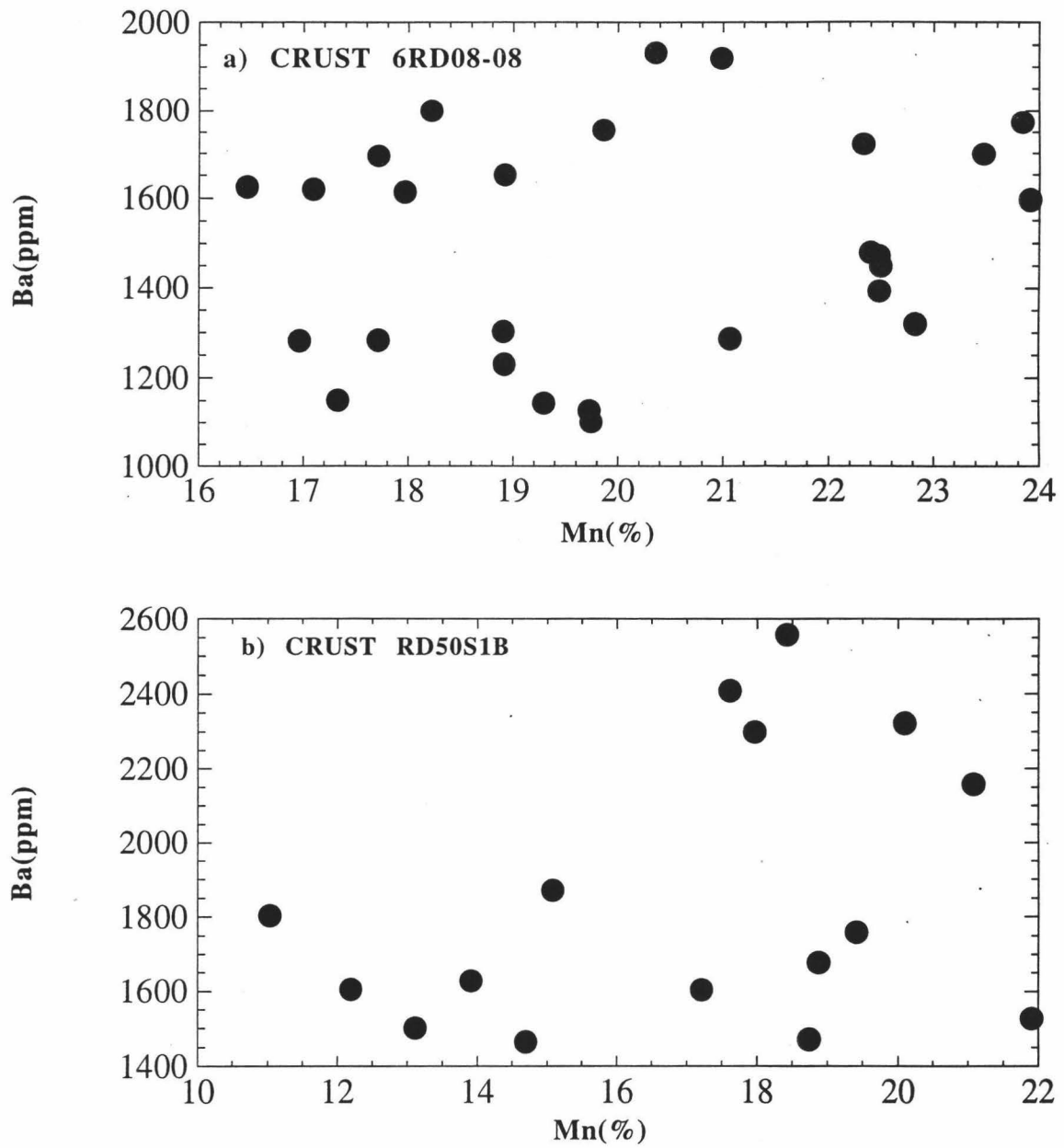


Figure 4.9 Ba vs. Mn a) Crust 6RD08-08 from Kiribati. b) Crust RD50S1B from Hawaii

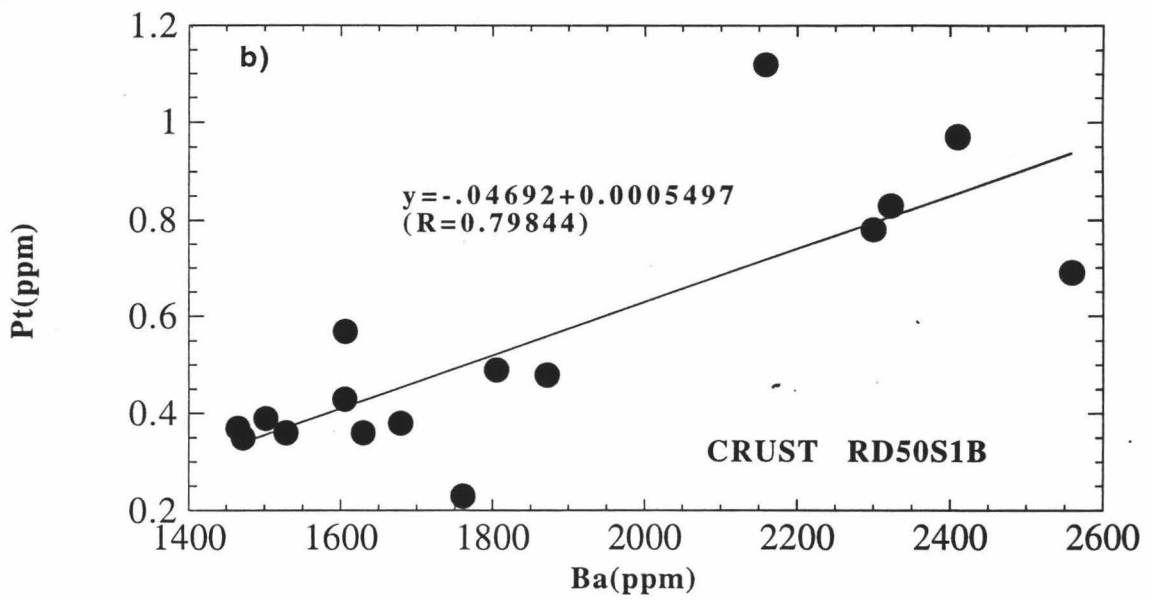
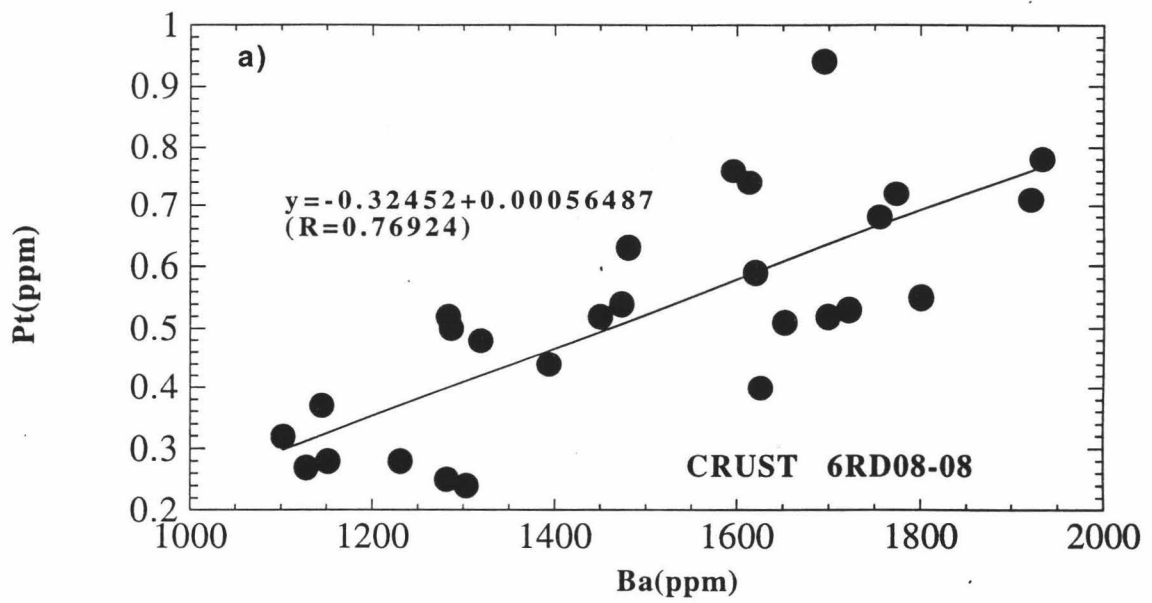


Figure 4.10 Pt vs. Ba. a) Crust 6RD08-08 from Kiribati. b) Crust RD50S1B from Hawaii

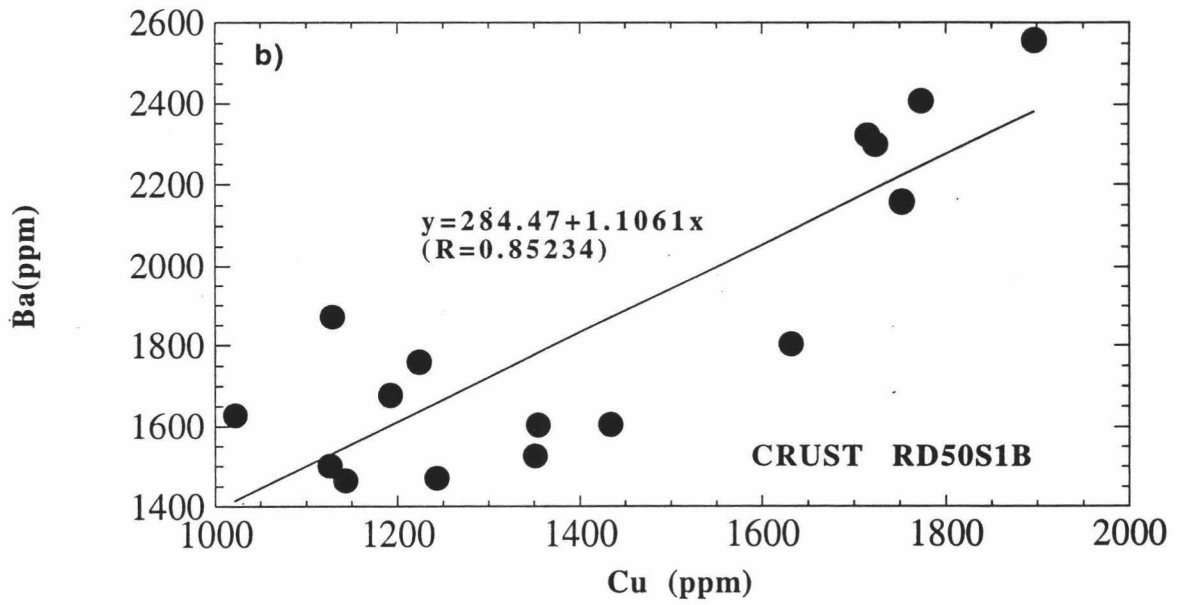
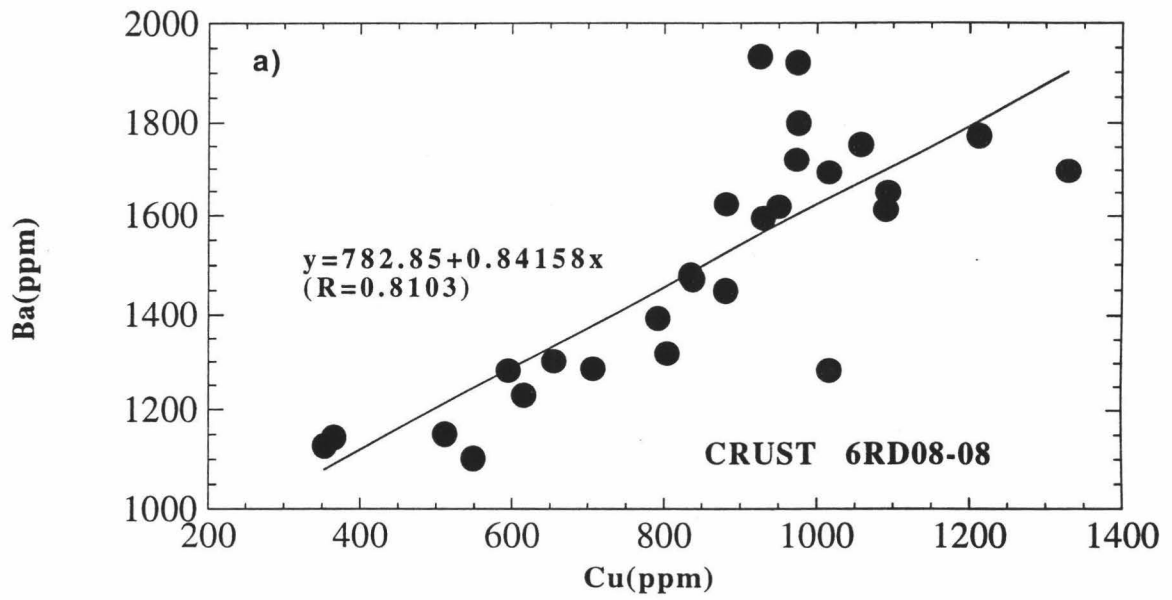


Figure 4.11 Cu vs. Ba a) Crust 6RD08-08 from Kiribati. b) Crust RD50S1B from Hawaii

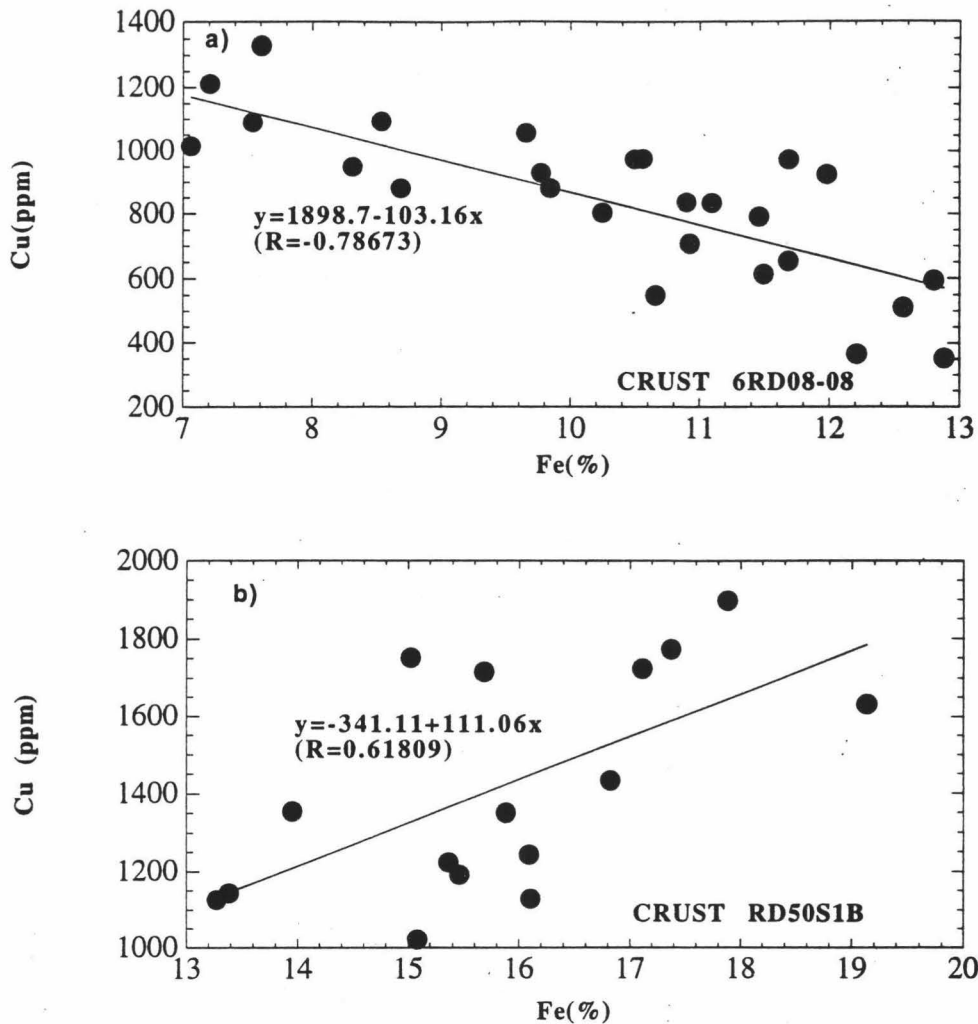


Figure 4.12 Cu vs. Fe a) Crust 6RD08-08 from Kiribati. b) Crust RD50S1B from Hawaii

4.4 Geochemistry of rare earth elements (REE)

REE are "scavenged" type elements. Their partition between crusts and seawater is influenced by competitive complexation of REE between hydrous surface of crusts and seawater (Koeppenkastrop and DeCarlo, 1992; DeCarlo and Wen, unpublished results). Therefore, changes in the chemistry of seawater

significantly affect REE uptake by crusts, especially the fractionation between HREE and LREE (Piper, 1974; Cantrell and Byrne, 1987; Elderfield, 1988; DeCarlo, 1991; DeCarlo and McMurtry, 1992; Piegras and Jacobsen, 1992; Wen and DeCarlo, 1994). The concentration of REE in the crusts is presented in Tables 4.5 and 4.6.

The concentrations of REE were normalized to the concentration in the North American Shale Composite (NASC) to eliminate the effect of the predominance of even atomic number nuclides that exists in the solar system (Henderson, 1984). The patterns of REE in various layers of the two crusts are presented in Figures 4.13 and 4.14. Several important features appear from the normalized patterns of REE in these two crusts: 1) cerium and gadolinium positive anomalies were observed in both crusts; 2) excepting Ce, patterns of REE are relatively flat in crust RD50S1B, whereas fractionation is extensive throughout crust 6RD08-08, particularly at the top and bottom of the crust sequence; 3) the REE patterns (Figure 4.13) within the CFA portion (60 mm-80 mm) of crust 6RD08-08 are, as anticipated, similar shape to that of seawater (De Baar et al., 1985); 4) The shale normalized HREE/LREE ratios in crust 6RD08-08 (Figure 4.13) are always greater than one, although there are obvious fluctuations throughout the crust (see chapter 6); the same ratios in crust RD50S1B (Figure 4.14) tend to be smaller than one.

The variable fractionation between HREE and LREE, such as observed in crust 6RD08-08 should reflect the competition between solution and surface complexation. Differences in the extent of fractionation observed in Figure 4.13 can be attributed in part to variations in the extent of REE complexation in seawater by carbonate ion through geologic time. Surface complexation reactions

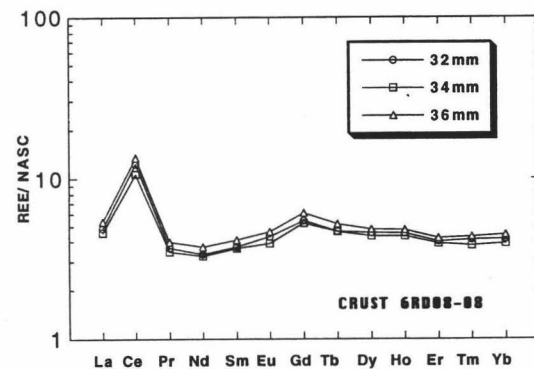
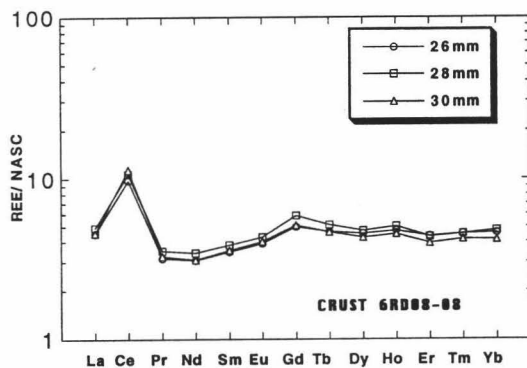
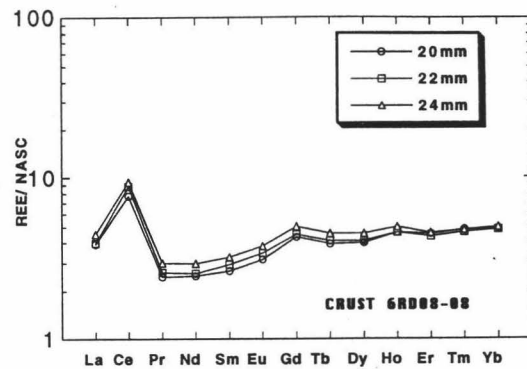
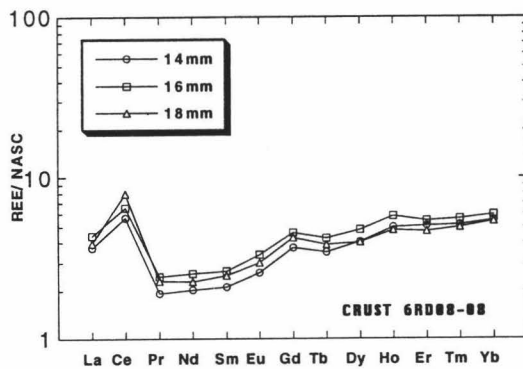
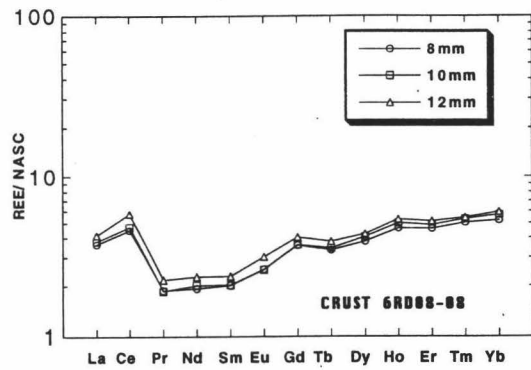
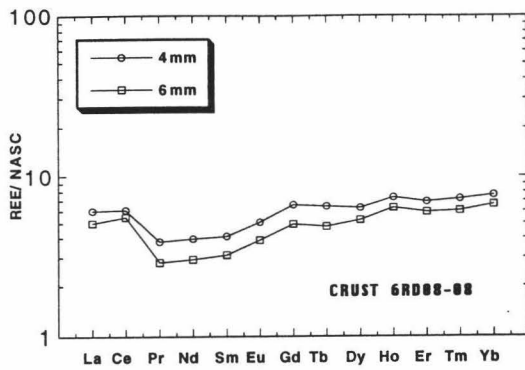


Figure 4.13 Shale (NASC) normalized REE patterns in different intervals of crust 6RD08-08 from Kiribati

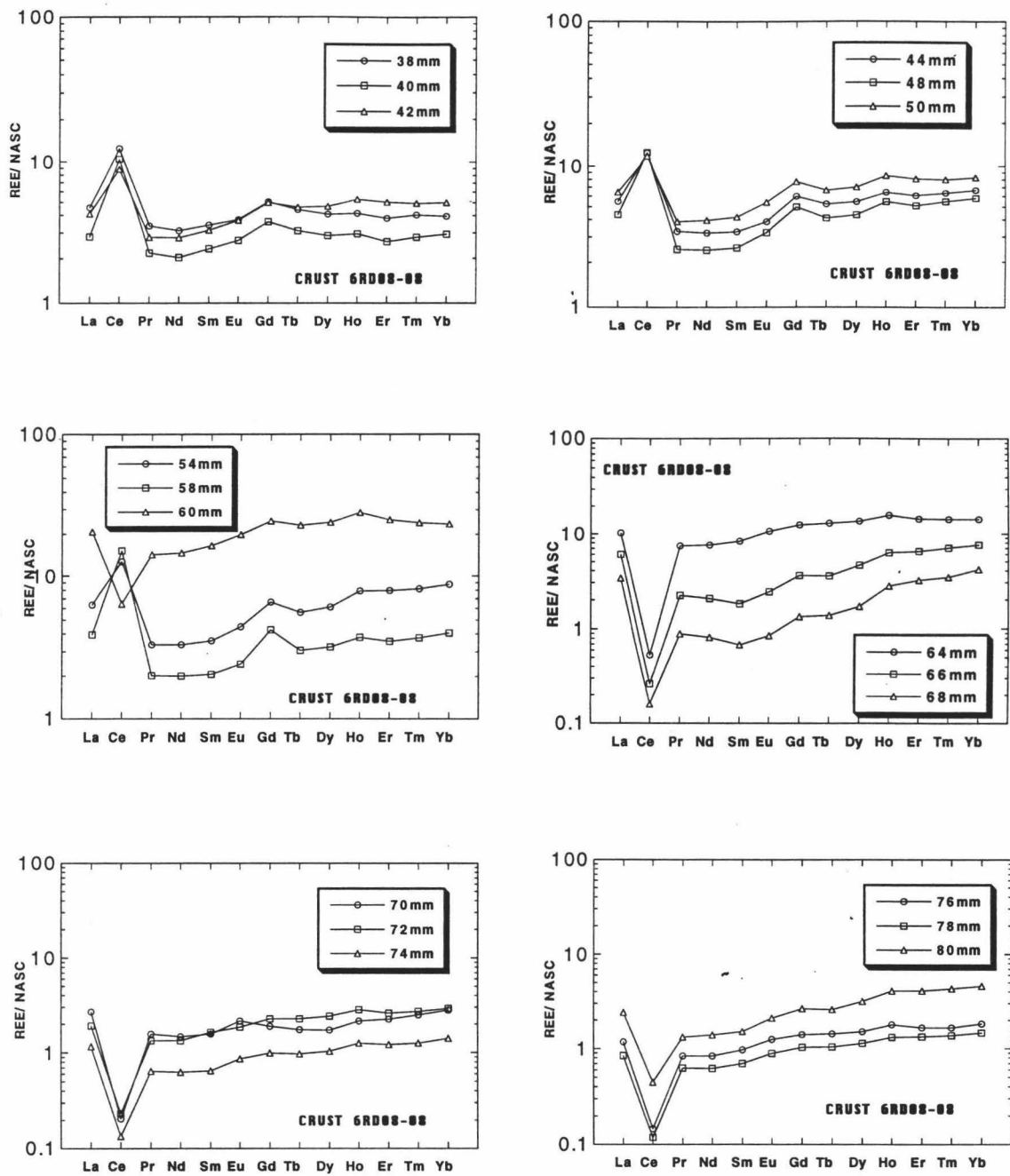


Figure 4.13 (continued) Shale (NASC) normalized REE patterns in different intervals of crust 6RD08-08 from Kiribati

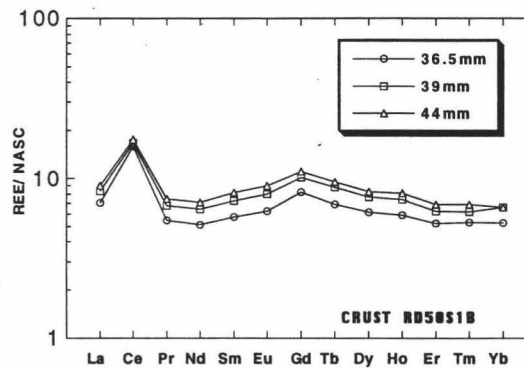
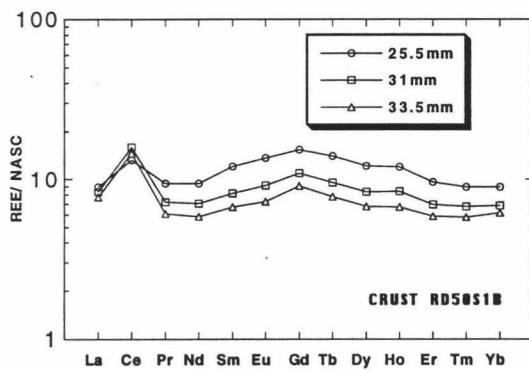
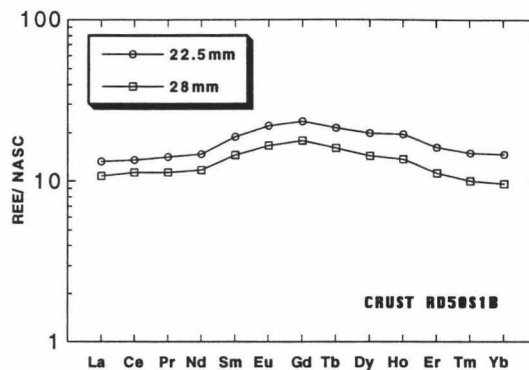
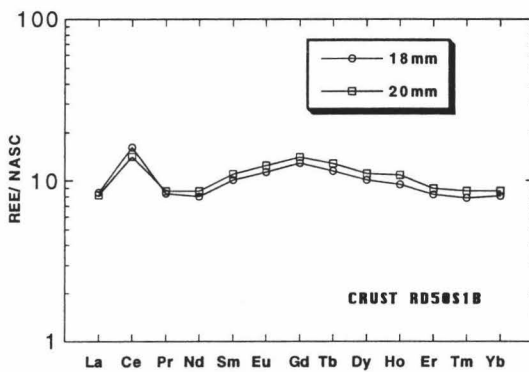
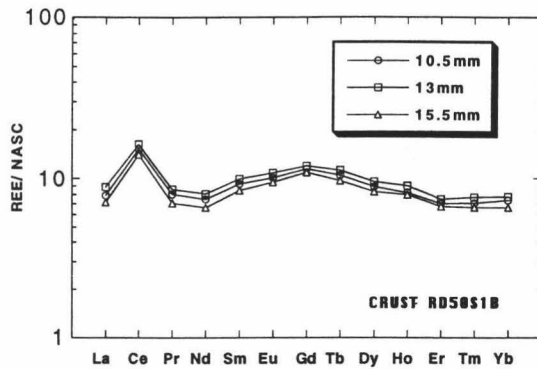
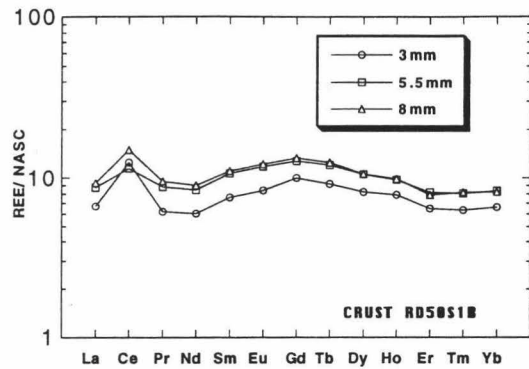


Figure 4.14 Shale (NASC) normalized REE patterns in different intervals of crust RD50S1B from Hawaii

on ferromanganese oxides are unlikely to have changed significantly over geologic time. Thus, differences in HREE/LREE ratios between the two crusts described here likely result from their exposure to different water masses or supply sources.

CHAPTER 5

THE FACTOR ANALYSIS APPROACH

5.1 Utility of factor analysis in ferromanganese crust studies

Factor analysis techniques have the advantage of taking into account intercorrelation patterns of the given geochemical data set, in this case for a ferromanganese crust. If particular elemental associations in crust are defined as a hydrogenetic group (e.g., elements Mn, Ni and Co), then there must be other elemental associations underlying the different components or elements of that geochemical data set. The purpose of factor analysis is to reveal these underlying elemental associations.

5.2 Brief introduction to factor analysis

Factor analysis is a multivariate statistical method which is based on the fundamental assumption that some underlying factors (unobserved variables) are equal to or smaller in number than the number of observed variables. This statistical method consists of a class of procedures used in treating data so as to simplify interrelationships that may exist between variables and objects.

A factor loading is equivalent to the correlation coefficient between factors and observed variables (elements). For ease of presentation, the factor loadings are usually shown in two dimensional plots that use additional graphic means to mark any group of variables which may have correlation coefficients of greater than 0.5 between any two variables (Li, personal communication). Factor scores,

are designed to portray interrelationships among objects. Factor loading and factor score results are discussed separately below.

5.3 Factor loadings

Four sets of data were subjected to factor analysis. The correlation coefficients between elements are presented in Appendix B. For ease of presentation and geochemical interpretation, each data set is discussed separately. The orthogonal transformation solution-varimax factor loadings in Appendix C (F1 vs. F2 and F3 vs. F4) are plotted for each data set.

Figure 5.1 presents the factor loading results (Appendix C.1) for the crust from Kiribati. Based on these results, elements in this crust can be divided into four major groups: 1) hydrogenetic (Mn, Co, Ni, Zn, Mg, and possibly Cu), 2) detrital (Si, Al, Fe possibly Pb), 3) fluorapatite (Ca, P, La, Pr, Sm, Nd, Eu, Gd, Tb, Dy, Ho, Er, Tm, Yb, Y), and 4) biogenetic (Ba, Pt, Ce, CeAN, Bi, Sr, Ca, P, Cu, and possibly Cr). Note that certain elements appear to be associated with two genetic groups (e.g., P, Ca).

In Figures 5.1a and 5.1b, Ca and P associate with both fluorapatite and the biogenetic groups. In the fluorapatite group, Ca and P are derived from the fluorapatite mineral phase. However, as discussed earlier, the Ca/P ratios are higher in crust from Kiribati than in CFA indicating additional Ca input to crust. This may explain why Ca also loads on the biogenetic factor. The REE as a unique elemental group are usually associated with each other under natural conditions. However, in Figure 5.1a and 5.1b the light (LREE) and heavy (HREE) appear segregated. This likely reflects REE fractionation as affected by solution

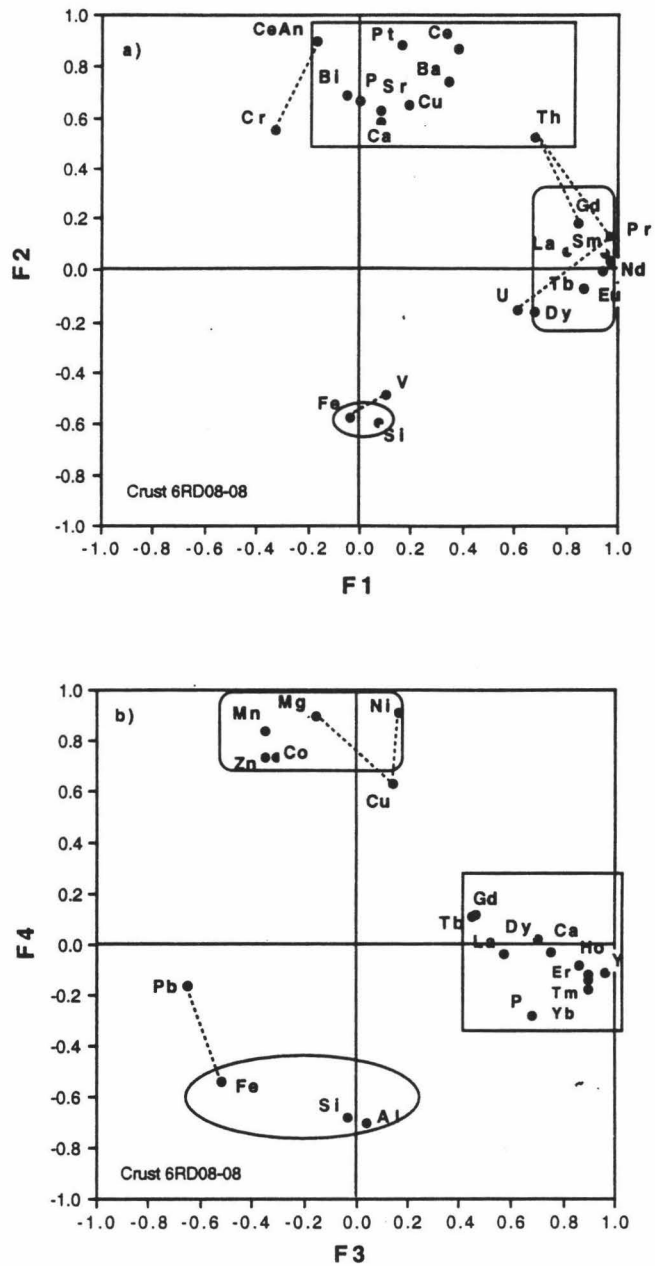


Figure 5.1 R-mode factor loading (ICP/OES and ICP/MS data), varimax rotation. Crust 6RD08-08 from Kiribati. a) Factor 1 and factor 2. b) Factor 3 and factor 4

complexation during the crust growth and rather than different sources of these elements and other processes (see chapter 6). Therefore, the LREE and HREE are still considered as a single genetic group.

Figure 5.2 is derived from microprobe data obtained at 0.5 mm resolution. The elements can be divided into three groups: 1) hydrogenetic group (Mn, Ni, Mg, K

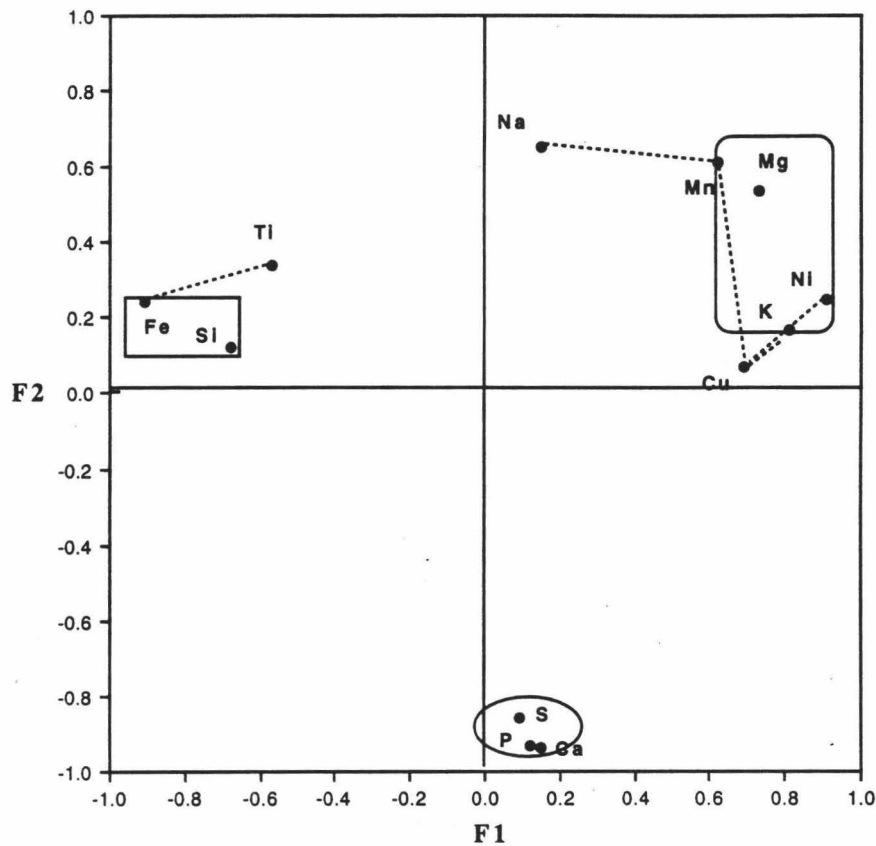


Figure 5.2 R-mode factor loading, varimax rotation, crust 6RD08-08 from Kiribati, factor 1 and factor 2 derived from 0.5mm interval microprobe data

and Cu), 2) fluorapatite group (Ca, P and SO_4^{2-}), and 3) detrital group (Si and Fe). The Si and Fe association in Figure 5.2 leads to the consideration of Fe as belonging to the detrital group. Note that this group is the same as the Si, Al and

Fe association in Figure 5.1b. Detrital group elements all show an inverse relationship to hydrogenetic group elements in both figures. In Figure 5.1a, a Si and Fe association is also generated. We know that Al is mainly detrital in hydrogenetic crusts and the Si/Al ratio is about 3 in detrital materials. But in crust 6RD08-08 Si/Al is much higher than in normal detrital material. The higher than expected value of this ratio indicates that there must be other input of Si besides detrital matter. It is possible then, that Si and Fe association in figure 5.1a is related to some other processes, such as Fe-hydrogenetic precipitates, hydrothermal input or biological activity. Factor analysis however does not allow us to elucidate this additional source.

The factor loadings (Appendix C.2) for the crust from Schumann Seamount are presented in Figure 5.3. Elements in this crust can also be split into four groups: 1) hydrogenetic (Mn, Ni, Zn, Co, Bi, Pb, Sr, Ce, Co, CeAN and U), 2) detrital (Si and Al), 3) biogenetic (Ba, Pt, Cu, Zn, V and Fe), and 4) fluorapatite (Ca, P, Y, La, Pr, Sm, Nd, Eu, Gd, Tb, Dy, Ho, Er, Tm and Yb). In Figure 5.3a, an association is generated among Co, U, Th, Pb and Ti , but except for Ti and Th, other these elements also load significantly on the hydrogenetic group factor.

Figure 5.4 presents factor loading results (Appendix C-4) for the crust from Horizon Guyot (Hein et al., 1992). Elements in this crust can be crudely divided into three groups: 1) hydrothermal group or possibly diagenetic group (Mn, Zn, Ba, Mg, Ni, Na, K, Co, Cu and likely Pb), 2) hydrogenetic group (Mn, Co, Ni, Mg, and Cu), 3) fluorapatite group (Ca and P). Compared with the elemental associations found in the two crusts from Kiribati and Hawaii, the elemental associations in crust of Horizon Guyot are unusual. There are at least two possible reasons for this. One is the possible existence of a hydrothermal input, the other is the potential occurrence of post-depositional diagenesis. Two lines of evidence

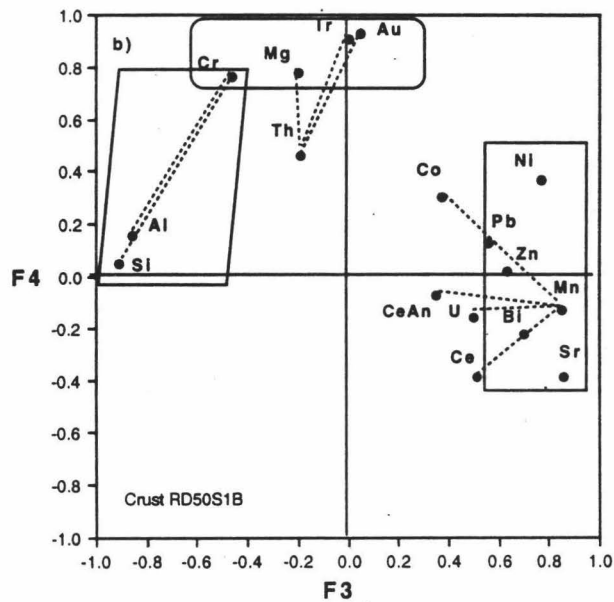
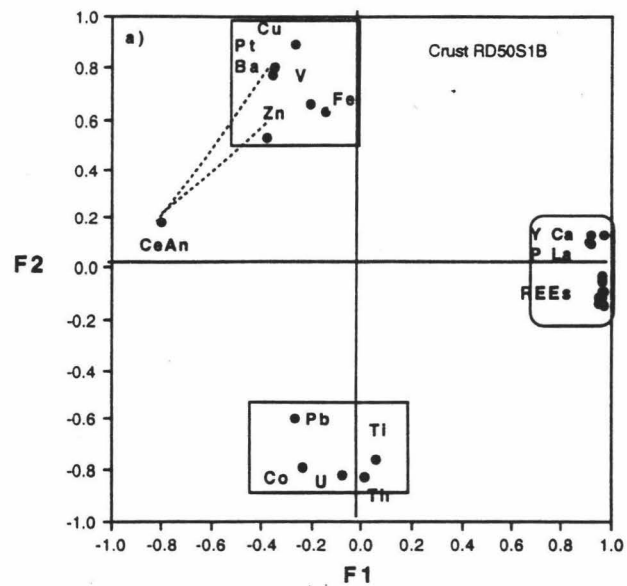


Figure 5.3 R-mode factor loading, varimax rotation. Crust from Schumann seamount, Hawaii. Four factors derived from ICP/OES and ICP/MS data at 2-3mm intervals. a) F1 vs. F2. b) F3 vs. F4

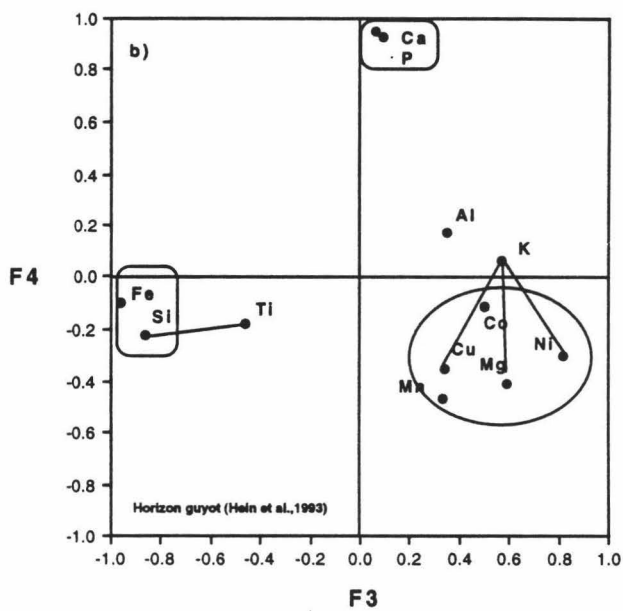
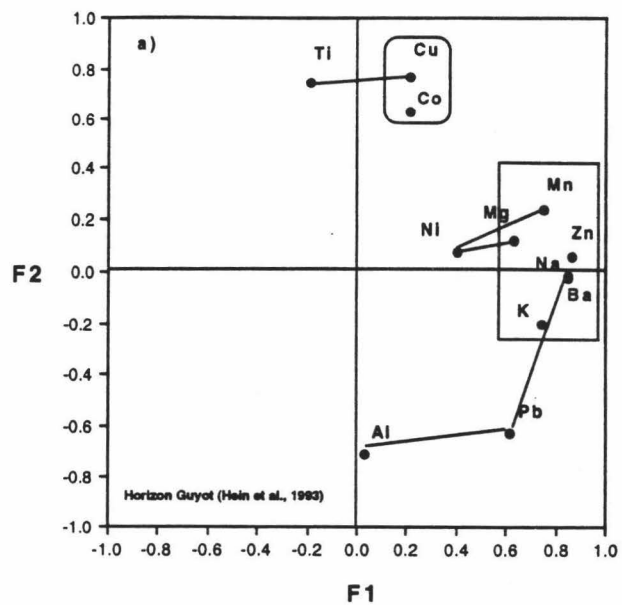


Figure 5.4 R-mode factor loading, varimax rotation. Crust from Horizon Guyot (Hein et al., 1992) a) factor 1 vs. factor 2. b) factor 3 vs. factor 4

suggest hydrothermal input. First, Al and Si are an inversely related (Figure 5.5a), and second Mn and Ba are correlated (Figure 5.5b).

The data from bulk crust samples recovered in the Marshall Island (Hein et al., 1988) were also subjected to factor analysis (Appendix C.3). According to Figures 5.6 a and 5.6 b, the elements can be divided into four groups: 1) hydrogenetic (Mn, Mg, Ni, Co, Cd, Zn), 2) fluorapatite (Ca, P, CO₂, Y), 3) biogenetic (Ba, Zn, Cu), and 4) detrital (Si, Al, K). The elemental associations, between Mn and Mo as well as Pb and Co may indicate that Mo and Pb are also of hydrogenous origin.

Comparing the factor loading results of detailed analysis from several individual crusts and from bulk samples leads to several important observations. In spite of slight differences in the elemental associations among individual data sets and possibility of a hydrothermal group of elements in one set, all associations yield very similar genetic groups (hydrogenetic, biogenetic, detrital, and fluorapatite groups). DeCarlo et al. (1987a) and DeCarlo and McMurtry (1992) reported that bulk samples of crusts from the Hawaiian Archipelago also exhibit similar genetic groups with the exception of a hydrothermal contribution to a few samples. One could readily argue that the elemental groupings are similar owing to similar geochemical processes forming crusts in general. However, although similar mechanisms occur during the formation of crusts over time, at any given time the sources of elements incorporated in crusts in different areas may be quite different.

Li (1982) has reported that, in ferromanganese nodules interelement relationships derived from electron microprobe data are not always directly comparable to the results of bulk analysis. He concluded that while bulk analysis

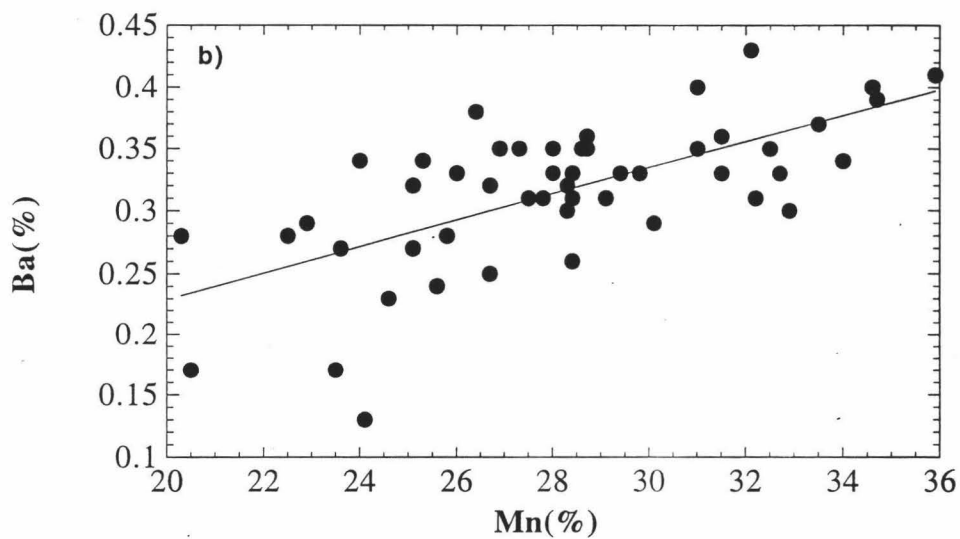
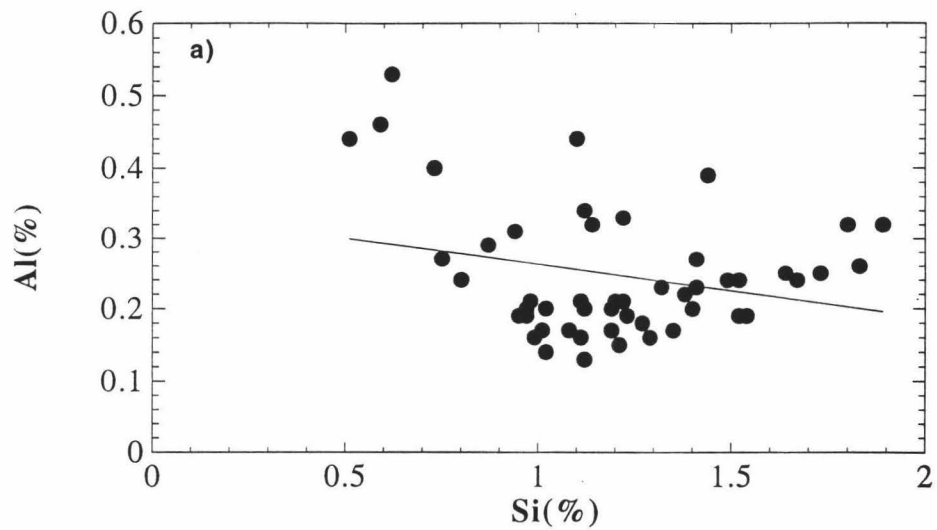


Figure 5.5 Scatter plots of elements, crust from Horizon Guyot (Hein et al., 1992). a) Al vs. Si. b) Ba vs. Mn

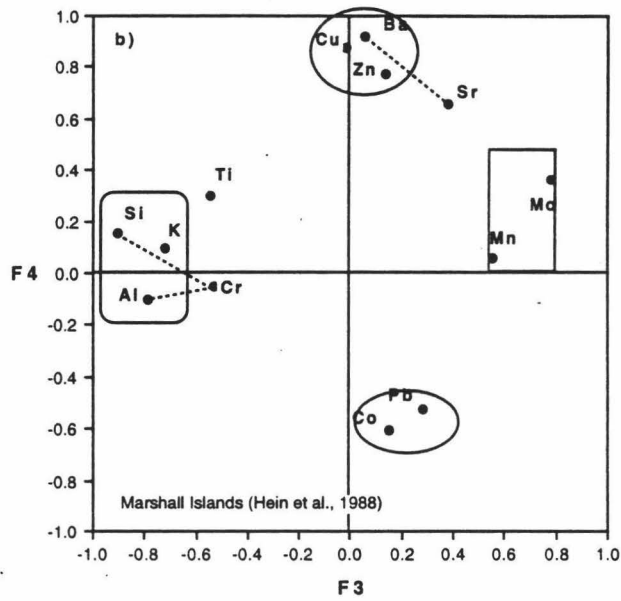
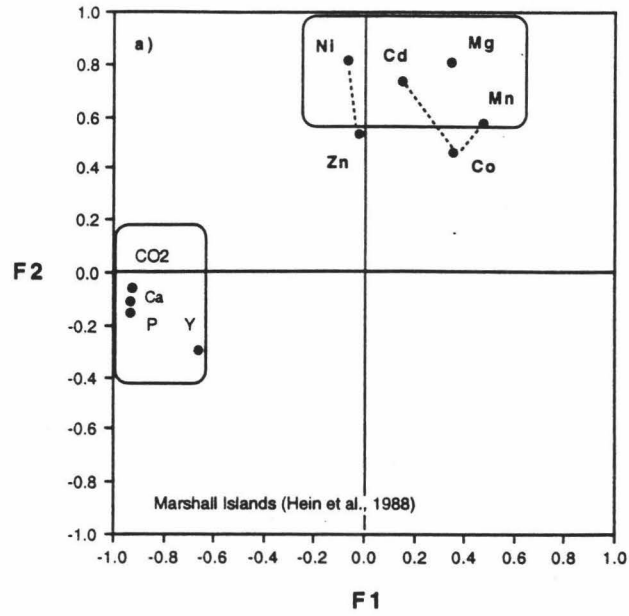


Figure 5.6 R-mode factor loading, varimax rotation. bulk crust samples from Marshall Islands (Hein et al., 1988) a) factor 1 vs. factor 2. b) factor 3 vs. factor 4

may provide overall interelement relationships that reflect how elements were first incorporated into nodules, microprobe analysis exposes the interelement relationships that reflect the influence of post-depositional diagenetic rearrangement. In this respect, crusts are obviously very different from nodules. Why are elemental associations similar between bulk and fine-scale analysis in crusts, but are very different in nodules?

In this study, data that effectively represent a time series (within a crust through geological time) are compared to a spatial series (a group of individual bulk samples from a given region). The stratigraphic analysis in crusts from Hawaii and Kiribati represent the time series and the bulk compositional data from the Marshall Islands represent the spatial series. The elemental associations are nearly identical in time and space; therefore, crusts appear not to experience significant post-depositional diagenesis and remobilization of elements as do nodules.

Slight differences in the elemental associations in terms of the various elements that comprise the genetic groups between crusts indicates that different crusts experienced different oceanic water conditions. The abundance of a given element in a crust is influenced first by the major genetic processes, and second by other factors such as local water conditions, including the oxygen concentration, the extent of biological activity, the depth of the CCD and lysocline, and the different sources of elements as well as their genetic associations (Halbach and Puteanus, 1984; Halbach, 1986; DeCarlo et al., 1987a, b). An important example of this is the element Ce which falls into different groupings in different crusts. In crust 6RD08-08 from Kiribati, Ce is mainly associated with the biogenetic elemental group (Figure 5.1a), however in crust RD50S1B from Hawaii Ce behaves as a transitional phase with significant loadings in both the hydrogenetic and biogenetic groups (Figure 5.3b), although

the hydrogenetic association is slightly favored. It thus appears that at least two parameters are necessary to describe the geochemical behavior of Ce in crusts. I propose that local environments may play as important a role as basin-wide conditions in controlling the incorporation into crusts of elements which are readily scavenged from seawater by Fe or Mn oxides. Specific geological processes such as hydrothermal activity or extensive weathering may also exert an influence on elemental associations. For example, the crust from Horizon Guyot is believed to have grown much faster (Hein et al., 1992) than other hydrogenetic crusts and may have been influenced by hydrothermal input. Finally, it should be pointed out that the enrichment of certain elements in crusts can result from several processes; sometimes these processes are superimposed. The Fe content of crusts, for example, can be attributed to biogenetic, detrital or hydrogenetic inputs or any combination thereof. However, factor analysis only identifies predominant elemental associations and does not allow resolution of minor differences.

5.4 Factor scores

A requirement for the calculation of factor scores to determine inter-object relationships by factor analysis is that the number of variables be less than the number of observations within the given data set. In order to meet this requirement, a smaller number of variables was chosen based on geochemical considerations and the results of the previous factor loadings.

Twenty five parameters (Al, Si, P, Ca, Cu, Mg, Co, Fe, Mn, Ni, Sr, CeAN, Ba, La, Pr, Sm, Eu, Gd, Tb, Ho, Yb, Pt, Th and Ca) were chosen for crust 6RD08-08. Fifteen parameters (Si, P, Ca, Cu, Co, Fe, Mn, Ni, CeAN, Ba, La, Ce, Eu and Bi) were selected for crust RD50S1B.

The loadings of factor 1 and factor 3 in the crust from Kiribati are presented in Figure 5.7a. The elements previously define as the "biogenetic" (Ba, Pt, Ce, Bi, Ca, P, Cu) load on factor 1 and the "hydrogenetic" (Mn, Co, Ni, Mg, Zn, Cu) load on factor 3. The scores for these two groups are plotted as a function of depth in Figures 5.7b and 5.7c. The biogenetic group factor score decreases sharply from bottom to top of the crust, suggesting lessened biogenetic influence on the crust composition as a function of geologic time. Figure 5.7c shows dramatic and seemingly random changing the hydrogenetic group throughout the crust.

Figure 5.8 shows factor loadings and factor scores of the crust from Schumann Seamount. Biogenetic (Ba, Pt, Cu, Fe) and hydrogenetic (Mn, Ni, Co, Ce) groups load on factors 2 and 1, respectively. The plot of the hydrogenetic group as a function of depth (Figure 5.8b) within the crust displays "valleys" at 15.5 mm and 28 mm. As previously mentioned these intervals also correspond to strong detrital inputs. The biogenetic group decreases from bottom to top (Figure 5.8 c) but exhibits a steeper decrease between 30 and 20 mm. A biogenetic factor peak in the middle (about 32 mm) part of the crust, is believed to be related to the passage of the seamount, on which the crust accreted, through the equatorial high productivity upwelling zone (VonderHaar 1990; Cowen et al., 1993)

The combined data (Kiribati 6RD08-08 and Hawaii RD50S1B) are comprised of forty three samples (twenty seven from crust 6RD08-08 and sixteen samples from crust RD50S1B) and thirty one elements (Fe, Mn, Al, Si, Ca, P, Mg, Ti, Co, Ni, Sr, Zn, Cu, Y, Ba, Pt, Pb, Bi, Th, U, V, La, Ce, Nd, Sm, Eu, Gd, Tb, Dy, Tm, Yb) and were also subjected to factor analysis. Factor loadings are shown in Figure 5.9. Based on these results, elements can be divided into and assigned to several major groups: 1) REE, 2) detrital (Al, Si, Fe), 3) hydrogenetic (Mn, Co, Ni, possibly Zn),

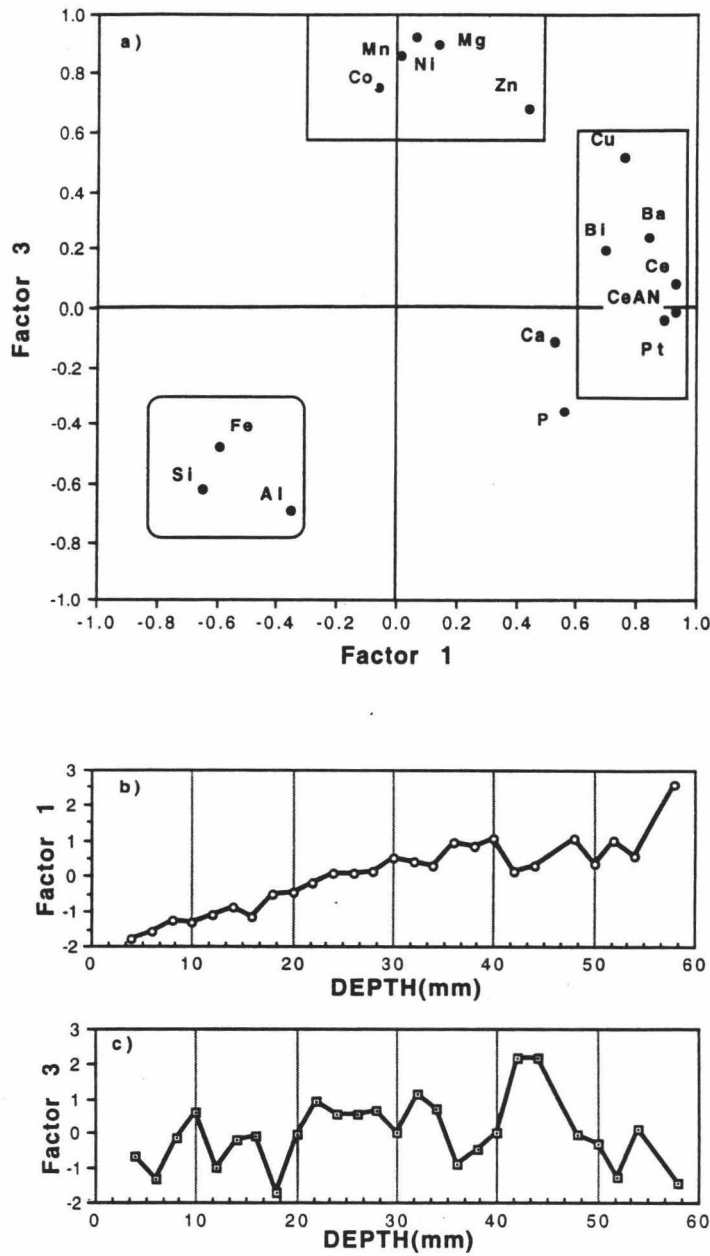


Figure 5.7 R-mode factor analysis for crust 6RD08-08 from Kiribati. a) R-mode factor loading, varimax rotation. factor 1 represents biogenetic group (Ba, Ce, Pt and Cu) and factor 3 represents hydrogenetic group (Mn, Ni, Co, Mg and Zn). b) Factor score, variations of factor 1 (biogenetic group) as a function of depth. c) Factor score, variations of factor 3 (hydrogenetic factor) as a function of depth.

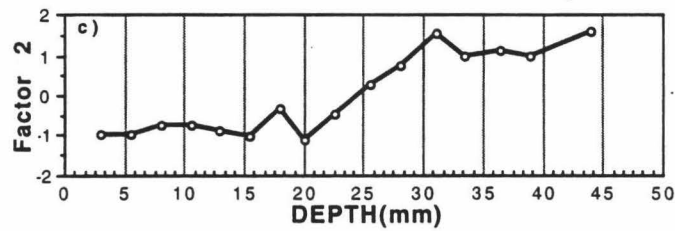
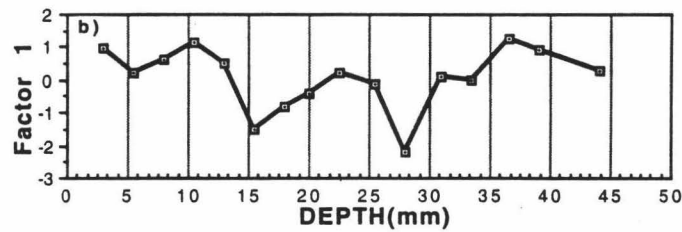
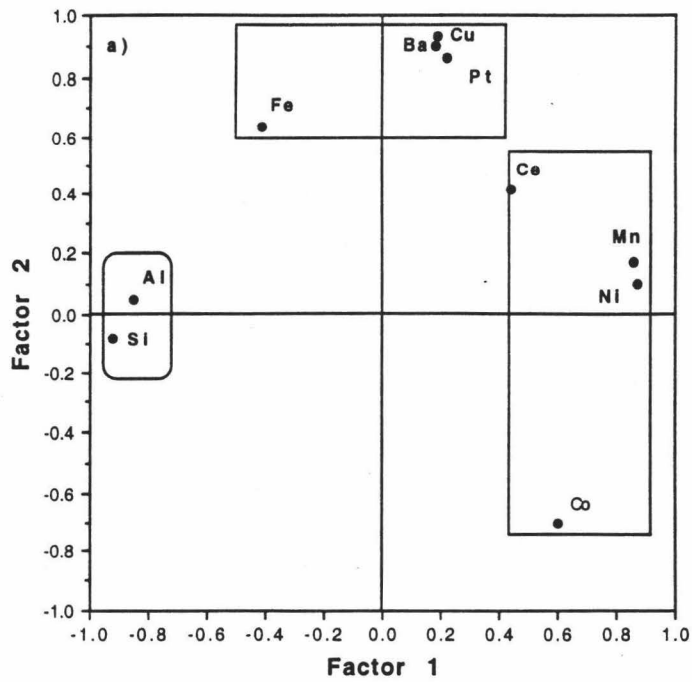


Figure 5.8 R-mode factor analysis for crust RD50S1B from Hawaii, a) R-mode factor loading, varimax rotation. factor 1 represents hydrogenetic group (Mn, Ni, Co and Ce) and factor 2 represents biogenetic group (Ba, Cu, Pt and Fe). b) Factor score, variation of factor 1 (hydrogenetic factor) as a function of depth. c) Factor score, variation of factor 2 (biogenetic factor) as a function of depth.

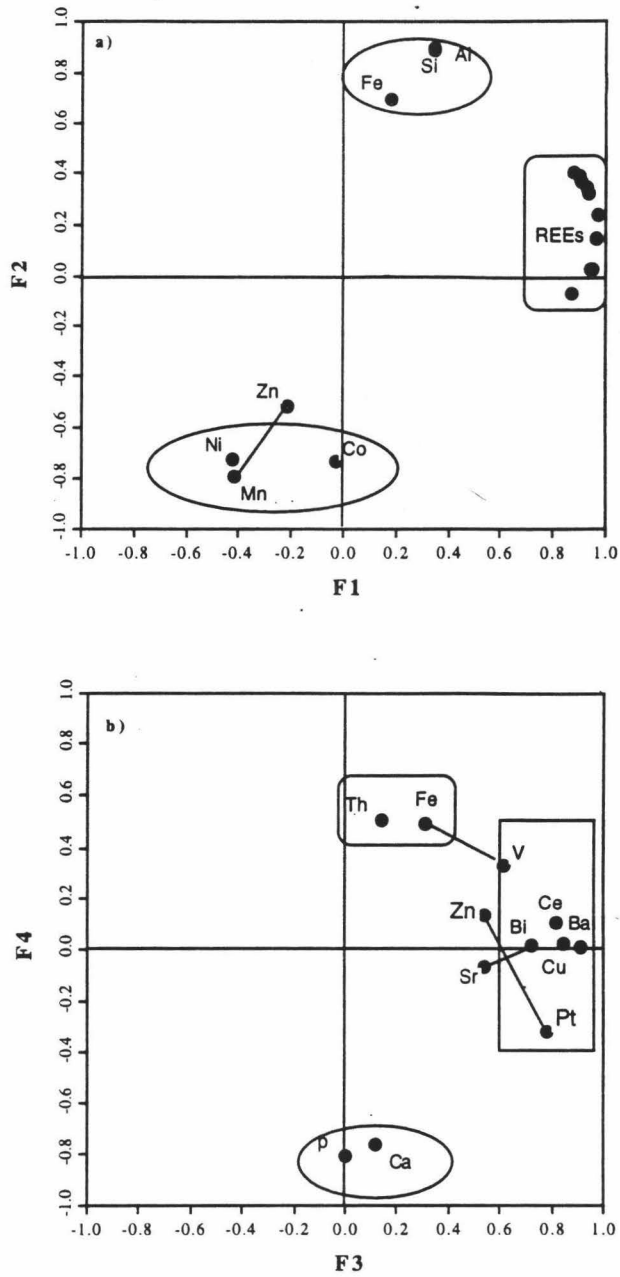


Figure 5.9 R-mode factor loading, varimax rotation. Crusts 6RD08-08 and RD50S1B.
 a) Factor 1 and Factor 2. b) Factor 3 and Factor 4

4) biogenetic (Ba, Cu, Pt, Ce, Bi, V, possibly Zn, Sr, Fe), and 5) fluorapatite (Ca, P). Elemental associations in Figure 5.9 are highly consistent with the results of factor loadings of crust 6RD08-08 from Kiribati rather than crust RD50S1B from Hawaii owing partly to two-thirds of the samples being from the Kiribati crust. For example, Fe and Ce (Figure 5.9) load on detrital and biogenetic factors respectively, which are the same as the factor loadings of crust 6RD08-08 from Kiribati (Figure 5.7a). However, Fe is biologically related and Ce is hydrogenetic in crust RD50S1B from Hawaii (Figure 5.8a). The importance of the combined data is apparent in Figure 5.10, which plots the factor score between the

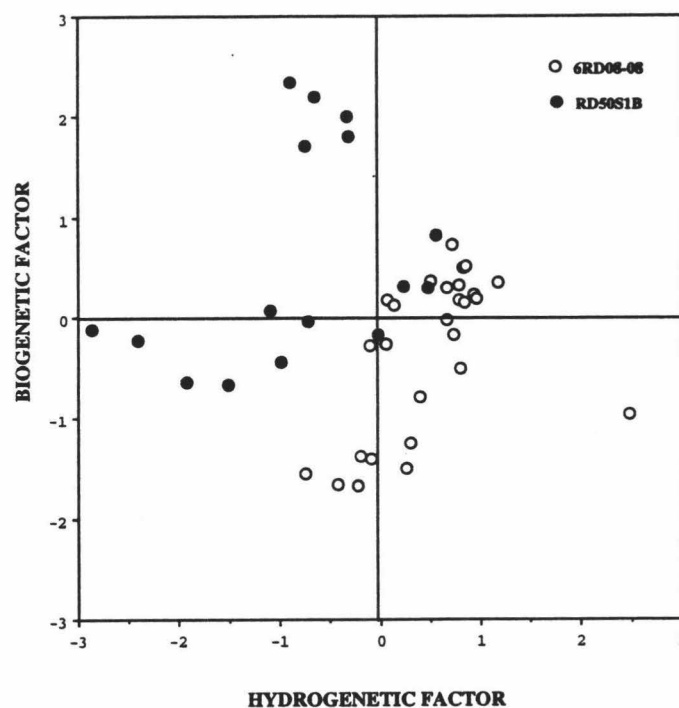


Figure 5.10 R-mode factor score, Biogenetic factor vs. hydrogenetic factor

biogenetic and hydrogenetic groups. A significant difference exists between the two crusts. The hydrogenetic group (Mn, Co, Ni and Zn) is highly enriched in crust 6RD08-08 from Kiribati, and the biogenetic group (Ba, Cu, Pt, Ce, Bi, V, possibly Zn, Sr and Fe) is slightly higher in crust RD50S1B than in crust 6RD08-08. The trends in the chemical variations in both crusts shown in Figure 5.10 are similar to those of the factor scores (Figures 5.7b, c and 5.8b, c), although these values of the factor scores are slightly different from what appears in the individual crust data.

CHAPTER 6

GENESIS AND PALEOCEANOGRAPHIC IMPLICATIONS

6.1 Genesis of ferromanganese crusts

It is generally accepted that ferromanganese crusts are predominately of hydrogenetic origin (Halbach, 1986; DeCarlo et al., 1987a, b), but in some instances other processes including post-depositional alteration or hydrothermal inputs, or both, may obscure evidence of the main hydrogenetic process. A significant result of the factor analysis study presented in this thesis is the realization that both the Kiribati and Schumann Seamount crusts are mainly hydrogenetic, whereas the elemental associations in the crust from Horizon Guyot (Hein et al., 1992) suggest potential diagenetic or hydrothermal inputs. A ternary diagram of variations in Fe, Mn, and (Co, Ni, Zn)*10 amongst the three crusts is presented in Figure 6.1. Crusts 6RD08-08 and RD50S1B exhibit a similar abundance of Mn but exhibit slight differences in the Fe and the hydrogenetic trace elements (Co, Ni, Zn); these could be attributed to different conditions leading to the enrichment of these elements. The crust from Horizon Guyot has a much higher abundance of Mn but relatively lower abundance of Co, Ni and Zn, which may result from a hydrothermal or diagenetic input in addition to hydrogenetic deposition. The hydrothermal or diagenetic input superimposes on the hydrogenetic imprint of the crust from Horizon Guyot. Furthermore, elemental associations in the crusts from Schumann Seamount and Kiribati are significantly different from those in the crust from Horizon Guyot.

On the basis of elemental associations in Fe-Mn crusts it can be

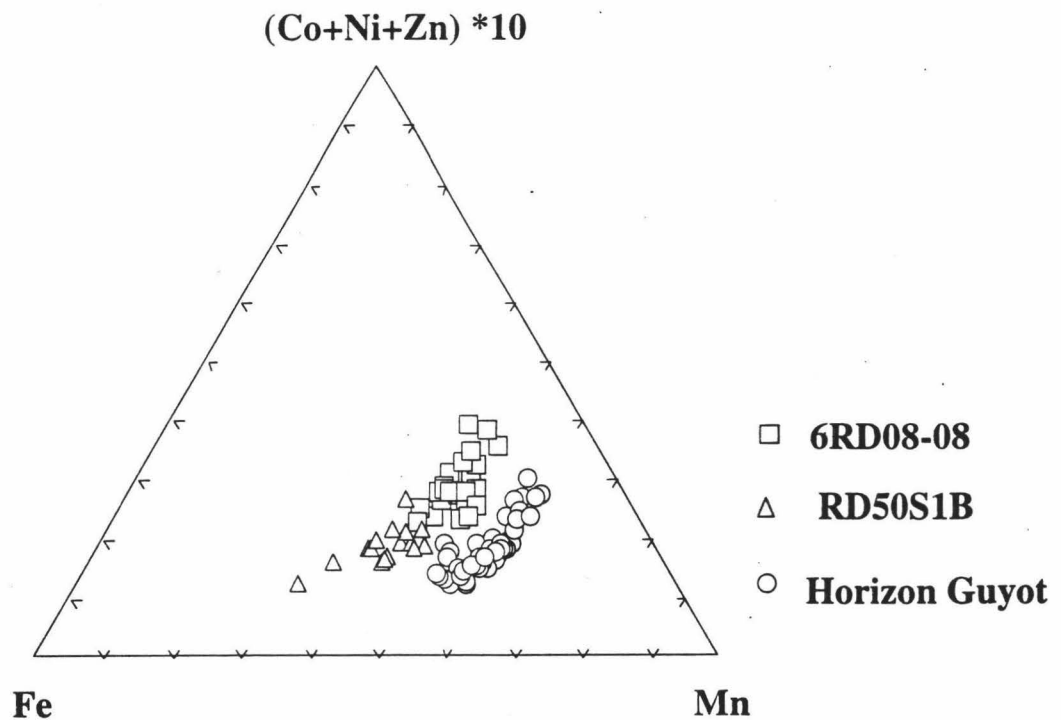


Figure 6.1 Plot of components Fe, Mn, (Co+Ni+Zn)*10 in ferromanganese crusts from different areas. The squares indicate the crust from Kiribati. The triangles represent the crust from Hawaii. The circles show the sample within crust from Horizon Guyot (Data from Hein et al., 1992)

deduced that manganese oxide (δMnO_2) exerts a primary control on the enrichment of hydrogenetic group elements. In general, the more MnO_2 precipitates directly from the water column, the more the hydrogenetic group elements (Co, Ni, Zn) can be enriched owing to strong interaction between the dissolved species and newly formed oxide surfaces. Although the crust from Horizon Guyot, is more enriched in Mn, it exhibits lower abundance of

hydrogenetic elements (Co, Ni, Zn). One explanation might be the fast growth of this crust proposed by Hein et al. (1992). However, this could also result from excess Mn derived from the hydrothermal inputs. Therefore, although the total Mn content of this crust is elevated relative to those from Kiribati and Schumann, the contribution from hydrogenetic processes appears smaller. The current approach however, can not resolve quantitatively multiple sources of individual elements but can only infer potential sources. It should also be pointed out that different intervals within each individual crust may have accreted under the influence of several geochemical processes. This could also lead to slightly different elemental associations. However, major elemental groupings should not change significantly.

Because the comparative study of factor loadings has shown that the hydrogenetic crusts, in general, exhibit almost no evidence of post-depositional remobilization, their geochemistry and elemental distributions within the crust should reflect the chemistry of oceanic water and its changes throughout the geological-time period during which the crust grew. Thus, when attempting to reconstruct paleoceanographic conditions which the crust experienced, it is important to know the growth rates of crusts and ages of particular intervals.

6.2 Chemical stratigraphy

Various aspects of crust stratigraphy have been studied over the past ten years (Janin, 1987; 1988; Puteanus and Halbach, 1988; Ingram et al., 1988; VonderHaar 1990; DeCarlo, 1991; Hein et al., 1992; Cowen et al., 1993; McMurtry et al., 1994). Dating methods for crusts include radiometric, biostratigraphic and empirical (Co chronometer) approaches. Amongst these,

nannofossil biostratigraphy appears to be the most reliable for old Fe-Mn crusts (Cowen et al., 1993, Cowen and DeCarlo, unpublished results). These authors conclude that the average growth rate of a crust from Hawaii was significantly slower than that of a crust from Kiribati. Their results are used as age constraints in this study and on a comparative basis to evaluate the reliability of other methods such as the Co-chronometer.

The Co-chronometer, in which the Co concentration is proposed to be inversely proportional to the growth rate, has been calculated by two different methods by Manheim and Lane-Bostwick (1988) and Puteanus and Halbach (1988). Relative growth rates were calculated for the two crusts in this study by both methods (Tables 6.1 and 6.2) using the empirical relationships: 1) R (growth rate in mm/Ma) = $6.8 \cdot 10^{-1} / (Co^n)^{1.67}$, $Co^n = Co \cdot 50 / (Fe + Mn)$ (Manheim and Lane-Bostwick, 1988) and 2) R (growth rate in mm/Ma) = $1.28 / Co - 0.24$ (Puteanus and Halbach, 1988). According to Manheim and Lane-Bostwick method, the growth rates of crust 6RD08-08 calculated in this manner range between 0.25 and 1.74 mm/m.y over the 60 mm crust sequence, whereas the growth rates of crust RD50S1B are calculated to be between 0.62 and 5.79 mm/m.y. in the first 44 mm of this thick sequence. The growth rates calculated by the two Co-chronometers are not entirely consistent with the biostratigraphy results (Cowen et al., 1993; Cowen and DeCarlo, unpublished data).

One can conclude that the Co-chronometer is only useful for estimating relative growth rates within a single crust, and even then fails when hiatuses, erosional or dissolutional features or any combination thereof are encountered in a crust sequence. Furthermore, the method can not be used to calculate absolute ages of the crusts, because different crusts and even different horizons within a single crust experienced quite different water chemistry over geologic time.

Although most of the Co content of crusts is derived from hydrogenetic scavenging, Co enrichment in the crusts may not only be dependent on the Co flux in the water column but also on how effectively Co is adsorbed onto Fe-Mn oxide surfaces. Because hydrogenetic crusts accumulate at a slow rate (less than

Table 6.1 Cobalt Accumulation and Growth Rate of Crust 6RD08-08 from Kiribati

| DEPTH(mm) | Growth rate (mm/Ma)* | Growth rate (mm/Ma)# |
|-----------|----------------------|----------------------|
| 4 | 0.78 | 3.66 |
| 6 | 0.81 | 3.90 |
| 8 | 0.69 | 3.55 |
| 10 | 0.51 | 2.75 |
| 12 | 0.82 | 4.19 |
| 14 | 0.70 | 3.55 |
| 16 | 0.71 | 3.74 |
| 18 | 1.17 | 5.77 |
| 20 | 0.80 | 3.54 |
| 22 | 0.67 | 2.88 |
| 24 | 0.80 | 3.48 |
| 26 | 0.96 | 4.47 |
| 28 | 0.84 | 3.65 |
| 30 | 0.83 | 3.56 |
| 32 | 0.37 | 1.81 |
| 34 | 0.29 | 1.77 |
| 36 | 0.70 | 3.22 |
| 38 | 0.45 | 2.14 |
| 40 | 0.51 | 2.56 |
| 42 | 0.35 | 1.87 |
| 44 | 0.25 | 1.52 |
| 48 | 0.61 | 3.70 |
| 50 | 1.25 | 11.76 |
| 52 | 1.74 | 25.45 |
| 54 | 0.39 | 2.75 |

* Manheim and Lane-Bostwick Method (1988)

Halbach and Puteanus Method (1988)

Table 6.2 Cobalt Accumulation and Growth Rate of Crust RD50S1B from Hawaii

| DEPTH(mm) | Growth rate (mm/Ma)* | Growth rate (mm/Ma)# |
|-----------|-----------------------|----------------------|
| 3 | 0.618 | 3.049 |
| 5.5 | 1.304 | 5.526 |
| 8 | 1.531 | 6.816 |
| 10.5 | 1.011 | 3.597 |
| 13 | 0.895 | 3.738 |
| 15.5 | 1.177 | 7.215 |
| 18 | 1.217 | 6.398 |
| 20 | 0.879 | 5.300 |
| 22.5 | 1.138 | 8.676 |
| 25.5 | 2.230 | 28.506 |
| 28 | 5.786 | - |
| 31 | 2.652 | 18.376 |
| 33.5 | 2.392 | 14.186 |
| 36.5 | 1.882 | 8.399 |
| 39 | 1.838 | 8.288 |
| 44 | 2.753 | 17.237 |

10 mm/Ma), there should be no kinetic limitation for the adsorption of Co onto the Fe-Mn oxide surface. As long as the environmental conditions favor Co being scavenged by Fe-Mn oxides during the time of Fe-Mn oxide precipitation in the water column, the available surface sites of Fe-Mn oxides should be similar.

Elemental abundance in crust 6RD08-08 from Kiribati are plotted as a function of depth in Figures 6.2 and 6.3. Si and Al decrease from top to bottom (Figures 6.2a, b). Ca and P are relatively constant throughout the top 40 mm of the crust, increase sharply from 40-55 mm, then decrease again toward the base (60 mm) (Figures 6.2c, d). Mn is particularly high between 40 mm and 18 mm, with the exception of one layer near 34 mm (Figure 6.2e). Fe concentrations generally increase from bottom to top, except for a minimum near 40 mm where Fe

is diluted by Mn, and also exhibits a large variability (Figure 6.2f). The Mn/Fe ratio increases from top to bottom, except near 40 mm. The Si/Al ratio is relatively constant, higher than in detrital component (see Figures 6.7 and 6.8), and displays a prominent maximum near 30 mm. Figure 6.3 presents minor element variations as a function of depth. The elements Pt, Cu, Ba and Bi generally decrease from bottom to top of the crust. Ni, Zn and Co variations are consistent with those of Mn. Pb exhibits a pattern intermediate to those of Fe and Si.

Elemental abundance for crust RD50S1B from Hawaii are presented as a function of depth in Figures 6.4 and 6.5. Si and Al covary strongly and are most abundant from 28 mm to 15mm (Figures 6.4a, b). There is a large peak at 21.5 mm for Ca and P (Figures 6.4c, d). Mn is abundant at the bottom and top, but lower concentrations are observed in the middle part of the crust (Figure 6.4e). Fe ranges between 13-18% through most of the crust with the exception of one peak at 28 mm (Figure 6.4f), that correlates with the peak in detrital components Si and Al. The Si/Al ratio is relatively constant except near 8mm (Figure 6.4h), the latter likely represents a non-detrital Si input. Figure 6.5 shows that minor elements Pt, Cu and Ba generally decrease from the bottom of the crust to the top; Ni, Co, Bi and Zn are correlated with Mn trend. Pb is correlated with Co.

Chemical paleotricks are shown in Figures 6.6 and 6.7. These describe the variations of biogenetic and hydrogenetic elemental associations as a function of depth in the crust, and are based on factor analysis and elemental variations throughout the Hawaiian and Kiribati crusts. The sedimentary records of most areas of the Pacific basin show that productivity decreases sharply away from the equatorial zone (Kennett, 1982). The data from this study indicate that this decrease is reflected by the composition between the 31 and 28 mm intervals of crust RD50S1B from Schumann Seamount. Biostratigraphic dating (Cowen et al.,

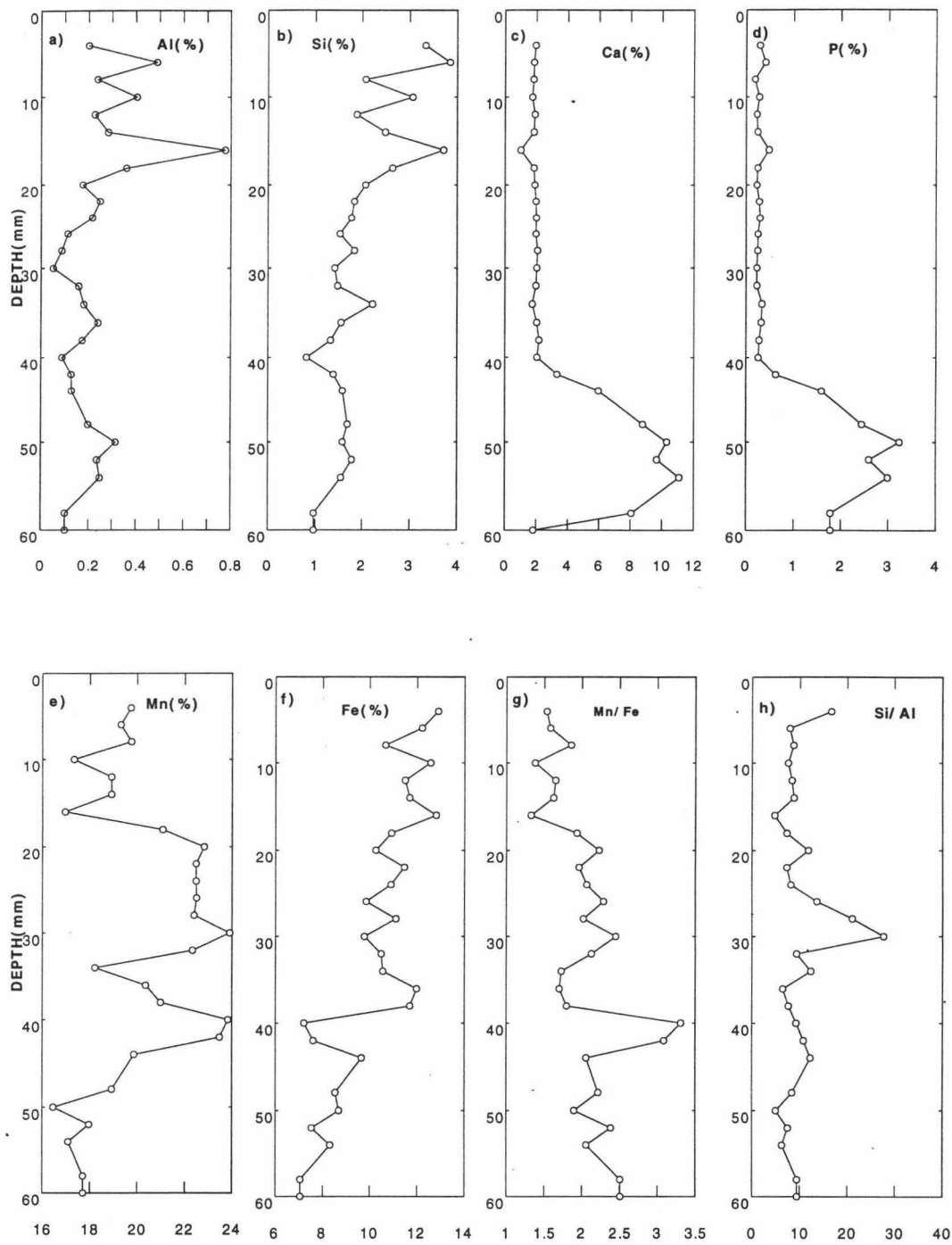


Figure 6.2 Variations of major elements and their ratios as a function of depth in crust from Kiribati (6RD08-08)

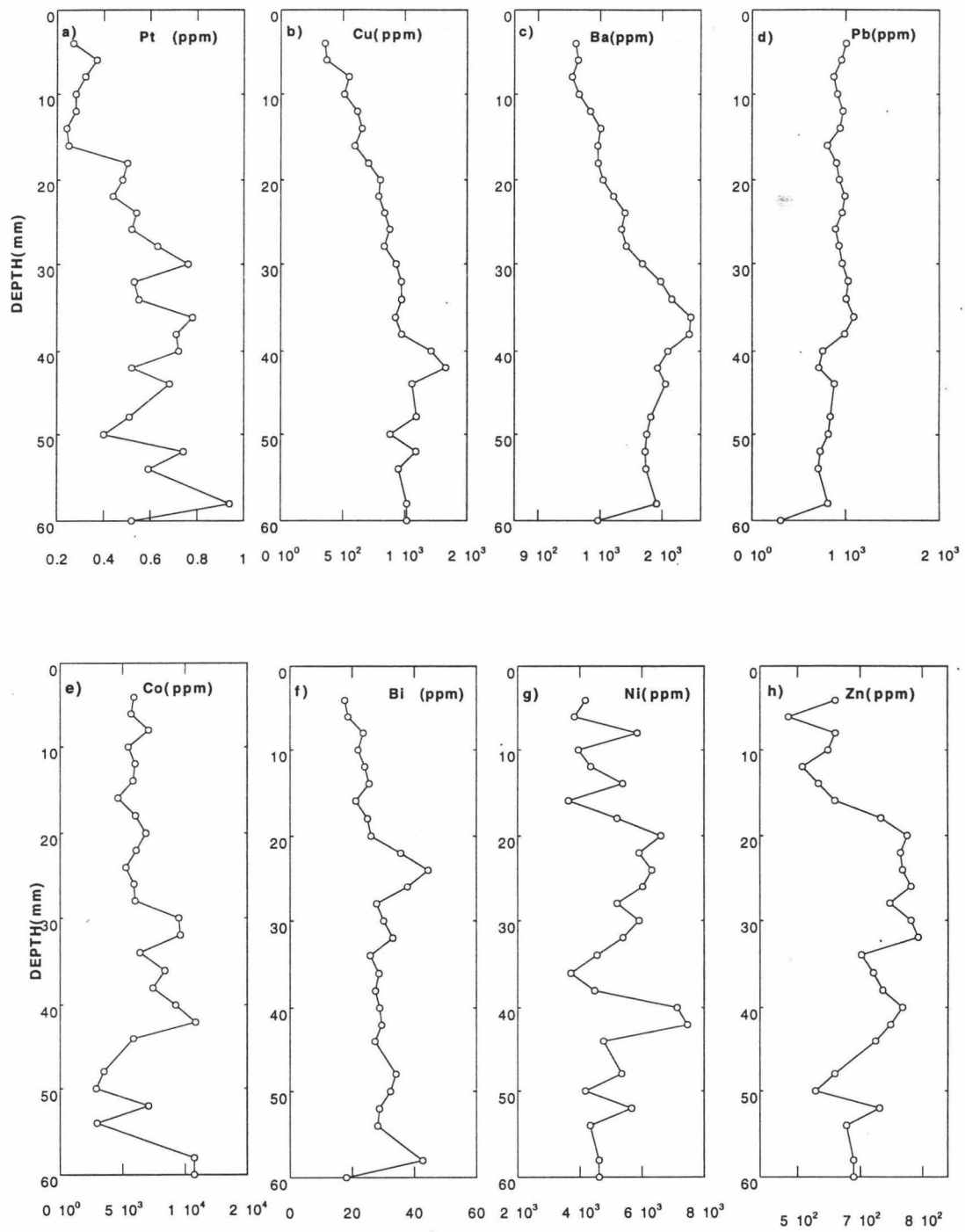


Figure 6.3 Variations of minor elements as a function of depth in crust from Kiribati 6RD08-08

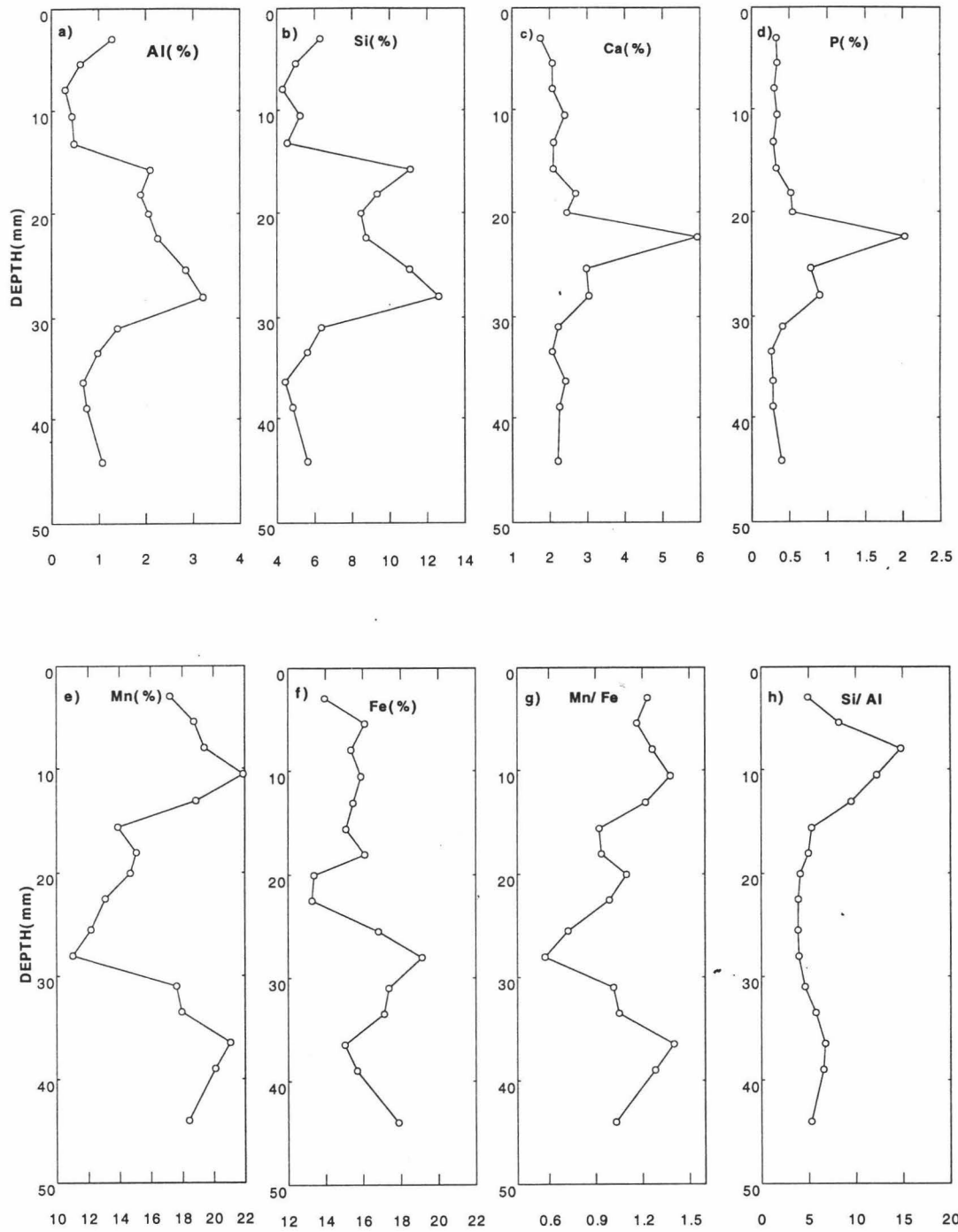


Figure 6.4 Variations of major elements and their ratios as a function of depth in crust from Hawaii (RD50S1B)

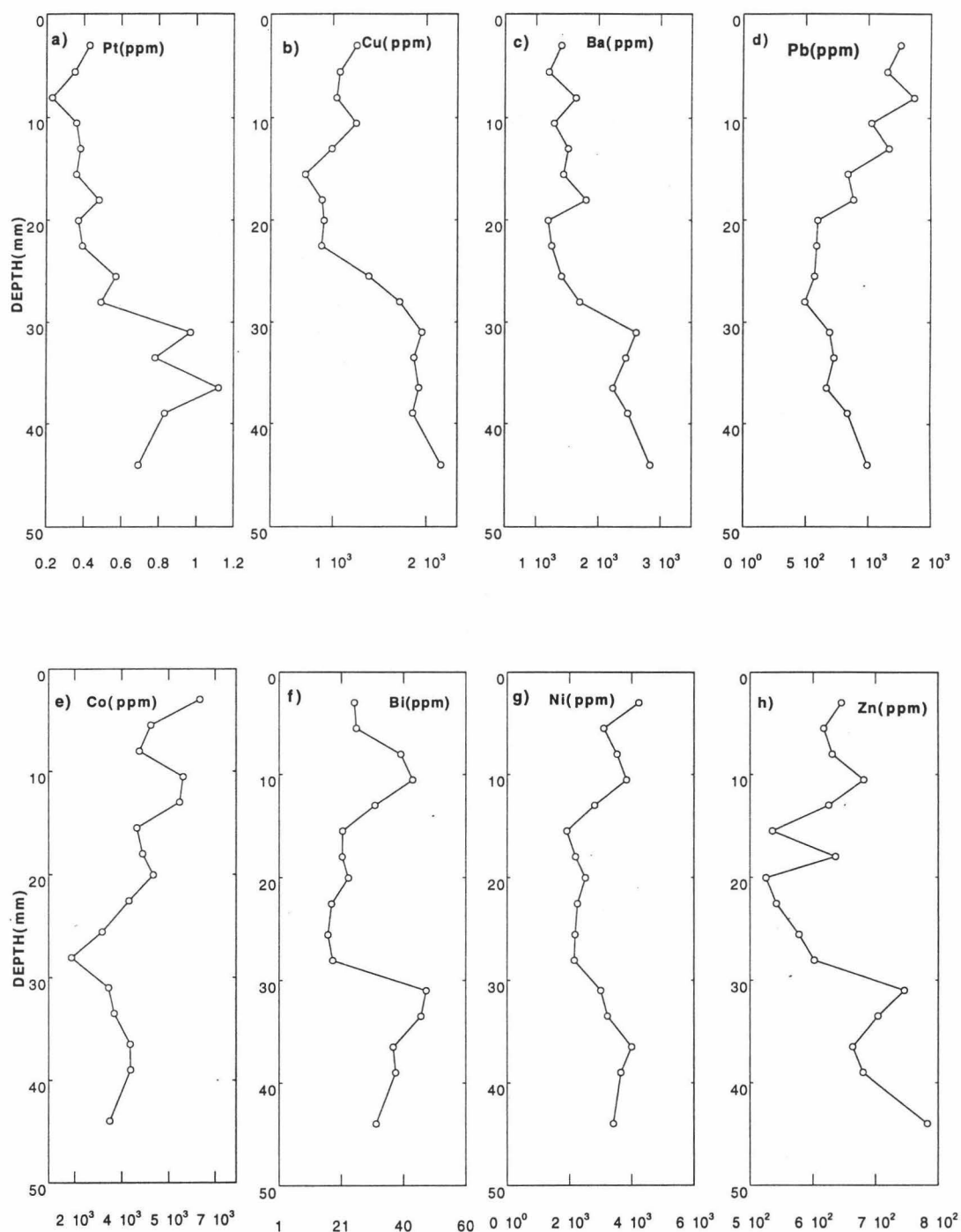


Figure 6.5 Variation of minor elements as a function of depth in crust from Hawaii (RD50S1B)

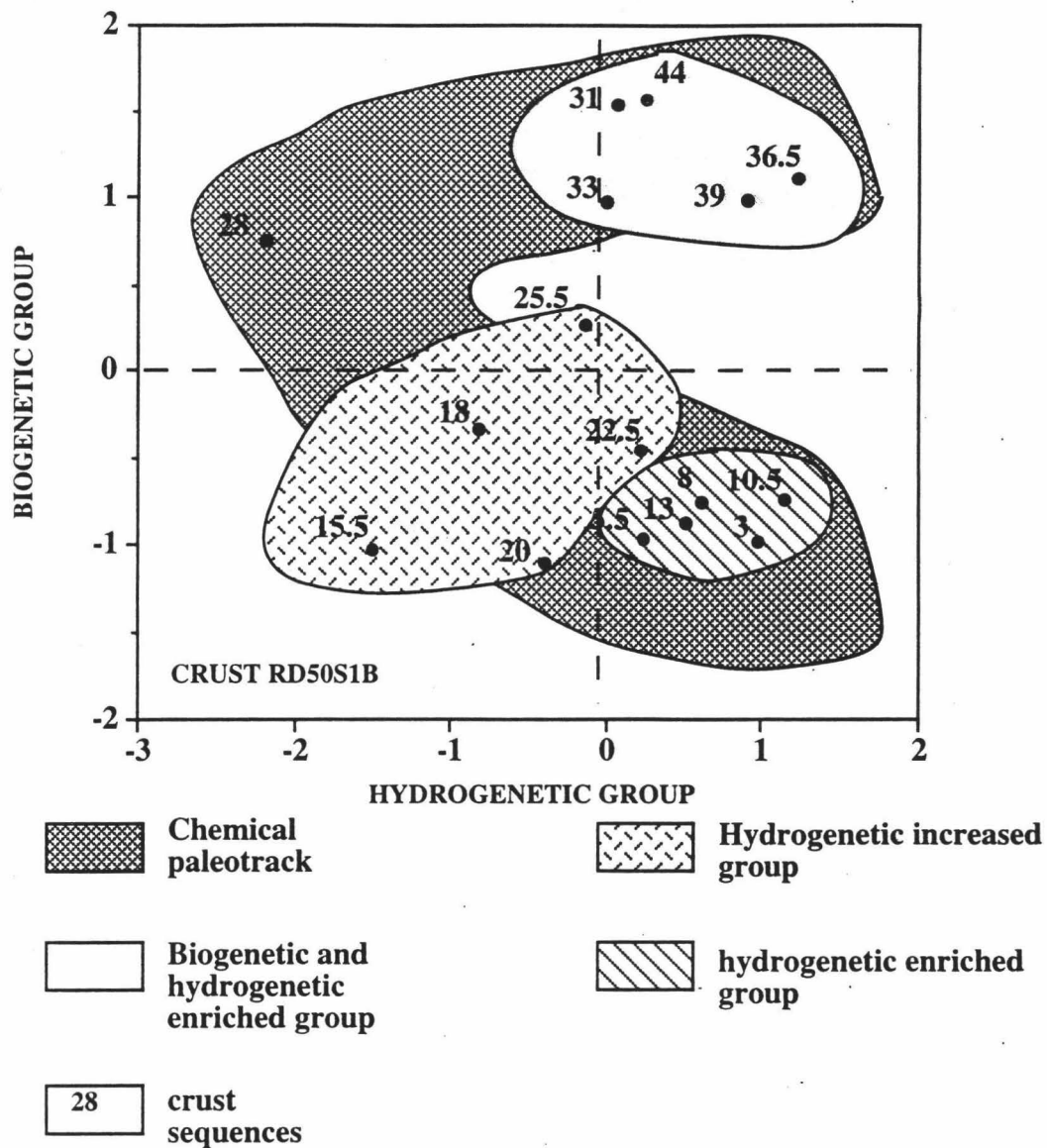


Figure 6.6 Chemical paleotrack of crust RD50S1B from Hawaii. Hydrogenetic group mainly represents elements Mn, Ni, Co and Zn. Biogenetic group elements are referred to Ba, Cu, Pt and Fe.

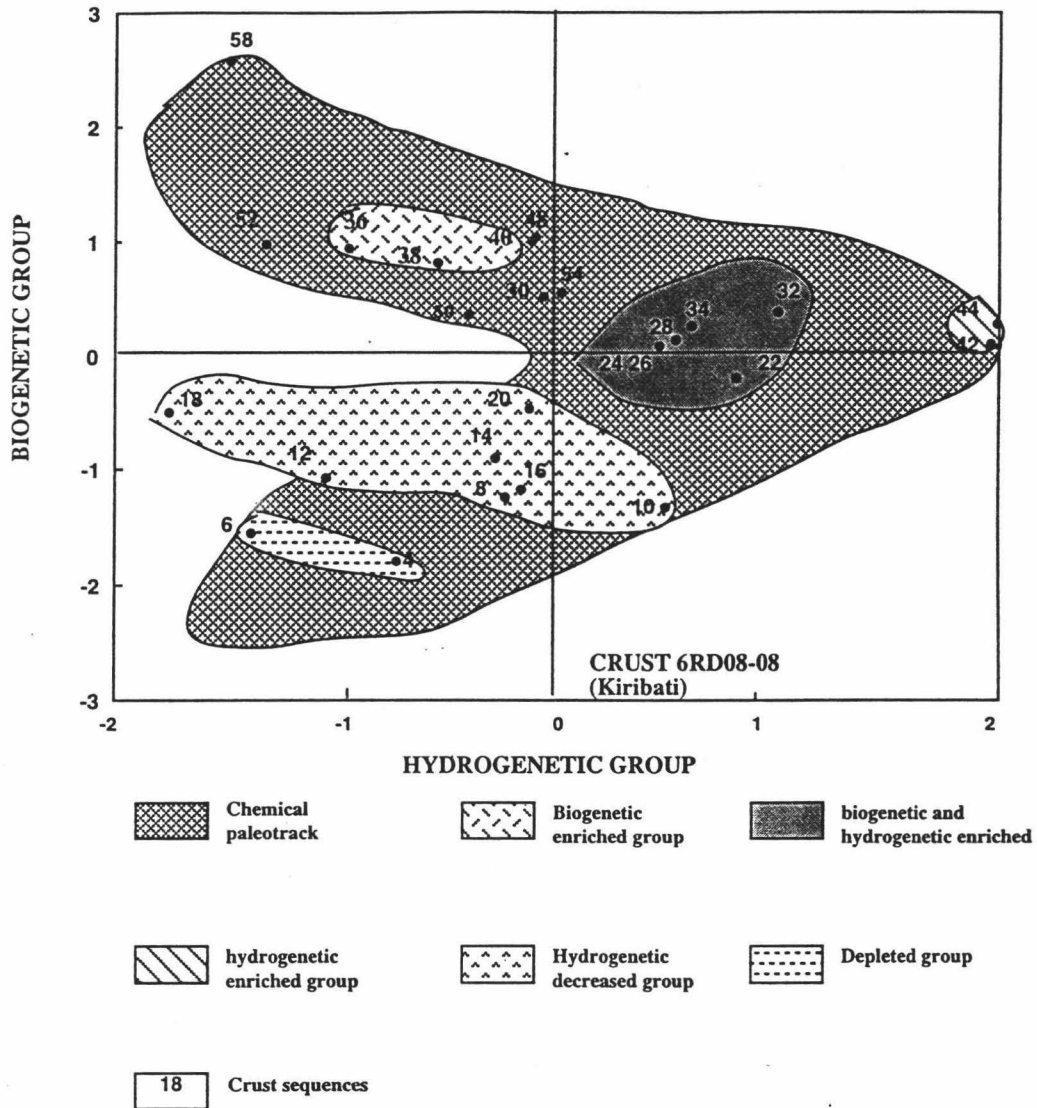


Figure 6.7 Chemical paleotrack of crust 6RD08-08 from Kiribati. Hydrogenetic group is representative of elements Mn, Co, Ni, Zn and Mg. Biogenetic group mainly represents elements Ba, Cu, Pt and Ce.

1993) indicates that the 31 mm interval is at least Eocene in age; approximately the time period when Schumann Seamount is proposed to have crossed the equator (VonderHaar, 1990). There is an internal consistency between the chemical paleotrack proposed here (Figure 6.8), the seamount paleotrack

Seamount Paleotrack

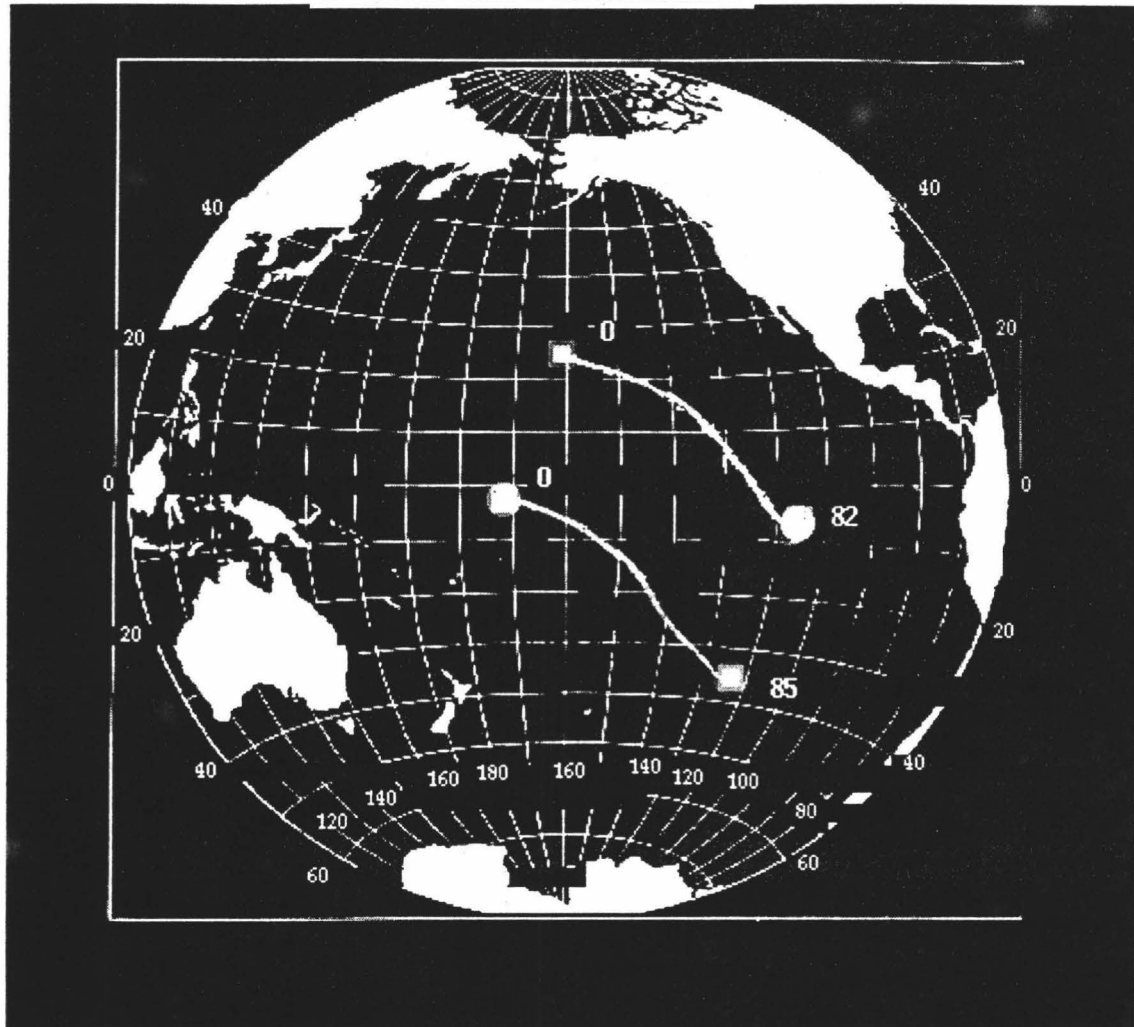


Figure 6.8 Seamount paleotrack. 0-85 Ma represents the McKean seamount crust 6RD08-08 from Kiribati (Yan and Kroenke, 1993), 0-82 Ma represents the Schumann seamount crust RD50S1B from Hawaii (VonderHaar, 1990; McMurtry et al., 1994)

proposed by VonderHaar (1990), and biostratigraphic dating (Cowen et al., 1993). Figure 6.6 also reveals an enrichment of biogenetic and hydrogenetic elements in the bottom part of crust RD50S1B indicating both extensive biological activity and a relatively strong water current regime that led to a slow growth rate. Along the paleotrack represented by the 28 mm interval within the crust, the biogenetic elemental group decreased. This suggests that the seamount on which the crust formed moved away from the equatorial upwelling area. The plot of the chemical paleotrack of crust 6RD08-08 (Figure 6.7) indicates that the biogenetic group elements also decreased from the bottom to the top, but that the hydrogenetic group elements increased from the bottom to the middle then decreased from the middle to the top of the crust. Therefore, the chemical paleotrack of the crust from Kiribati also suggests a move away from high productivity area, which may relate to high upwelling area. But, this high productivity area can not be related the equatorial upwelling zone, because the Kiribati crust 6RD08-08 was recovered south of the equator and the seamount is believed to be moving in North-West to Western (Figure 6-8) (Yan and Kroenke, 1993).

6.3 Rare earth elements as paleoindicators

The rare earth elements (REE), as a group of elements with slightly differing chemical properties across the family can provide unique insight into geochemical processes of the formation of Fe-Mn crusts. The paleotracks of the two seamounts have traversed different regions of Pacific Ocean. Hence, it would be expected that differences in the depositional environments to which these crusts were exposed would be reflected in their composition. For example, as mentioned

above, the crust from the Musicians Seamount spent a significant portion of its early growth history in the equatorial zone of high productivity. Later passage within the tradewind belt, where continental eolian dust is an important source of sediments, led to a greater influence of detrital matter on crust accumulation. The crust from Kiribati, on the other hand, traveled WNW and accumulated near the equatorial zone and experienced a significantly different environment (i.e., a much shallower CCD, Van Andel et al., 1975) during the corresponding time period. Variations in the elemental profiles within both crusts discussed so far lead to the conclusion that conditions controlling the incorporation of the elements into crusts have not remained constant over geologic time.

REE abundances have been previously used to help elucidate modes of crust genesis (Piper, 1974; Aplin, 1984; Fleet, 1984; DeCarlo, 1991; DeCarlo and McMurtry, 1992). Moreover the extent of fractionation between the light (LREE) and heavy (HREE) members of the REE may be useful in interpreting past oceanic conditions (Wen and DeCarlo, 1994). It is known that the fractionation of the REE is influenced by both the conditions in the water column and the composition of the particles that scavenge them from seawater (Cantrell and Byrne, 1987; Byrne and Kim, 1990; Koeppenkastrop and DeCarlo, 1992 1993; DeCarlo and Wen, unpublished results). Cantrell and Byrne (1987) have demonstrated that CO_3^{2-} complexation largely controls the speciation of REE in seawater and greatly influences their availability for scavenging onto surfaces. This causes fractionation upon removal of REE from seawater and results in the well-known HREE-enriched shale-normalized pattern of seawater (De Baar et al., 1985; Piegras and Jacobsen, 1992). The REE patterns in the crust from Kiribati presented earlier clearly show that REE fractionation also exists in ferromanganese crusts.

Figure 6.9 depicts the extent of REE fractionation through a plot of the $(Sm/Yb)_N$ ratio as a function of depth in crust 6RD08-08. Cyclic variations of the $(Sm/Yb)_N$ ratio suggest some important factors that control the REE fractionation changed through geological time. The plots in Figure 6.10 also indicate that there is no simple relationship observed between $(Sm/Yb)_N$ ratio and major elements. On the other hand, cyclic variations of the $(Sm/Yb)_N$ ratio in crust 6RD08-08 as a function of age (Figure 6.11) bear a striking inverse relationship to variations in the CCD (Van Andel et al., 1975), at least over the past 50 my. A similar $(Sm/Yb)_N$ cyclicity has been observed in several other crusts. One of these was recovered from the same seamount (DeCarlo and Pruszkowski, 1992, Wen and DeCarlo, unpublished data, 1994), another from Christmas Island in Indian ocean (Wen and DeCarlo, unpublished data, 1994), one from the Ellice Island chain, and two from

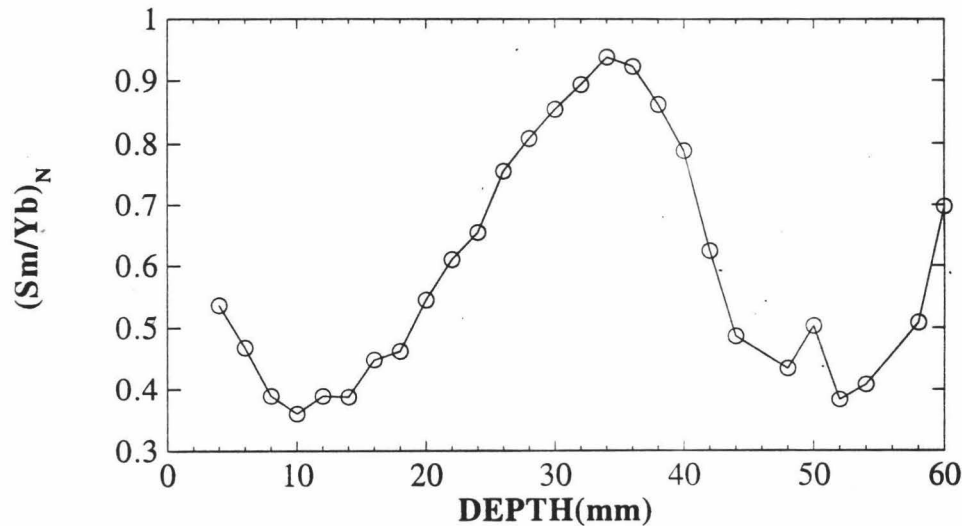


Figure 6.9 Cyclic variations in the shale-normalized $(Sm/Yb)_N$ ratio as a function of depth within crust 6RD08-08 from Kiribati.

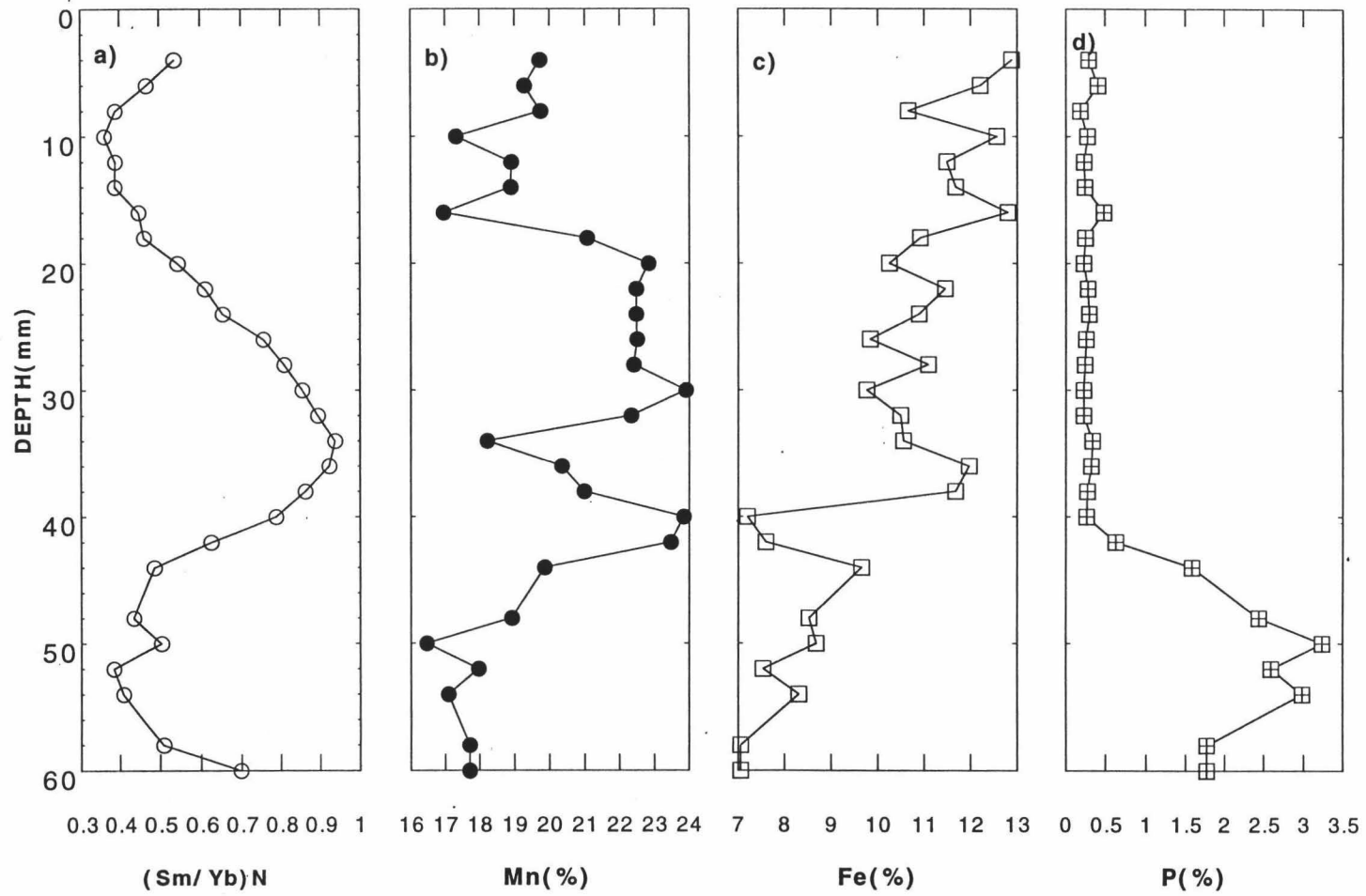


Figure 6.10 Plots of elements and ratio as a function of depth. a) $(Sm/Yb)_N$ vs. depth b) Mn vs. depth c) Fe vs. depth d) P vs. depth

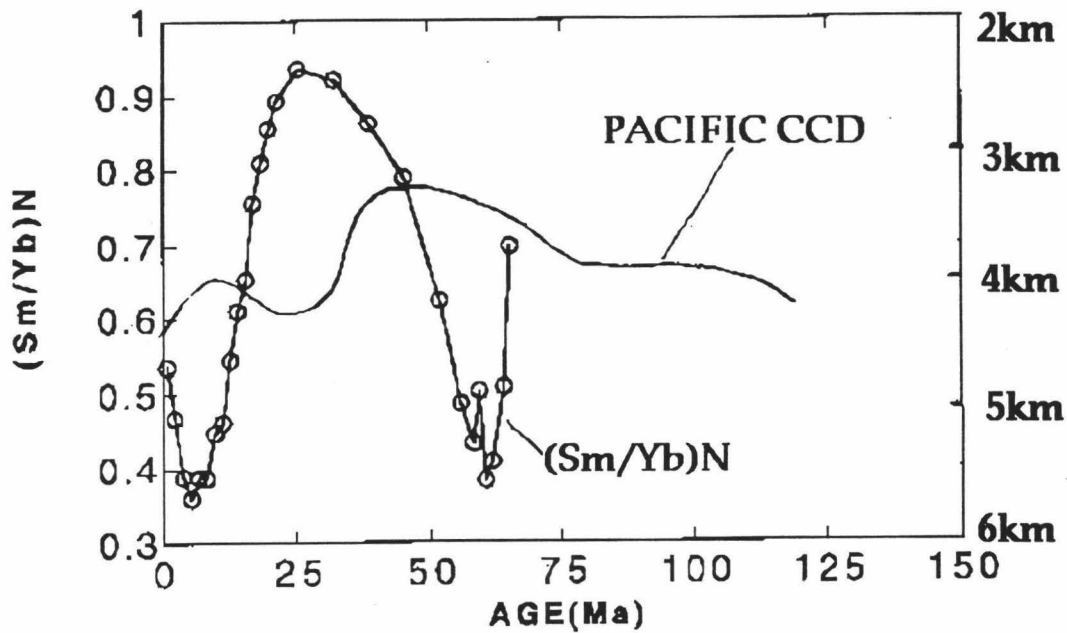


Figure 6.11 Cyclic variations in the shale-normalized $(Sm/Yb)_N$ ratio as a function of age (Cowen and DeCarlo, unpublished data, 1994) within crust 6RD08-08 from Kiribati and the depth of the Pacific Ocean CCD over geological time on the basis of DSDP sediment data (Modified after Van Andel et al., 1975)

the Marshall Islands (McMurtry, unpublished data, 1993). Hence, it is possible that crust 6RD08-08 and others record changes in past climatic conditions in terms of the CO_2 variations in seawater during the Tertiary.

In the Equatorial Pacific Ocean, the depth and shape of the Calcite lysocline appear to have changed significantly in response to climate forcing (Archer, 1991). Farrell and Prell (1989, 1991) also demonstrated that the depth of the calcite lysocline changed significantly in response to glacial/interglacial climate fluctuations. However, how carbonate ion concentrations change in the water column during glacial/interglacial periods still remains unclear. In Figure 6.11, we clearly see a systematic variation in REE fractionation within crust 6RD08-08 as a function of time. Cantrell and Byrne (1987) and Elderfield (1988) showed that rare earth speciation in seawater is dominated by carbonate complexation, and that the proportion of each REE complexed with carbonate increases with increasing atomic number. Hence the proportion of the free REE ion decreases with increasing atomic number. This is important when the ability of the REE to adsorb onto particle surfaces is considered. On the basis of theory and our observation, I hypothesize that a large value of the $(\text{Sm}/\text{Yb})_N$ ratio in crusts reflects a lower concentration of CO_3^{2-} in seawater. According to the following chemical equilibrium reaction in seawater, when CO_2 increases, CO_3^{2-} decreases.



The relationship between carbonate ion and carbon dioxide imply that relatively low concentrations of carbonate ion in seawater are a response to relatively high CO_2 in seawater. The relatively high CO_2 will deepen the lysocline and CCD level if the lysocline and CCD generally covary.

Cerium exists in the oceanic environment either in the soluble trivalent state or as the highly insoluble CeO_2 ; the latter occurs primarily under

highly oxidizing conditions (Henderson, 1984). The Ce anomaly has been previously proposed as a potentially useful tool to deduce paleoredox conditions (Glasby et al., 1987; Wright et al., 1987; Elderfield, 1988; DeCarlo, 1991). Recent evidence, however, indicates that Ce anomalies can also be influenced by biological factors (Moffett, 1990; Wen and DeCarlo, 1994). The Ce anomalies (Figures 6.12 and 6.13) in crust RD50S1B from Schumann Seamount and in crust 6RD08-08 from Kiribati reveal a contrasting behavior of this parameter based on results of factor analysis. In crust RD50S1B the Ce anomaly appears to be a good redox indicator that is highly correlated with MnO₂ as previously reported by DeCarlo (1991), whereas in crust 6RD08-08 from Kiribati the Ce anomaly is not strongly correlated with the MnO₂ phase. Rather it is strongly correlated with Ba, Cu and Pt, thereby falling in the biogenetic group. Hence it is possible that Ce anomalies may be better suited as an indicator of local environmental conditions rather than for the interpretation of basin-wide conditions.

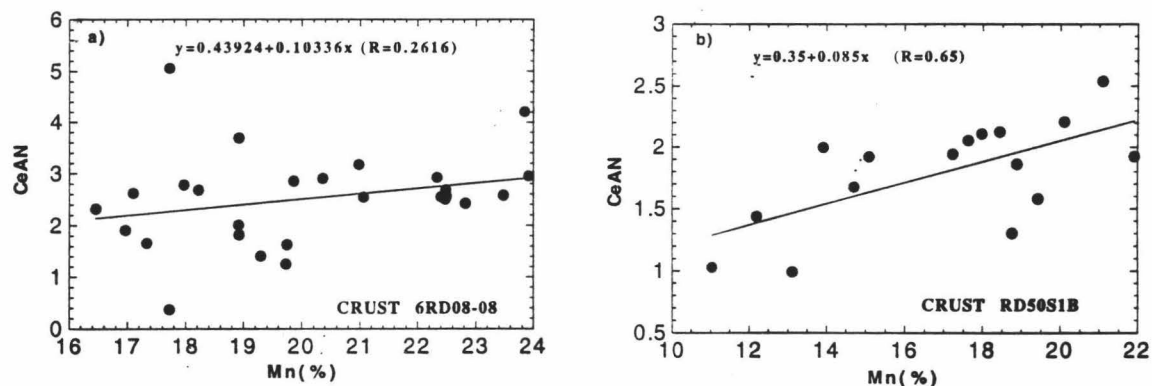


Figure 6.12 Mn vs. CeAN. a) Crust 6RD08-08 from Kiribati. b) Crust RD50S1B from Hawaii

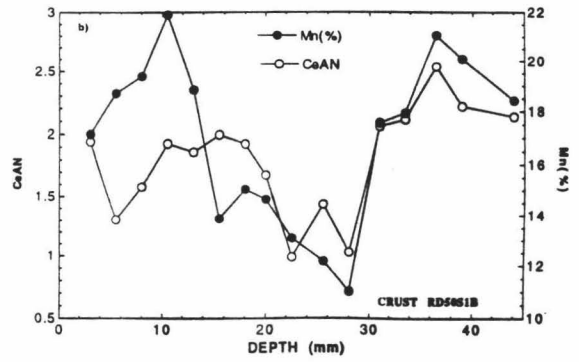
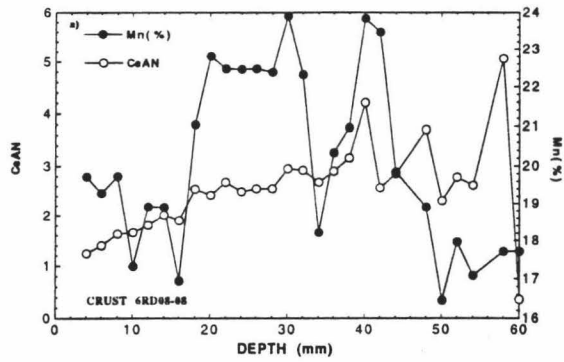


Figure 6.13 Mn and CeAN as a function of depth. a) Crust 6RD08-08 from Kiribati. b) Crust RD50S1B from Hawaii

CHAPTER 7

CONCLUSIONS

1. Examination of internal structures and elemental distributions allowed inferences to be made regarding conditions under which crusts accumulated. Botryoidal and columnar layers appear to have accumulated during conditions of intensified water flow and are characterized by slow deposition. Mottled and compact layers, in contrast, are representative of crust accretion during calm water conditions which lead to more rapid accumulation rates and a greater incorporation of detrital elements. There is no significant relationship between internal structure and the concentration of hydrogenetic elements (Mn, Co, Ni).

2. A strong covariance was observed between the inverse distribution coefficient ($\log C_{sw}/C_{mn}$) and the mean residence time (τ) of elements in seawater. These associations exemplify how the chemistry of oceanic water and crusts are intimately related. This study revealed that crusts experienced several changes in oceanic current regimes over geologic time, although these changes do not strongly influence biogenetically related elements. The concentrations of REE and of other elements (most of which have residence time less than oceanic mixing time) indicate that the geochemistry of crust is highly dependent on local environments and that regional seawater chemistry plays a more important role in elemental distribution than previously thought.

3. Results of factor analysis indicate that the chemical composition of crusts in general can be characterized by assigning the elements to four major genetic groups. These are inferred to represent a hydrogenetic group (Mn, Ni, Co, Zn, Cu, Ce, CeAN), a biogenetic group (Ba, Zn, Cu, Pt, Fe, CeAN), a detrital group (Si, Al, Fe) and a carbonate fluorapatite group (Ca, P, REEs). The latter group includes

the REE likely due to statistical forcing. The hydrogenetic and detrital groups display the expected strong inverse correlation, whereas the biogenetic elements exhibit environment dependence. Results of a comparative study of major elemental associations among different crusts suggest that hydrogenetic Fe-Mn crusts have experienced almost no post-depositional diagenesis or remobilization of elements after they initially formed.

4. There is high internal consistency between the chemical paleotrack proposed here, the seamount paleotrack proposed by VonderHaar (1990), and biostratigraphic dating results (Cowen et al., 1993) in a crust from Hawaii.

5. Rare earth elements appear to have potential as paleoindicators. The cyclic variations of the $(\text{Sm}/\text{Yb})_N$ ratio (a measure of REE fractionation) as a function of depth in the crust, when combined with biostratigraphic data (Cowen et al., 1993), may be useful in inferring carbonate variations in seawater through geologic time.

7.1 Future research

Further experimental work and field research are needed to test hypotheses and answer questions that arose from this study. First, an important hypothesis derived from this study is that the cyclic variations of $(\text{Sm}/\text{Yb})_N$ as a function of depth within the Fe-Mn crust from Kiribati are inversely correlated with fluctuations of CCD through geological time. It has been previously shown that the fractionation of LREE and HREE in crust can be attributed to the variations in carbonate ion concentration in seawater. Thus, in order to test this hypothesis, experiments should be conducted to investigate the sorption of REE onto metal oxide phases as a function carbonate concentration in solution. The thermodynamic modeling program FITEQL 3 (Herbelin and Westall, 1994) can be

used to model results of such experiments. This would produce quantitative results as to how changes in carbonate ion in solution affect REE fractionation during uptake onto either αFeOOH or δMnO_2 surfaces. This work would also help to reconstruct the relationship between carbonate ion in solution and variations of Sm/Yb on the surface of natural metal oxides. The relationship between CO_3^{2-} and Sm/Yb will be used as a model for an observational study designed to evaluate changes of carbonate ion concentration over geological time by examining the variations of Sm/Yb as a function of age in Fe-Mn crusts. Fe-Mn crusts from different areas need to be examined in order to determine whether the cyclic variations of $(\text{Sm}/\text{Yb})_N$ within crusts are a common phenomenon. Because of an excellent chronological record in carbonate sediments (CCD is highly constrained temporally), it is possible that the inverse correlation between CCD and REE fractionation can also be used to date crusts.

Ce anomalies in crusts are attributed to oxidative scavenging of Ce by δMnO_2 . However, this study also indicates that cerium concentrations can be controlled in part by biological activity. According to molecular orbital theory, cerium (Ce^{3+}) is very similar to iron (Fe^{2+}); both are high spin species that lose one electron from a π orbital upon oxidation. This intuitively implies that cerium should be oxidized in the seawater column and not only at the surface of δMnO_2 . Hence, the occurrence of CeO_2 may be either hydrogenetically or biologically related in natural Fe-Mn deposits. Experiments with Ce^{3+} can be conducted as function of pH and time. Similar experiments also can be conducted under similar conditions as described above, except in the absence of oxygen in the solution or in the presence of δMnO_2 particles. These will help elucidate whether dissolved O_2 is involved in the oxidation of Ce^{3+} in seawater or whether the catalytic

properties of δMnO_2 are need to effect the oxidation of Ce^{3+} in the marine environment.

In order to complete the above proposed research, the individual sorptive properties of αFeOOH , HFO and δMnO_2 should also be further investigated through batch experiments. Previous experiments (Koeppenkastrop and DeCarlo, 1992, 1993) indicated that αFeOOH and HFO play a key role in controlling the distribution of REE in Fe-Mn deposits and seawater. This hypothesis is only based on the results of experiments conducted with single pure phases (αFeOOH , HFO and δMnO_2). It is believed (Honeyman et al., 1988) that when two phases coexist the interaction with various dissolved species in seawater will be quite different from the results obtained with single phases. Therefore, an experiment designed to investigate competitive sorption using these two mineral phases to simulate natural Fe-Mn oxides should also be conducted.

APPENDIX A

Appendix A. Elemental Abundance (%) of Microprobe Data for Crust 6RD08-08 from Kiribati

| DEPTH (mm) | Na(%) | Mg(%) | Al(%) | Si(%) | S(%) | P(%) | K(%) | Ca(%) | Cl(%) |
|---------------|-------|-------|-------|-------|------|------|------|-------|-------|
| 6.00 | 0.83 | 1.11 | 0.49 | 3.31 | 0.34 | 0.71 | 0.30 | 2.39 | 0.42 |
| 6.48 | 1.05 | 1.14 | 0.43 | 3.06 | 0.37 | 0.67 | 0.31 | 2.56 | 0.41 |
| 6.98 | 0.88 | 1.15 | 0.47 | 2.95 | 0.34 | 0.66 | 0.32 | 2.49 | 0.40 |
| 7.52 | 0.99 | 1.07 | 0.65 | 3.74 | 0.32 | 0.57 | 0.38 | 2.29 | 0.42 |
| 8.07 | 0.76 | 1.11 | 0.43 | 2.90 | 0.39 | 0.57 | 0.36 | 2.45 | 0.30 |
| 8.55 | 0.83 | 0.88 | 0.50 | 2.25 | 0.32 | 0.54 | 0.34 | 2.16 | 0.36 |
| 9.05 | 1.11 | 1.14 | 0.43 | 3.13 | 0.38 | 0.56 | 0.38 | 2.63 | 0.35 |
| 9.53 | 1.24 | 1.13 | 0.30 | 2.24 | 0.36 | 0.45 | 0.45 | 2.68 | 0.39 |
| 10.07 | 1.06 | 1.25 | 0.17 | 1.84 | 0.29 | 0.45 | 0.45 | 2.46 | 0.46 |
| 10.56 | 0.93 | 0.81 | 0.36 | 3.06 | 0.33 | 0.51 | 0.32 | 2.13 | 0.48 |
| 11.06 | 1.26 | 1.14 | 0.25 | 2.15 | 0.33 | 0.39 | 0.42 | 2.37 | 0.55 |
| 11.66 | 1.26 | 1.26 | 0.31 | 2.30 | 0.47 | 0.64 | 0.43 | 2.97 | 0.55 |
| 12.14 | 0.98 | 1.04 | 0.31 | 2.32 | 0.37 | 0.53 | 0.40 | 2.64 | 0.45 |
| 12.64 | 1.15 | 1.14 | 0.24 | 2.31 | 0.43 | 0.47 | 0.44 | 2.68 | 0.44 |
| 13.18 | 0.90 | 1.15 | 0.33 | 2.51 | 0.36 | 0.54 | 0.38 | 2.66 | 0.40 |
| 13.62 | 1.39 | 1.23 | 0.19 | 1.97 | 0.39 | 0.44 | 0.42 | 2.74 | 0.37 |
| 14.10 | 1.28 | 1.11 | 0.38 | 2.50 | 0.38 | 0.50 | 0.42 | 2.65 | 0.55 |
| 14.60 | 0.91 | 0.97 | 0.28 | 2.28 | 0.32 | 0.45 | 0.37 | 2.42 | 0.51 |
| 15.10 | 1.31 | 1.07 | 0.32 | 2.62 | 0.39 | 0.56 | 0.41 | 2.61 | 0.46 |
| 15.63 | 1.14 | 1.08 | 0.31 | 2.15 | 0.42 | 0.50 | 0.37 | 2.65 | 0.53 |
| 16.11 | 1.23 | 1.43 | 0.18 | 2.39 | 0.35 | 0.62 | 0.52 | 2.57 | 0.45 |
| 16.66 | 0.89 | 1.05 | 0.28 | 2.50 | 0.36 | 0.53 | 0.38 | 2.59 | 0.41 |
| 17.18 | 1.33 | 1.49 | 0.19 | 1.37 | 0.39 | 0.34 | 0.64 | 2.56 | 0.46 |
| 17.62 | 1.07 | 1.34 | 0.14 | 2.28 | 0.40 | 0.49 | 0.49 | 2.56 | 0.41 |
| 18.26 | 1.19 | 1.59 | 0.15 | 1.51 | 0.40 | 0.48 | 0.58 | 2.59 | 0.49 |
| 18.81 | 1.40 | 1.48 | 0.14 | 1.37 | 0.44 | 0.36 | 0.58 | 2.70 | 0.69 |
| 19.28 | 1.17 | 1.52 | 0.16 | 1.40 | 0.31 | 0.32 | 0.54 | 2.39 | 0.51 |
| 19.77 | 1.17 | 1.30 | 0.16 | 1.08 | 0.36 | 0.27 | 0.47 | 2.50 | 0.78 |
| 20.37 | 1.29 | 1.46 | 0.15 | 1.49 | 0.40 | 0.33 | 0.50 | 2.49 | 0.78 |
| 20.85 | 1.56 | 1.33 | 0.17 | 1.93 | 0.40 | 0.50 | 0.45 | 2.75 | 0.51 |
| 21.40 | 1.08 | 1.80 | 0.21 | 1.17 | 0.34 | 0.18 | 0.70 | 2.48 | 0.39 |
| 22.02 | 1.03 | 1.52 | 0.17 | 1.83 | 0.37 | 0.34 | 0.49 | 2.36 | 0.51 |
| 22.39 | 1.14 | 1.59 | 0.15 | 1.36 | 0.39 | 0.38 | 0.54 | 2.62 | 0.55 |
| 22.90 | 1.29 | 1.47 | 0.13 | 1.04 | 0.35 | 0.29 | 0.54 | 2.39 | 0.56 |
| 23.43 | 1.13 | 1.37 | 0.14 | 1.28 | 0.40 | 0.37 | 0.56 | 2.62 | 0.61 |

Appendix A. (Continued) Elemental Abundance (%) of Microprobe Data for Crust 6RD08-08 from Kiribati

| DEPTH (mm) | Na(%) | Mg(%) | Al(%) | Si(%) | S(%) | P(%) | K(%) | Ca(%) | Cl(%) |
|---------------|-------|-------|-------|-------|------|------|------|-------|-------|
| 23.87 | 0.91 | 1.44 | 0.14 | 1.53 | 0.41 | 0.35 | 0.53 | 2.69 | 0.64 |
| 24.32 | 1.12 | 1.40 | 0.17 | 2.08 | 0.37 | 0.41 | 0.46 | 2.56 | 0.62 |
| 24.89 | 0.94 | 1.51 | 0.12 | 1.36 | 0.29 | 0.27 | 0.57 | 2.48 | 0.53 |
| 25.43 | 1.03 | 1.55 | 0.17 | 1.37 | 0.31 | 0.39 | 0.55 | 2.47 | 0.45 |
| 25.90 | 1.03 | 1.16 | 0.31 | 1.91 | 0.40 | 0.42 | 0.36 | 2.61 | 0.62 |
| 26.41 | 0.72 | 0.77 | 0.21 | 1.71 | 0.30 | 0.36 | 0.26 | 2.00 | 0.66 |
| 26.90 | 0.78 | 1.05 | 0.23 | 2.16 | 0.41 | 0.54 | 0.33 | 2.63 | 0.54 |
| 27.41 | 0.96 | 1.06 | 0.27 | 2.04 | 0.37 | 0.44 | 0.38 | 2.62 | 0.64 |
| 27.89 | 0.98 | 1.12 | 0.17 | 1.68 | 0.42 | 0.45 | 0.40 | 2.92 | 0.48 |
| 28.30 | 1.01 | 1.06 | 0.14 | 1.60 | 0.37 | 0.40 | 0.38 | 2.71 | 0.45 |
| 28.90 | 1.16 | 1.10 | 0.21 | 2.33 | 0.40 | 0.51 | 0.43 | 2.84 | 0.39 |
| 29.50 | 1.14 | 1.06 | 0.19 | 2.07 | 0.37 | 0.34 | 0.42 | 2.68 | 0.69 |
| 30.01 | 1.25 | 1.13 | 0.24 | 2.44 | 0.37 | 0.45 | 0.37 | 2.80 | 0.44 |
| 30.39 | 1.16 | 0.91 | 0.19 | 2.54 | 0.42 | 0.52 | 0.38 | 2.67 | 0.47 |
| 31.03 | 1.51 | 1.16 | 0.19 | 1.91 | 0.32 | 0.32 | 0.48 | 2.84 | 0.54 |
| 31.50 | 1.20 | 1.10 | 0.20 | 1.96 | 0.37 | 0.43 | 0.47 | 2.73 | 0.54 |
| 31.98 | 1.24 | 1.06 | 0.22 | 2.16 | 0.41 | 0.43 | 0.42 | 2.78 | 0.47 |
| 32.51 | 0.93 | 1.13 | 0.23 | 2.03 | 0.37 | 0.40 | 0.37 | 2.77 | 0.61 |
| 32.94 | 1.20 | 1.15 | 0.36 | 2.31 | 0.43 | 0.45 | 0.41 | 2.73 | 0.63 |
| 33.55 | 1.25 | 1.22 | 0.17 | 1.27 | 0.33 | 0.30 | 0.50 | 2.63 | 0.65 |
| 34.00 | 1.16 | 1.12 | 0.26 | 2.80 | 0.37 | 0.43 | 0.45 | 2.69 | 0.44 |
| 34.29 | 1.36 | 1.35 | 0.17 | 1.24 | 0.33 | 0.33 | 0.59 | 2.75 | 0.55 |
| 34.74 | 1.53 | 1.11 | 0.14 | 1.07 | 0.33 | 0.32 | 0.53 | 2.57 | 0.65 |
| 35.16 | 1.07 | 1.26 | 0.21 | 1.03 | 0.31 | 0.28 | 0.48 | 2.10 | 0.99 |
| 35.58 | 0.99 | 0.97 | 0.15 | 0.93 | 0.29 | 0.30 | 0.34 | 2.22 | 0.91 |
| 36.08 | 1.11 | 1.13 | 0.28 | 1.85 | 0.44 | 0.40 | 0.36 | 2.88 | 0.50 |
| 37.06 | 1.06 | 1.14 | 0.25 | 2.61 | 0.42 | 0.43 | 0.37 | 2.85 | 0.50 |
| 37.49 | 1.30 | 1.05 | 0.21 | 1.99 | 0.46 | 0.31 | 0.42 | 2.84 | 0.52 |
| 38.16 | 1.01 | 1.26 | 0.18 | 0.99 | 0.32 | 0.29 | 0.47 | 2.58 | 0.76 |
| 38.52 | 1.48 | 1.39 | 0.20 | 1.67 | 0.42 | 0.56 | 0.57 | 2.94 | 0.56 |
| 39.11 | 1.21 | 1.35 | 0.25 | 1.17 | 0.35 | 0.27 | 0.53 | 2.48 | 0.59 |
| 39.62 | 1.48 | 1.58 | 0.20 | 1.14 | 0.38 | 0.27 | 0.65 | 2.40 | 0.51 |
| 40.65 | 1.25 | 1.52 | 0.26 | 1.19 | 0.43 | 0.43 | 0.58 | 2.74 | 0.58 |
| 41.09 | 1.49 | 1.36 | 0.23 | 1.53 | 0.46 | 0.91 | 0.56 | 3.67 | 0.56 |
| 41.70 | 1.25 | 1.39 | 0.22 | 1.24 | 0.44 | 0.74 | 0.55 | 3.52 | 0.61 |
| 42.14 | 1.35 | 1.34 | 0.21 | 1.12 | 0.43 | 0.79 | 0.50 | 3.76 | 0.57 |

Appendix A. (Continued) Elemental Abundance (%) of Microprobe Data for Crust 6RD08-08 from Kiribati

| DEPTH (mm) | Na(%) | Mg(%) | Al(%) | Si(%) | S(%) | P(%) | K(%) | Ca(%) | Cl(%) |
|---------------|-------|-------|-------|-------|------|-------|------|-------|-------|
| 42.62 | 1.08 | 1.45 | 0.24 | 2.10 | 0.44 | 0.87 | 0.53 | 3.71 | 0.46 |
| 43.19 | 1.01 | 1.11 | 0.20 | 1.73 | 0.50 | 1.82 | 0.41 | 5.88 | 0.55 |
| 43.71 | 1.14 | 1.03 | 0.17 | 1.32 | 0.48 | 3.19 | 0.43 | 8.53 | 0.46 |
| 44.19 | 1.13 | 0.98 | 0.21 | 1.25 | 0.56 | 3.71 | 0.40 | 9.40 | 0.51 |
| 44.69 | 1.00 | 1.10 | 0.18 | 1.21 | 0.44 | 3.02 | 0.42 | 8.20 | 0.44 |
| 45.20 | 1.38 | 1.06 | 0.27 | 1.54 | 0.44 | 0.88 | 0.51 | 4.01 | 0.63 |
| 48.02 | 1.38 | 1.26 | 0.19 | 1.29 | 0.39 | 1.01 | 0.57 | 4.22 | 0.48 |
| 48.51 | 0.41 | 0.97 | 0.13 | 1.12 | 0.45 | 2.40 | 0.34 | 6.74 | 0.48 |
| 49.11 | 0.40 | 1.03 | 0.18 | 1.23 | 0.49 | 1.94 | 0.45 | 6.18 | 0.42 |
| 49.59 | 0.54 | 1.14 | 0.14 | 0.76 | 0.57 | 4.36 | 0.41 | 11.00 | 0.42 |
| 50.13 | 0.56 | 0.93 | 0.14 | 1.27 | 0.48 | 2.44 | 0.40 | 7.22 | 0.52 |
| 50.65 | 0.59 | 0.88 | 0.18 | 1.27 | 0.50 | 3.51 | 0.34 | 9.84 | 0.43 |
| 51.20 | 0.66 | 1.19 | 0.24 | 1.31 | 0.45 | 0.72 | 0.51 | 4.09 | 0.59 |
| 51.70 | 0.74 | 1.20 | 0.17 | 1.08 | 0.43 | 1.76 | 0.52 | 5.94 | 0.53 |
| 52.20 | 0.53 | 1.11 | 0.15 | 0.80 | 0.50 | 4.41 | 0.42 | 11.20 | 0.53 |
| 52.70 | 0.48 | 1.41 | 0.18 | 0.73 | 0.41 | 3.02 | 0.55 | 7.96 | 0.48 |
| 53.25 | 0.68 | 1.11 | 0.20 | 1.01 | 0.51 | 3.15 | 0.40 | 8.71 | 0.42 |
| 53.71 | 0.68 | 0.85 | 0.60 | 2.68 | 0.44 | 2.87 | 0.51 | 7.42 | 0.55 |
| 54.18 | 0.77 | 1.01 | 0.15 | 0.69 | 0.55 | 4.75 | 0.47 | 11.70 | 0.40 |
| 54.77 | 0.99 | 1.18 | 0.19 | 0.97 | 0.46 | 2.32 | 0.47 | 7.08 | 0.58 |
| 55.18 | 0.92 | 1.05 | 0.79 | 2.82 | 0.39 | 1.28 | 0.51 | 4.59 | 0.68 |
| 55.59 | 1.17 | 0.99 | 0.20 | 1.20 | 0.47 | 2.10 | 0.52 | 6.81 | 0.65 |
| 56.18 | 0.88 | 0.94 | 0.32 | 1.24 | 0.46 | 2.47 | 0.38 | 7.00 | 0.72 |
| 56.79 | 0.79 | 1.11 | 1.09 | 3.56 | 0.46 | 3.31 | 0.60 | 7.67 | 0.50 |
| 57.32 | 1.03 | 1.14 | 0.26 | 1.67 | 0.43 | 1.36 | 0.47 | 5.12 | 0.65 |
| 57.85 | 0.80 | 0.96 | 0.40 | 1.97 | 0.50 | 2.11 | 0.50 | 6.24 | 0.61 |
| 58.33 | 0.97 | 1.06 | 0.20 | 1.51 | 0.44 | 1.09 | 0.43 | 4.75 | 0.73 |
| 58.71 | 1.03 | 0.97 | 0.14 | 1.25 | 0.47 | 1.28 | 0.44 | 5.15 | 0.51 |
| 59.34 | 1.02 | 1.16 | 0.18 | 1.20 | 0.42 | 1.55 | 0.47 | 5.74 | 0.61 |
| 59.77 | 0.78 | 0.85 | 0.74 | 2.37 | 0.60 | 7.09 | 0.48 | 16.10 | 0.33 |
| 60.30 | 0.64 | 0.77 | 0.93 | 3.25 | 0.71 | 11.20 | 0.54 | 23.90 | 0.18 |
| 60.84 | 0.71 | 1.01 | 0.14 | 1.24 | 0.45 | 2.28 | 0.41 | 7.06 | 0.52 |
| 61.32 | 0.92 | 1.11 | 0.25 | 1.56 | 0.45 | 1.00 | 0.47 | 4.42 | 0.55 |
| 61.77 | 0.64 | 1.11 | 0.15 | 1.07 | 0.43 | 1.28 | 0.51 | 5.09 | 0.46 |
| 62.27 | 0.77 | 0.97 | 0.10 | 1.02 | 0.46 | 2.71 | 0.39 | 8.04 | 0.51 |
| 62.74 | 1.14 | 1.09 | 0.14 | 1.07 | 0.48 | 2.58 | 0.41 | 7.45 | 0.59 |

Appendix A. (Continued) Elemental Abundance (%) of Microprobe Data for Crust 6RD08-08 from Kiribati

| DEPTH (MM) | Ti(%) | V(%) | Fe(%) | Mn(%) | Ni(%) | Cu(%) | Zn(%) | Ba(%) | Sr(%) | Pb(%) |
|------------|-------|------|-------|-------|-------|-------|-------|-------|-------|-------|
| 6.00 | 1.10 | 0.04 | 21.00 | 24.40 | 0.61 | 0.10 | 0.00 | 0.20 | 0.18 | 0.27 |
| 6.48 | 1.10 | 0.07 | 21.20 | 24.60 | 0.65 | 0.08 | 0.08 | 0.26 | 0.33 | 0.17 |
| 6.98 | 1.05 | 0.04 | 20.40 | 25.00 | 0.78 | 0.08 | 0.00 | 0.23 | 0.25 | 0.33 |
| 7.52 | 1.10 | 0.07 | 20.00 | 23.40 | 0.65 | 0.11 | 0.07 | 0.32 | 0.44 | 0.33 |
| 8.07 | 1.03 | 0.04 | 18.90 | 25.60 | 0.81 | 0.18 | 0.08 | 0.23 | 0.44 | 0.18 |
| 8.55 | 1.04 | 0.01 | 17.30 | 22.20 | 0.70 | 0.13 | 0.08 | 0.21 | 0.02 | 0.29 |
| 9.05 | 1.11 | 0.00 | 18.90 | 26.30 | 0.92 | 0.07 | 0.10 | 0.32 | 0.40 | 0.09 |
| 9.53 | 1.14 | 0.03 | 15.90 | 28.00 | 0.98 | 0.12 | 0.08 | 0.13 | 0.22 | 0.16 |
| 10.07 | 0.81 | 0.04 | 11.20 | 31.60 | 1.87 | 0.12 | 0.07 | 0.24 | 0.39 | 0.07 |
| 10.56 | 0.84 | 0.05 | 17.20 | 22.20 | 0.65 | 0.05 | 0.05 | 0.16 | 0.13 | 0.34 |
| 11.06 | 0.92 | 0.08 | 14.10 | 29.40 | 1.50 | 0.18 | 0.09 | 0.20 | 0.48 | 0.00 |
| 11.66 | 1.14 | 0.03 | 19.80 | 30.50 | 1.03 | 0.09 | 0.04 | 0.35 | 0.11 | 0.16 |
| 12.14 | 1.10 | 0.08 | 17.80 | 28.30 | 1.03 | 0.08 | 0.03 | 0.28 | 0.31 | 0.00 |
| 12.64 | 0.92 | 0.05 | 14.80 | 30.50 | 1.44 | 0.11 | 0.05 | 0.28 | 0.00 | 0.36 |
| 13.18 | 1.00 | 0.07 | 18.20 | 27.90 | 0.90 | 0.09 | 0.09 | 0.24 | 0.20 | 0.49 |
| 13.62 | 1.11 | 0.07 | 15.90 | 30.70 | 1.30 | 0.19 | 0.07 | 0.29 | 0.29 | 0.16 |
| 14.10 | 1.43 | 0.06 | 18.90 | 27.80 | 0.99 | 0.20 | 0.05 | 0.32 | 0.34 | 0.38 |
| 14.60 | 1.27 | 0.08 | 16.30 | 26.10 | 0.89 | 0.02 | 0.08 | 0.24 | 0.14 | 0.11 |
| 15.10 | 1.35 | 0.05 | 17.70 | 27.80 | 0.89 | 0.11 | 0.04 | 0.23 | 0.09 | 0.31 |
| 15.63 | 1.21 | 0.02 | 17.70 | 28.30 | 0.85 | 0.13 | 0.08 | 0.23 | 0.26 | 0.22 |
| 16.11 | 1.16 | 0.06 | 9.86 | 33.80 | 1.90 | 0.25 | 0.11 | 0.25 | 0.16 | 0.15 |
| 16.66 | 1.29 | 0.05 | 17.20 | 27.20 | 0.87 | 0.17 | 0.06 | 0.27 | 0.00 | 0.31 |
| 17.18 | 0.97 | 0.04 | 9.38 | 36.80 | 2.40 | 0.23 | 0.05 | 0.32 | 0.39 | 0.21 |
| 17.62 | 0.95 | 0.06 | 10.60 | 33.30 | 2.05 | 0.23 | 0.04 | 0.29 | 0.00 | 0.23 |
| 18.26 | 0.89 | 0.05 | 8.09 | 36.40 | 2.40 | 0.27 | 0.08 | 0.22 | 0.14 | 0.36 |
| 18.81 | 0.95 | 0.05 | 9.50 | 35.20 | 2.27 | 0.27 | 0.10 | 0.31 | 0.39 | 0.15 |
| 19.28 | 0.86 | 0.03 | 7.73 | 35.10 | 2.67 | 0.29 | 0.12 | 0.35 | 0.08 | 0.21 |
| 19.77 | 0.84 | 0.04 | 9.90 | 31.80 | 1.87 | 0.23 | 0.08 | 0.23 | 0.00 | 0.00 |
| 20.37 | 0.88 | 0.00 | 9.19 | 34.60 | 2.27 | 0.30 | 0.10 | 0.26 | 0.35 | 0.00 |
| 20.85 | 1.07 | 0.06 | 12.10 | 31.80 | 1.66 | 0.28 | 0.06 | 0.23 | 0.57 | 0.30 |
| 21.40 | 0.79 | 0.00 | 7.27 | 37.90 | 2.90 | 0.31 | 0.14 | 0.42 | 0.38 | 0.23 |
| 22.02 | 0.79 | 0.00 | 8.86 | 34.30 | 2.39 | 0.21 | 0.03 | 0.32 | 0.22 | 0.05 |
| 22.39 | 0.77 | 0.02 | 9.67 | 35.70 | 2.56 | 0.23 | 0.11 | 0.38 | 0.37 | 0.00 |
| 22.90 | 0.87 | 0.03 | 8.61 | 35.00 | 2.58 | 0.32 | 0.08 | 0.27 | 0.10 | 0.00 |
| 23.43 | 0.80 | 0.03 | 9.36 | 35.00 | 2.53 | 0.33 | 0.15 | 0.34 | 0.33 | 0.24 |

Appendix A. (Continued) Elemental Abundance (%) of Microprobe Data for Crust 6RD08-08 from Kiribati

| DEPTH (mm) | Ti(%) | V(%) | Fe(%) | Mn(%) | Ni(%) | Cu(%) | Zn(%) | Ba(%) | Sr(%) | Pb(%) |
|---------------|-------|------|-------|-------|-------|-------|-------|-------|-------|-------|
| 23.87 | 0.95 | 0.01 | 10.30 | 34.10 | 1.91 | 0.29 | 0.08 | 0.30 | 0.04 | 0.23 |
| 24.32 | 0.90 | 0.02 | 10.60 | 33.10 | 2.13 | 0.28 | 0.09 | 0.18 | 0.00 | 0.19 |
| 24.89 | 0.74 | 0.02 | 8.29 | 35.00 | 2.57 | 0.23 | 0.12 | 0.38 | 0.00 | 0.00 |
| 25.43 | 0.83 | 0.02 | 9.03 | 35.30 | 2.41 | 0.35 | 0.12 | 0.30 | 0.25 | 0.19 |
| 25.90 | 1.30 | 0.01 | 15.60 | 27.40 | 1.08 | 0.12 | 0.08 | 0.19 | 0.02 | 0.07 |
| 26.41 | 0.99 | 0.07 | 14.40 | 20.00 | 0.65 | 0.15 | 0.02 | 0.20 | 0.26 | 0.08 |
| 26.90 | 1.21 | 0.01 | 16.50 | 26.50 | 0.98 | 0.15 | 0.04 | 0.27 | 0.11 | 0.14 |
| 27.41 | 1.41 | 0.08 | 18.00 | 26.80 | 0.87 | 0.26 | 0.09 | 0.27 | 0.04 | 0.21 |
| 27.89 | 1.08 | 0.03 | 14.90 | 30.70 | 1.31 | 0.15 | 0.10 | 0.28 | 0.33 | 0.17 |
| 28.30 | 1.06 | 0.06 | 14.10 | 28.40 | 1.13 | 0.17 | 0.04 | 0.23 | 0.46 | 0.13 |
| 28.90 | 1.13 | 0.07 | 15.90 | 30.10 | 1.19 | 0.21 | 0.08 | 0.33 | 0.19 | 0.15 |
| 29.50 | 0.95 | 0.07 | 14.40 | 28.60 | 1.12 | 0.22 | 0.01 | 0.22 | 0.14 | 0.11 |
| 30.01 | 1.19 | 0.02 | 17.30 | 28.50 | 0.93 | 0.12 | 0.03 | 0.30 | 0.39 | 0.25 |
| 30.39 | 1.25 | 0.07 | 19.20 | 26.60 | 0.85 | 0.03 | 0.04 | 0.35 | 0.38 | 0.44 |
| 31.03 | 1.29 | 0.02 | 13.30 | 30.50 | 1.05 | 0.19 | 0.09 | 0.30 | 0.10 | 0.12 |
| 31.50 | 1.43 | 0.04 | 14.50 | 29.60 | 0.91 | 0.19 | 0.08 | 0.24 | 0.41 | 0.17 |
| 31.98 | 1.48 | 0.03 | 16.10 | 28.90 | 0.94 | 0.19 | 0.02 | 0.31 | 0.08 | 0.42 |
| 32.51 | 1.62 | 0.00 | 16.10 | 28.50 | 0.90 | 0.06 | 0.11 | 0.38 | 0.14 | 0.14 |
| 32.94 | 1.72 | 0.03 | 17.20 | 28.40 | 0.82 | 0.09 | 0.06 | 0.33 | 0.08 | 0.34 |
| 33.55 | 1.11 | 0.02 | 10.60 | 30.10 | 1.29 | 0.18 | 0.05 | 0.32 | 0.10 | 0.00 |
| 34.00 | 1.58 | 0.04 | 15.30 | 28.40 | 0.76 | 0.15 | 0.08 | 0.30 | 0.58 | 0.29 |
| 34.29 | 1.24 | 0.03 | 9.52 | 33.40 | 1.60 | 0.26 | 0.02 | 0.26 | 0.00 | 0.00 |
| 34.74 | 1.12 | 0.02 | 9.94 | 30.00 | 1.30 | 0.29 | 0.03 | 0.19 | 0.18 | 0.18 |
| 35.16 | 1.06 | 0.00 | 8.17 | 30.40 | 1.55 | 0.23 | 0.10 | 0.34 | 0.09 | 0.33 |
| 35.58 | 1.16 | 0.00 | 9.75 | 27.80 | 1.20 | 0.17 | 0.03 | 0.18 | 0.34 | 0.05 |
| 36.08 | 1.71 | 0.01 | 16.40 | 29.00 | 0.98 | 0.07 | 0.15 | 0.33 | 0.43 | 0.48 |
| 37.06 | 1.54 | 0.02 | 15.60 | 29.40 | 1.08 | 0.20 | 0.09 | 0.35 | 0.36 | 0.21 |
| 37.49 | 1.32 | 0.05 | 13.40 | 30.10 | 1.17 | 0.20 | 0.06 | 0.30 | 0.34 | 0.17 |
| 38.16 | 0.97 | 0.04 | 8.98 | 30.60 | 1.83 | 0.25 | 0.08 | 0.35 | 0.10 | 0.09 |
| 38.52 | 1.19 | 0.00 | 9.79 | 34.50 | 1.74 | 0.34 | 0.09 | 0.26 | 0.15 | 0.14 |
| 39.11 | 1.05 | 0.00 | 8.23 | 32.80 | 1.92 | 0.34 | 0.13 | 0.29 | 0.00 | 0.11 |
| 39.62 | 1.08 | 0.08 | 7.24 | 35.60 | 2.30 | 0.30 | 0.12 | 0.34 | 0.49 | 0.00 |
| 40.65 | 1.17 | 0.02 | 7.78 | 36.70 | 2.36 | 0.32 | 0.15 | 0.30 | 0.55 | 0.19 |
| 41.09 | 1.14 | 0.01 | 8.95 | 33.50 | 1.75 | 0.28 | 0.06 | 0.32 | 0.30 | 0.19 |
| 41.70 | 1.09 | 0.01 | 8.68 | 34.30 | 1.98 | 0.32 | 0.07 | 0.32 | 0.35 | 0.26 |
| 42.14 | 1.06 | 0.03 | 10.00 | 33.40 | 1.64 | 0.19 | 0.07 | 0.38 | 0.13 | 0.23 |

Appendix A. (Continued) Elemental Abundance (%) of Microprobe Data for Crust 6RD08-08 from Kiribati . .

| DEPTH (mm) | Ti(%) | V(%) | Fe(%) | Mn(%) | Ni(%) | Cu(%) | Zn(%) | Ba(%) | Sr(%) | Pb(%) |
|---------------|-------|------|-------|-------|-------|-------|-------|-------|-------|-------|
| 42.62 | 0.94 | 0.04 | 8.81 | 34.00 | 1.92 | 0.23 | 0.11 | 0.30 | 0.61 | 0.00 |
| 43.19 | 1.27 | 0.03 | 12.30 | 28.90 | 1.17 | 0.13 | 0.09 | 0.20 | 0.60 | 0.14 |
| 43.71 | 0.97 | 0.04 | 9.10 | 28.10 | 1.40 | 0.18 | 0.11 | 0.28 | 0.00 | 0.13 |
| 44.19 | 1.17 | 0.00 | 11.40 | 26.30 | 1.00 | 0.25 | 0.12 | 0.39 | 0.25 | 0.37 |
| 44.69 | 0.92 | 0.00 | 10.20 | 28.40 | 1.49 | 0.24 | 0.08 | 0.24 | 0.24 | 0.08 |
| 45.20 | 1.38 | 0.05 | 13.10 | 30.30 | 1.31 | 0.28 | 0.05 | 0.31 | 0.28 | 0.29 |
| 48.02 | 1.07 | 0.09 | 10.30 | 32.10 | 1.73 | 0.29 | 0.07 | 0.29 | 0.57 | 0.30 |
| 48.51 | 0.85 | 0.01 | 10.10 | 26.10 | 1.18 | 0.28 | 0.04 | 0.23 | 0.41 | 0.00 |
| 49.11 | 0.91 | 0.01 | 10.90 | 28.00 | 1.54 | 0.28 | 0.01 | 0.32 | 0.00 | 0.02 |
| 49.59 | 0.61 | 0.02 | 6.18 | 25.50 | 1.93 | 0.07 | 0.05 | 0.15 | 0.51 | 0.12 |
| 50.13 | 0.92 | 0.03 | 10.90 | 28.00 | 1.48 | 0.18 | 0.07 | 0.28 | 0.36 | 0.26 |
| 50.65 | 1.00 | 0.03 | 11.40 | 25.00 | 1.04 | 0.21 | 0.02 | 0.27 | 0.00 | 0.14 |
| 51.20 | 1.14 | 0.06 | 12.60 | 32.20 | 1.63 | 0.28 | 0.06 | 0.31 | 0.00 | 0.28 |
| 51.70 | 0.95 | 0.00 | 8.92 | 31.50 | 1.95 | 0.32 | 0.03 | 0.39 | 0.21 | 0.21 |
| 52.20 | 0.61 | 0.00 | 6.62 | 25.90 | 1.89 | 0.20 | 0.07 | 0.25 | 0.21 | 0.13 |
| 52.70 | 0.65 | 0.01 | 5.36 | 29.30 | 2.46 | 0.26 | 0.10 | 0.37 | 0.00 | 0.25 |
| 53.25 | 0.75 | 0.03 | 8.70 | 27.20 | 1.58 | 0.19 | 0.04 | 0.35 | 0.19 | 0.16 |
| 53.71 | 1.35 | 0.01 | 16.00 | 22.30 | 0.86 | 0.25 | 0.11 | 0.47 | 0.63 | 0.83 |
| 54.18 | 0.66 | 0.03 | 6.14 | 25.60 | 1.89 | 0.24 | 0.09 | 0.24 | 0.29 | 0.05 |
| 54.77 | 0.94 | 0.04 | 8.78 | 30.00 | 1.76 | 0.19 | 0.10 | 0.28 | 0.51 | 0.02 |
| 55.18 | 1.05 | 0.05 | 17.30 | 25.20 | 0.85 | 0.24 | 0.04 | 0.37 | 0.57 | 0.23 |
| 55.59 | 0.88 | 0.06 | 11.70 | 28.30 | 1.44 | 0.22 | 0.11 | 0.32 | 0.19 | 0.07 |
| 56.18 | 0.88 | 0.00 | 11.30 | 22.70 | 0.99 | 0.23 | 0.00 | 0.28 | 0.00 | 0.24 |
| 56.79 | 1.00 | 0.05 | 14.20 | 18.20 | 0.82 | 0.30 | 0.08 | 0.22 | 0.30 | 0.33 |
| 57.32 | 1.11 | 0.06 | 13.90 | 28.70 | 1.28 | 0.18 | 0.07 | 0.42 | 0.58 | 0.09 |
| 57.85 | 1.21 | 0.02 | 14.20 | 26.70 | 0.99 | 0.24 | 0.06 | 0.34 | 0.37 | 0.24 |
| 58.33 | 1.07 | 0.01 | 14.10 | 30.20 | 1.25 | 0.29 | 0.06 | 0.36 | 0.21 | 0.08 |
| 58.71 | 0.90 | 0.08 | 12.90 | 29.80 | 1.18 | 0.28 | 0.07 | 0.39 | 0.13 | 0.02 |
| 59.34 | 1.00 | 0.00 | 11.80 | 29.70 | 1.32 | 0.37 | 0.09 | 0.29 | 0.00 | 0.28 |
| 59.77 | 0.79 | 0.03 | 9.66 | 18.40 | 0.71 | 0.23 | 0.06 | 0.14 | 0.28 | 0.34 |
| 60.30 | 0.54 | 0.00 | 6.35 | 9.30 | 0.30 | 0.07 | 0.02 | 0.13 | 0.40 | 0.18 |
| 60.84 | 1.06 | 0.03 | 12.30 | 28.80 | 1.14 | 0.21 | 0.08 | 0.19 | 0.77 | 0.11 |
| 61.32 | 1.24 | 0.00 | 13.40 | 30.10 | 1.23 | 0.20 | 0.05 | 0.28 | 0.60 | 0.33 |
| 61.77 | 1.16 | 0.04 | 10.00 | 32.00 | 1.73 | 0.33 | 0.11 | 0.34 | 0.18 | 0.36 |
| 62.27 | 1.01 | 0.00 | 9.51 | 27.60 | 1.45 | 0.24 | 0.04 | 0.30 | 0.18 | 0.00 |
| 62.74 | 1.03 | 0.00 | 10.40 | 26.90 | 1.29 | 0.17 | 0.08 | 0.27 | 0.14 | 0.12 |

APPENDIX B

Appendix B.1 Elemental Correlation Matrix for Crust 6RD08-08 from Kiribati.

104

| | Al | Si | P | Cu | Mg | Co | Fe | Mn | Ni | Sr | Zn | Ti | V |
|----|--------------|--------------|--------------|--------------|-------------|-------------|--------------|-------------|-------------|-------|-------|------|------|
| Al | 1.00 | | | | | | | | | | | | |
| Si | 0.79 | 1.00 | | | | | | | | | | | |
| P | 0.04 | -0.23 | 1.00 | | | | | | | | | | |
| Cu | -0.57 | -0.80 | 0.36 | 1.00 | | | | | | | | | |
| Mg | -0.54 | -0.57 | -0.36 | 0.59 | 1.00 | | | | | | | | |
| Co | -0.46 | -0.36 | -0.52 | 0.37 | 0.76 | 1.00 | | | | | | | |
| Fe | 0.53 | 0.70 | -0.59 | -0.83 | -0.39 | -0.17 | 1.00 | | | | | | |
| Mn | -0.63 | -0.47 | -0.53 | 0.36 | 0.84 | 0.70 | -0.19 | 1.00 | | | | | |
| Ni | -0.60 | -0.55 | -0.16 | 0.53 | 0.82 | 0.52 | -0.60 | 0.75 | 1.00 | | | | |
| Sr | -0.30 | -0.39 | 0.51 | 0.24 | -0.12 | -0.21 | -0.24 | -0.04 | -0.12 | 1.00 | | | |
| Zn | -0.58 | -0.59 | -0.21 | 0.62 | 0.74 | 0.55 | -0.38 | 0.78 | 0.65 | 0.19 | 1.00 | | |
| Ti | -0.23 | -0.31 | -0.14 | 0.33 | 0.17 | 0.20 | 0.02 | 0.12 | -0.04 | 0.20 | 0.23 | 1.00 | |
| V | -0.11 | 0.13 | -0.54 | -0.26 | 0.03 | 0.32 | 0.51 | 0.09 | -0.23 | -0.25 | -0.22 | 0.33 | 1.00 |

Appendix B.1 (Continued) Elemental Correlation Matrix for Crust 6RD08-08 from Kiribati.

| | Al | Si | P | Cu | Mg | Co | Fe | Mn | Ni | Sr | Zn | Ti | V |
|------|--------------|--------------|-------------|-------------|-------|-------|--------------|-------|-------|-------------|-------------|-------|-------|
| CeAN | -0.27 | -0.56 | 0.41 | 0.64 | 0.14 | -0.02 | -0.43 | 0.04 | -0.00 | 0.50 | 0.41 | 0.34 | -0.28 |
| Cr | 0.04 | -0.10 | 0.46 | 0.05 | -0.28 | -0.37 | -0.23 | -0.31 | -0.17 | 0.36 | -0.13 | -0.09 | -0.36 |
| Y | 0.08 | 0.02 | 0.73 | 0.17 | -0.26 | -0.34 | -0.47 | -0.45 | 0.01 | 0.13 | -0.38 | -0.24 | -0.25 |
| Ba | -0.51 | -0.70 | 0.27 | 0.86 | 0.38 | 0.35 | -0.55 | 0.24 | 0.18 | 0.34 | 0.56 | 0.44 | -0.09 |
| La | -0.13 | 0.04 | 0.45 | 0.25 | -0.03 | -0.07 | -0.37 | -0.12 | 0.10 | 0.14 | -0.02 | -0.24 | -0.16 |
| Ce | -0.41 | -0.59 | 0.53 | 0.81 | 0.24 | 0.07 | -0.63 | 0.10 | 0.15 | 0.49 | 0.51 | 0.21 | -0.36 |
| Pr | -0.39 | -0.16 | 0.04 | 0.39 | 0.27 | 0.25 | -0.24 | 0.32 | 0.23 | 0.14 | 0.43 | 0.00 | 0.02 |
| Nd | -0.33 | -0.06 | 0.07 | 0.30 | 0.20 | 0.17 | -0.22 | 0.25 | 0.21 | 0.11 | 0.32 | -0.05 | 0.03 |
| Sm | -0.37 | -0.12 | 0.01 | 0.33 | 0.25 | 0.20 | -0.21 | 0.34 | 0.25 | 0.12 | 0.42 | -0.02 | 0.03 |
| Eu | -0.30 | -0.02 | 0.12 | 0.27 | 0.14 | 0.09 | -0.23 | 0.21 | 0.20 | 0.10 | 0.26 | -0.12 | 0.01 |
| Gd | -0.29 | -0.13 | 0.40 | 0.43 | 0.12 | 0.00 | -0.45 | 0.06 | 0.21 | 0.20 | 0.19 | -0.10 | -0.14 |
| Tb | -0.23 | 0.02 | 0.22 | 0.24 | 0.12 | 0.04 | -0.28 | 0.11 | 0.21 | 0.06 | 0.12 | -0.13 | 0.00 |
| Dy | -0.09 | 0.11 | 0.36 | 0.14 | -0.02 | -0.08 | -0.31 | -0.09 | 0.16 | 0.00 | -0.14 | -0.27 | -0.05 |

Appendix B.1 (Continued) Elemental Correlation Matrix for Crust 6RD08-08 from Kiribati.

| | Al | Si | P | Cu | Mg | Co | Fe | Mn | Ni | Sr | Zn | Ti | V |
|----|-------|--------------|--------------|-------------|-------|-------|--------------|-------|-------|-------------|-------------|-------|--------------|
| Ho | 0.05 | 0.19 | 0.48 | 0.05 | -0.16 | -0.21 | -0.31 | -0.28 | 0.08 | -0.01 | -0.33 | -0.31 | -0.10 |
| Er | 0.12 | 0.20 | 0.52 | 0.01 | -0.21 | -0.25 | -0.31 | -0.35 | 0.04 | -0.03 | -0.39 | -0.33 | -0.14 |
| Tm | 0.15 | 0.23 | 0.52 | -0.03 | -0.23 | -0.26 | -0.28 | -0.38 | 0.02 | -0.02 | -0.42 | -0.34 | -0.15 |
| Yb | 0.20 | 0.28 | 0.51 | -0.07 | -0.26 | -0.28 | -0.25 | -0.42 | -0.01 | -0.03 | -0.45 | -0.35 | -0.14 |
| Ir | 0.08 | -0.17 | 0.66 | 0.08 | -0.31 | -0.43 | -0.30 | -0.41 | -0.22 | 0.23 | -0.27 | -0.13 | -0.38 |
| Pt | -0.24 | -0.48 | 0.39 | 0.63 | 0.18 | 0.01 | -0.45 | 0.07 | 0.02 | 0.47 | 0.44 | 0.33 | -0.36 |
| Au | 0.06 | -0.11 | 0.54 | 0.04 | -0.25 | -0.31 | -0.22 | -0.34 | -0.21 | 0.16 | -0.24 | -0.11 | -0.24 |
| Pb | 0.03 | 0.35 | -0.60 | -0.37 | 0.00 | 0.22 | 0.54 | 0.23 | -0.14 | -0.18 | 0.13 | -0.06 | 0.17 |
| Bi | -0.31 | -0.54 | 0.32 | 0.52 | 0.27 | -0.15 | -0.42 | 0.26 | 0.33 | 0.38 | 0.52 | 0.04 | -0.49 |
| Th | -0.39 | -0.39 | 0.22 | 0.51 | 0.32 | 0.09 | -0.34 | 0.31 | 0.26 | 0.38 | 0.59 | 0.04 | -0.20 |
| U | 0.02 | 0.22 | -0.37 | 0.01 | 0.15 | 0.37 | 0.27 | 0.11 | -0.14 | -0.21 | 0.08 | 0.15 | 0.32 |
| Ca | -0.11 | -0.33 | 0.93 | 0.53 | -0.14 | -0.31 | -0.71 | -0.36 | 0.03 | 0.47 | -0.07 | -0.07 | -0.48 |

Appendix B.1 (Continued) Elemental Correlation Matrix for Crust 6RD08-08 from Kiribati.

| | CeAN | Cr | Y | Ba | La | Ce | Pr | Nd | Sm | Eu | Gd | Tb | Dy |
|------|--------------|-------|-------------|-------------|-------------|-------------|-------------|-------------|-------------|-------------|-------------|-------------|------|
| CeAN | 1.00 | | | | | | | | | | | | |
| Cr | 0.56 | 1.00 | | | | | | | | | | | |
| Y | -0.19 | -0.05 | 1.00 | | | | | | | | | | |
| Ba | 0.72 | 0.10 | -0.09 | 1.00 | | | | | | | | | |
| La | -0.23 | -0.18 | 0.66 | 0.19 | 1.00 | | | | | | | | |
| Ce | 0.79 | 0.31 | 0.08 | 0.89 | 0.35 | 1.00 | | | | | | | |
| Pr | -0.04 | -0.31 | 0.12 | 0.49 | 0.78 | 0.50 | 1.00 | | | | | | |
| Nd | -0.17 | -0.32 | 0.24 | 0.35 | 0.85 | 0.40 | 0.98 | 1.00 | | | | | |
| Sm | -0.11 | -0.34 | 0.12 | 0.40 | 0.77 | 0.43 | 0.99 | 0.99 | 1.00 | | | | |
| Eu | -0.21 | -0.35 | 0.33 | 0.29 | 0.87 | 0.35 | 0.95 | 0.98 | 0.97 | 1.00 | | | |
| Gd | -0.06 | -0.19 | 0.55 | 0.37 | 0.95 | 0.50 | 0.88 | 0.92 | 0.87 | 0.94 | 1.00 | | |
| Tb | -0.30 | -0.35 | 0.52 | 0.18 | 0.93 | 0.26 | 0.87 | 0.94 | 0.89 | 0.96 | 0.96 | 1.00 | |
| Dy | -0.43 | -0.32 | 0.75 | -0.02 | 0.94 | 0.10 | 0.65 | 0.77 | 0.68 | 0.82 | 0.88 | 0.93 | 1.00 |

Appendix B.1 (Continued) Elemental Correlation Matrix for Crust 6RD08-08 from Kiribati.

| | CeAN | Cr | Y | Ba | La | Ce | Pr | Nd | Sm | Eu | Gd | Tb | Dy |
|----|--------------|-------|--------------|-------------|-------------|-------------|-------------|-------------|-------------|-------------|-------------|-------------|-------------|
| Ho | -0.45 | -0.24 | 0.90 | -0.18 | 0.84 | -0.03 | 0.40 | 0.54 | 0.42 | 0.62 | 0.74 | 0.78 | 0.95 |
| Er | -0.46 | -0.22 | 0.93 | -0.22 | 0.78 | -0.07 | 0.28 | 0.43 | 0.31 | 0.51 | 0.65 | 0.69 | 0.90 |
| Tm | -0.47 | -0.22 | 0.93 | -0.27 | 0.76 | -0.10 | 0.23 | 0.38 | 0.25 | 0.46 | 0.61 | 0.65 | 0.87 |
| Yb | -0.47 | -0.19 | 0.92 | -0.31 | 0.73 | -0.13 | 0.19 | 0.33 | 0.21 | 0.42 | 0.57 | 0.62 | 0.84 |
| Ir | 0.21 | 0.24 | 0.35 | 0.14 | 0.18 | 0.24 | -0.08 | -0.08 | -0.12 | -0.07 | 0.09 | 0.00 | 0.11 |
| Pt | 0.82 | 0.40 | -0.18 | 0.78 | 0.07 | 0.85 | 0.28 | 0.15 | 0.21 | 0.08 | 0.19 | -0.01 | -0.20 |
| Au | 0.03 | -0.05 | 0.40 | 0.11 | 0.30 | 0.15 | 0.06 | 0.08 | 0.04 | 0.09 | 0.20 | 0.17 | 0.26 |
| Pb | -0.27 | -0.18 | -0.60 | -0.09 | -0.01 | -0.14 | 0.31 | 0.27 | 0.30 | 0.19 | -0.03 | 0.05 | -0.12 |
| Bi | 0.66 | 0.40 | -0.11 | 0.46 | -0.07 | 0.61 | 0.08 | 0.00 | 0.06 | 0.00 | 0.06 | -0.10 | -0.20 |
| Th | 0.36 | 0.00 | -0.05 | 0.62 | 0.52 | 0.72 | 0.78 | 0.70 | 0.74 | 0.65 | 0.63 | 0.53 | 0.31 |
| U | -0.08 | -0.17 | -0.33 | 0.27 | 0.26 | 0.18 | 0.49 | 0.45 | 0.43 | 0.35 | 0.25 | 0.28 | 0.12 |
| Ca | 0.37 | 0.26 | 0.82 | 0.34 | 0.54 | 0.56 | 0.14 | 0.18 | 0.10 | 0.23 | 0.52 | 0.35 | 0.48 |

Appendix B.1 (Continued) Elemental Correlation Matrix for Crust 6RD08-08 from Kiribati.

109

| | Ho | Er | Tm | Yb | Ir | Pt | Au | Pb | Bi | Th | U | Ca |
|----|-------------|-------------|-------------|-------------|-------------|-------------|-------|--------------|-------------|------|-------|------|
| Ho | 1.00 | | | | | | | | | | | |
| Er | 0.99 | 1.00 | | | | | | | | | | |
| Tm | 0.97 | 0.99 | 1.00 | | | | | | | | | |
| Yb | 0.97 | 0.99 | 1.00 | 1.00 | | | | | | | | |
| Ir | 0.17 | 0.24 | 0.25 | 0.23 | 1.00 | | | | | | | |
| Pt | -0.31 | -0.33 | -0.34 | -0.36 | 0.34 | 1.00 | | | | | | |
| Au | 0.29 | 0.35 | 0.36 | 0.34 | 0.95 | 0.23 | 1.00 | | | | | |
| Pb | -0.29 | -0.35 | -0.35 | -0.35 | -0.37 | -0.14 | -0.31 | 1.00 | | | | |
| Bi | -0.25 | -0.27 | -0.28 | -0.30 | 0.11 | 0.53 | -0.06 | -0.11 | 1.00 | | | |
| Th | 0.07 | -0.01 | -0.04 | -0.08 | 0.13 | 0.58 | 0.17 | 0.16 | 0.52 | 1.00 | | |
| U | -0.05 | -0.11 | -0.12 | -0.13 | -0.31 | 0.10 | -0.24 | 0.72 | -0.17 | 0.26 | 1.00 | |
| Ca | 0.59 | 0.62 | 0.61 | 0.60 | 0.46 | 0.33 | 0.40 | -0.63 | 0.31 | 0.24 | -0.32 | 1.00 |

Appendix B.2 Elemental Correlation Matrix for Crust RD50S1B from Hawaii.

| | Cr | Y | Ba | La | Ce | Pr | Nd | Sm | Eu | Gd | Tb | Du | Ho |
|----|--------------|-------------|--------------|-------------|-------|-------------|-------------|-------------|-------------|-------------|-------------|-------------|------|
| Cr | 1.00 | | | | | | | | | | | | |
| Y | 0.50 | 1.00 | | | | | | | | | | | |
| Ba | -0.53 | -0.35 | 1.00 | | | | | | | | | | |
| La | 0.13 | 0.88 | -0.19 | 1.00 | | | | | | | | | |
| Ce | -0.55 | -0.42 | 0.64 | -0.23 | 1.00 | | | | | | | | |
| Pr | 0.29 | 0.89 | -0.49 | 0.94 | -0.42 | 1.00 | | | | | | | |
| Nd | 0.34 | 0.93 | -0.47 | 0.94 | -0.45 | 1.00 | 1.00 | | | | | | |
| Sm | 0.40 | 0.92 | -0.54 | 0.91 | -0.48 | 0.99 | 0.99 | 1.00 | | | | | |
| Eu | 0.41 | 0.94 | -0.53 | 0.91 | -0.48 | 0.99 | 0.99 | 1.00 | 1.00 | | | | |
| Gd | 0.42 | 0.96 | -0.48 | 0.92 | -0.45 | 0.98 | 0.99 | 0.99 | 1.00 | 1.00 | | | |
| Tb | 0.43 | 0.94 | -0.54 | 0.91 | -0.48 | 0.99 | 0.99 | 1.00 | 1.00 | 1.00 | 1.00 | | |
| Dy | 0.45 | 0.95 | -0.51 | 0.91 | -0.48 | 0.98 | 0.99 | 0.99 | 1.00 | 1.00 | 1.00 | 1.00 | |
| Ho | 0.46 | 0.97 | -0.47 | 0.92 | -0.46 | 0.97 | 0.98 | 0.98 | 0.99 | 1.00 | 0.99 | 1.00 | 1.00 |

Appendix B.2 (continued) Elemental Correlation Matrix for Crust RD50S1B from Hawaii.

| | Cr | Y | Ba | La | Ce | Pr | Nd | Sm | Eu | Gd | Tb | Du | Ho |
|----|--------------|--------------|--------------|-------------|--------------|--------------|--------------|--------------|--------------|--------------|--------------|--------------|--------------|
| Er | 0.45 | 0.97 | -0.46 | 0.92 | -0.44 | 0.96 | 0.98 | 0.98 | 0.99 | 0.99 | 0.99 | 0.99 | 1.00 |
| Tm | 0.42 | 0.95 | -0.49 | 0.92 | -0.41 | 0.97 | 0.98 | 0.98 | 0.99 | 0.99 | 0.99 | 0.99 | 0.99 |
| Yb | 0.42 | 0.94 | -0.52 | 0.91 | -0.41 | 0.96 | 0.97 | 0.98 | 0.98 | 0.98 | 0.98 | 0.99 | 0.99 |
| Ir | 0.70 | -0.13 | -0.21 | -0.36 | -0.32 | -0.27 | -0.24 | -0.20 | -0.20 | -0.20 | -0.18 | -0.15 | -0.15 |
| Pt | -0.36 | -0.24 | 0.80 | -0.28 | 0.44 | -0.52 | -0.47 | -0.53 | -0.51 | -0.46 | -0.51 | -0.47 | -0.42 |
| Au | 0.68 | -0.12 | -0.18 | -0.33 | -0.30 | -0.26 | -0.23 | -0.19 | -0.19 | -0.19 | -0.17 | -0.15 | -0.15 |
| Pb | -0.13 | -0.54 | -0.13 | -0.29 | 0.13 | -0.24 | -0.31 | -0.29 | -0.31 | -0.37 | -0.30 | -0.33 | -0.37 |
| Bi | -0.68 | -0.61 | 0.58 | -0.38 | 0.55 | -0.55 | -0.57 | -0.61 | -0.62 | -0.62 | -0.62 | -0.62 | -0.61 |
| Th | 0.66 | 0.02 | -0.73 | -0.13 | -0.36 | 0.12 | 0.10 | 0.18 | 0.17 | 0.13 | 0.18 | 0.17 | 0.13 |
| U | -0.17 | -0.38 | -0.38 | -0.15 | 0.16 | -0.04 | -0.12 | -0.08 | -0.11 | -0.17 | -0.10 | -0.13 | -0.18 |
| Al | 0.58 | 0.69 | -0.24 | 0.39 | -0.48 | 0.49 | 0.54 | 0.56 | 0.58 | 0.60 | 0.57 | 0.57 | 0.59 |
| Ca | 0.37 | 0.93 | -0.27 | 0.85 | -0.20 | 0.82 | 0.84 | 0.84 | 0.85 | 0.88 | 0.85 | 0.88 | 0.89 |
| Si | 0.53 | 0.58 | -0.32 | 0.30 | -0.48 | 0.45 | 0.49 | 0.52 | 0.53 | 0.54 | 0.51 | 0.51 | 0.52 |

Appendix B.2 (continued) Elemental Correlation Matrix for Crust RD50S1B from Hawaii.

| | Cr | Y | Ba | La | Ce | Pr | Nd | Sm | Eu | Gd | Tb | Du | Ho |
|-------------|--------------|--------------|--------------|--------------|-------------|--------------|--------------|--------------|--------------|--------------|--------------|--------------|--------------|
| P | 0.49 | 0.98 | -0.32 | 0.87 | -0.34 | 0.86 | 0.89 | 0.89 | 0.90 | 0.93 | 0.91 | 0.93 | 0.95 |
| Ti | 0.15 | -0.07 | -0.42 | -0.02 | 0.23 | 0.12 | 0.06 | 0.12 | 0.11 | 0.08 | 0.11 | 0.09 | 0.06 |
| Cu | -0.42 | -0.23 | 0.85 | -0.15 | 0.33 | -0.41 | -0.37 | -0.45 | -0.43 | -0.39 | -0.44 | -0.41 | -0.38 |
| Mg | 0.57 | 0.22 | -0.12 | -0.05 | -0.37 | 0.02 | 0.07 | 0.09 | 0.09 | 0.12 | 0.12 | 0.13 | 0.15 |
| Co | 0.22 | -0.38 | -0.47 | -0.40 | 0.07 | -0.25 | -0.29 | -0.23 | -0.25 | -0.28 | -0.23 | -0.23 | -0.26 |
| Fe | -0.47 | -0.13 | 0.52 | 0.03 | 0.03 | -0.08 | -0.08 | -0.13 | -0.13 | -0.13 | -0.16 | -0.17 | -0.18 |
| Mn | -0.60 | -0.72 | 0.33 | -0.46 | 0.54 | -0.58 | -0.62 | -0.65 | -0.66 | -0.67 | -0.65 | -0.65 | -0.67 |
| Ni | -0.22 | -0.57 | 0.32 | -0.45 | 0.28 | -0.56 | -0.57 | -0.60 | -0.60 | -0.60 | -0.59 | -0.57 | -0.57 |
| Sr | -0.76 | -0.53 | 0.40 | -0.18 | 0.64 | -0.35 | -0.40 | -0.44 | -0.45 | -0.47 | -0.45 | -0.45 | -0.47 |
| Zn | -0.55 | -0.51 | 0.82 | -0.28 | 0.57 | -0.52 | -0.52 | -0.58 | -0.59 | -0.57 | -0.59 | -0.57 | -0.56 |
| V | -0.38 | -0.28 | 0.84 | -0.12 | 0.52 | -0.39 | -0.38 | -0.44 | -0.43 | -0.39 | -0.43 | -0.41 | -0.37 |
| CeAN | -0.39 | -0.78 | 0.62 | -0.78 | 0.72 | -0.90 | -0.90 | -0.92 | -0.91 | -0.89 | -0.91 | -0.89 | -0.87 |

Appendix B.2 (continued) Elemental Correlation Matrix for Crust RD50S1B from Hawaii.

113

| | Er | Tm | Yb | Ir | Pt | Au | Pb | Bi | Th | U | Al | Ca | Si | P |
|----|--------------|--------------|--------------|-------------|--------------|-------------|--------------|--------------|-------------|--------------|-------------|-------------|-------------|------|
| Er | 1.00 | | | | | | | | | | | | | |
| Tm | 0.99 | 1.00 | | | | | | | | | | | | |
| Yb | 0.99 | 1.00 | 1.00 | | | | | | | | | | | |
| Ir | -0.17 | -0.18 | -0.17 | 1.00 | | | | | | | | | | |
| Pt | -0.41 | -0.45 | -0.47 | -0.15 | 1.00 | | | | | | | | | |
| Au | -0.16 | -0.18 | -0.16 | 1.00 | -0.13 | 1.00 | | | | | | | | |
| Pb | -0.39 | -0.32 | -0.29 | 0.38 | -0.43 | 0.39 | 1.00 | | | | | | | |
| Bi | -0.61 | -0.58 | -0.56 | -0.16 | 0.48 | -0.13 | 0.26 | 1.00 | | | | | | |
| Th | 0.12 | 0.14 | 0.17 | 0.65 | -0.75 | 0.62 | 0.52 | -0.49 | 1.00 | | | | | |
| U | -0.18 | -0.09 | -0.05 | 0.09 | -0.55 | 0.09 | 0.84 | 0.18 | 0.53 | 1.00 | | | | |
| Al | 0.59 | 0.52 | 0.49 | -0.01 | -0.11 | -0.03 | -0.72 | -0.74 | 0.07 | -0.68 | 1.00 | | | |
| Ca | 0.91 | 0.90 | 0.90 | -0.23 | -0.13 | -0.22 | -0.50 | -0.45 | -0.06 | -0.25 | 0.48 | 1.00 | | |
| Si | 0.52 | 0.45 | 0.42 | -0.04 | -0.24 | -0.08 | -0.61 | -0.75 | 0.17 | -0.56 | 0.96 | 0.39 | 1.00 | |
| P | 0.96 | 0.94 | 0.93 | -0.13 | -0.21 | -0.11 | -0.49 | -0.54 | 0.03 | -0.30 | 0.59 | 0.98 | 0.49 | 1.00 |

Appendix B.2 (continued) Elemental Correlation Matrix for Crust RD50S1B from Hawaii.

| | Er | Tm | Yb | Ir | Pt | Au | Pb | Bi | Th | U | Al | Ca | Si | P |
|------|--------------|--------------|--------------|-------------|--------------|-------------|-------------|-------------|--------------|--------------|--------------|--------------|--------------|--------------|
| Ti | 0.08 | 0.13 | 0.17 | 0.06 | -0.57 | 0.05 | 0.45 | -0.23 | 0.64 | 0.71 | -0.16 | 0.06 | -0.04 | 0.02 |
| Cu | -0.38 | -0.42 | -0.45 | -0.11 | 0.82 | -0.06 | -0.25 | 0.52 | -0.76 | -0.57 | -0.14 | -0.23 | -0.27 | -0.25 |
| Mg | 0.12 | 0.08 | 0.08 | 0.56 | 0.11 | 0.58 | -0.16 | -0.25 | 0.24 | -0.36 | 0.39 | 0.04 | 0.26 | 0.16 |
| Co | -0.26 | -0.21 | -0.16 | 0.53 | -0.42 | 0.52 | 0.67 | 0.10 | 0.71 | 0.76 | -0.54 | -0.27 | -0.47 | -0.29 |
| Fe | -0.18 | -0.22 | -0.26 | -0.35 | 0.31 | -0.32 | -0.18 | 0.19 | -0.50 | -0.42 | 0.16 | -0.26 | 0.18 | -0.22 |
| Mn | -0.66 | -0.61 | -0.58 | -0.01 | 0.28 | 0.02 | 0.58 | 0.79 | -0.18 | 0.52 | -0.96 | -0.49 | -0.94 | -0.61 |
| Ni | -0.58 | -0.55 | -0.53 | 0.40 | 0.32 | 0.44 | 0.52 | 0.66 | -0.08 | 0.28 | -0.77 | -0.44 | -0.82 | -0.50 |
| Sr | -0.45 | -0.40 | -0.38 | -0.33 | 0.30 | -0.29 | 0.44 | 0.78 | -0.36 | 0.49 | -0.89 | -0.25 | -0.85 | -0.40 |
| Zn | -0.55 | -0.55 | -0.56 | -0.02 | 0.58 | 0.03 | 0.24 | 0.73 | -0.47 | -0.04 | -0.52 | -0.42 | -0.57 | -0.46 |
| V | -0.37 | -0.37 | -0.40 | 0.01 | 0.64 | 0.05 | 0.09 | 0.54 | -0.52 | -0.24 | -0.35 | -0.21 | -0.46 | -0.23 |
| CeAN | -0.86 | -0.85 | -0.86 | 0.09 | 0.62 | 0.09 | 0.16 | 0.61 | -0.25 | 0.05 | -0.54 | -0.60 | -0.51 | -0.70 |

Appendix B.2 (continued) Elemental Correlation Matrix for Crust RD50S1B from Hawaii.

| | Ti | Cu | Mg | Co | Fe | Mn | Ni | Sr | Zn | V | Ce An |
|-------------|--------------|--------------|-------|--------------|-------------|-------------|-------------|-------------|-------------|-------------|-------|
| Ti | 1.00 | | | | | | | | | | |
| Cu | -0.70 | 1.00 | | | | | | | | | |
| Mg | -0.20 | 0.21 | 1.00 | | | | | | | | |
| Co | 0.61 | -0.51 | 0.00 | 1.00 | | | | | | | |
| Fe | -0.40 | 0.62 | 0.10 | -0.66 | 1.00 | | | | | | |
| Mn | 0.06 | 0.30 | -0.28 | 0.48 | -0.09 | 1.00 | | | | | |
| Ni | -0.18 | 0.45 | 0.11 | 0.44 | -0.12 | 0.84 | 1.00 | | | | |
| Sr | 0.12 | 0.30 | -0.44 | 0.27 | 0.05 | 0.91 | 0.62 | 1.00 | | | |
| Zn | -0.21 | 0.79 | 0.06 | -0.11 | 0.54 | 0.61 | 0.61 | 0.62 | 1.00 | | |
| V | -0.37 | 0.82 | 0.10 | -0.24 | 0.42 | 0.44 | 0.51 | 0.46 | 0.88 | 1.00 | |
| CeAN | -0.02 | 0.44 | -0.18 | 0.22 | -0.01 | 0.65 | 0.55 | 0.52 | 0.58 | 0.50 | 1.00 |

Appendix B.3 Elemental Correlation Matrix for Crust from Horizon Guyot (Hein et al., 1992)

116

| | Na | Mg | Al | Si | P | K | Ca | Ti | Mn | Fe | Co | Ni | Cu | Zn | Ba | Pb |
|----|-------------|-------------|--------------|--------------|--------------|--------------|-------|-------------|-------------|--------------|-------------|-------------|--------------|-------------|-------------|------|
| Na | 1.00 | | | | | | | | | | | | | | | |
| Mg | 0.45 | 1.00 | | | | | | | | | | | | | | |
| Al | 0.11 | 0.12 | 1.00 | | | | | | | | | | | | | |
| Si | -0.29 | -0.46 | -0.26 | 1.00 | | | | | | | | | | | | |
| P | 0.18 | -0.37 | 0.44 | -0.28 | 1.00 | | | | | | | | | | | |
| K | 0.75 | 0.73 | 0.37 | -0.66 | 0.11 | 1.00 | | | | | | | | | | |
| Ca | -0.07 | -0.05 | 0.12 | 0.27 | -0.03 | -0.10 | 1.00 | | | | | | | | | |
| Ti | -0.28 | -0.23 | -0.58 | 0.59 | -0.39 | -0.57 | 0.02 | 1.00 | | | | | | | | |
| Mn | 0.55 | 0.88 | -0.20 | -0.34 | -0.52 | 0.67 | -0.05 | -0.09 | 1.00 | | | | | | | |
| Fe | -0.03 | -0.45 | -0.32 | 0.88 | -0.19 | -0.52 | 0.31 | 0.43 | -0.21 | 1.00 | | | | | | |
| Co | 0.19 | 0.60 | -0.19 | -0.27 | -0.27 | 0.31 | -0.11 | 0.17 | 0.50 | -0.37 | 1.00 | | | | | |
| Ni | 0.24 | 0.88 | 0.24 | -0.67 | -0.20 | 0.70 | -0.12 | -0.28 | 0.70 | -0.75 | 0.53 | 1.00 | | | | |
| Cu | 0.07 | 0.58 | -0.39 | -0.14 | -0.50 | 0.15 | -0.12 | 0.50 | 0.59 | -0.29 | 0.65 | 0.57 | 1.00 | | | |
| Zn | 0.65 | 0.69 | 0.05 | -0.34 | -0.01 | 0.70 | 0.04 | -0.25 | 0.71 | -0.17 | 0.37 | 0.56 | 0.27 | 1.00 | | |
| Ba | 0.57 | 0.51 | 0.00 | -0.07 | -0.21 | 0.55 | 0.08 | 0.03 | 0.66 | 0.10 | 0.02 | 0.38 | 0.28 | 0.66 | 1.00 | |
| Pb | 0.54 | 0.06 | 0.43 | -0.05 | 0.43 | 0.41 | 0.29 | -0.53 | 0.07 | 0.24 | -0.38 | -0.07 | -0.55 | 0.45 | 0.48 | 1.00 |

Appendix B.4 Elemental Correlation Matrix for Bulk Sample Crusts from Marshall Islands (Hein et al., 1988).

| | Si | Al | Fe | Mg | Ca | Na | K | Ti | P | Mn | CO ₂ | As | Ba |
|-----------------|--------------|--------------|-------|-------------|--------------|-------|-------|-------|--------------|-------------|-----------------|--------------|--------------|
| Si | 1.00 | | | | | | | | | | | | |
| Al | 0.89 | 1.00 | | | | | | | | | | | |
| Fe | -0.13 | -0.14 | 1.00 | | | | | | | | | | |
| Mg | -0.02 | 0.10 | 0.03 | 1.00 | | | | | | | | | |
| Ca | -0.35 | -0.19 | -0.12 | -0.42 | 1.00 | | | | | | | | |
| Na | -0.07 | -0.19 | 0.05 | 0.44 | -0.25 | 1.00 | | | | | | | |
| K | 0.62 | 0.76 | -0.02 | 0.34 | -0.41 | -0.09 | 1.00 | | | | | | |
| Ti | 0.26 | 0.39 | 0.05 | 0.33 | -0.40 | -0.11 | 0.43 | 1.00 | | | | | |
| P | -0.30 | -0.16 | -0.13 | -0.44 | 1.00 | -0.24 | -0.42 | -0.42 | 1.00 | | | | |
| Mn | -0.57 | -0.59 | 0.18 | 0.47 | -0.39 | 0.33 | -0.06 | 0.14 | -0.46 | 1.00 | | | |
| CO ₂ | -0.27 | -0.11 | -0.12 | -0.37 | 0.96 | -0.25 | -0.35 | -0.30 | 0.95 | -0.40 | 1.00 | | |
| As | 0.31 | -0.01 | -0.15 | 0.02 | -0.59 | 0.22 | 0.01 | -0.27 | -0.55 | 0.10 | -0.58 | 1.00 | |
| Ba | -0.26 | -0.01 | 0.09 | -0.06 | 0.21 | -0.38 | -0.03 | 0.33 | 0.16 | 0.10 | 0.19 | -0.51 | 1.00 |
| Cd | -0.44 | -0.43 | 0.23 | 0.52 | -0.20 | 0.32 | -0.05 | 0.23 | -0.24 | 0.66 | -0.17 | -0.17 | 0.01 |
| Co | -0.21 | -0.35 | 0.18 | 0.40 | -0.45 | 0.42 | -0.02 | 0.24 | -0.46 | 0.57 | -0.41 | 0.21 | -0.53 |
| Cr | 0.44 | 0.40 | -0.09 | 0.10 | -0.12 | -0.15 | 0.18 | 0.24 | -0.08 | -0.36 | -0.11 | 0.00 | -0.07 |
| Cu | -0.21 | 0.10 | -0.03 | 0.12 | 0.27 | -0.26 | 0.04 | 0.21 | 0.23 | 0.00 | 0.23 | -0.51 | 0.85 |
| Mo | -0.57 | -0.57 | 0.02 | 0.11 | 0.03 | 0.08 | -0.31 | -0.34 | -0.02 | 0.64 | -0.04 | 0.16 | 0.27 |
| Ni | -0.59 | -0.37 | 0.11 | 0.58 | 0.06 | 0.13 | -0.03 | 0.18 | -0.01 | 0.65 | 0.06 | -0.50 | 0.44 |
| Pb | -0.15 | -0.37 | 0.27 | 0.19 | -0.46 | 0.35 | -0.08 | -0.03 | -0.45 | 0.43 | -0.50 | 0.41 | -0.34 |
| Sr | -0.25 | -0.15 | -0.06 | -0.34 | 0.58 | -0.33 | -0.33 | -0.17 | 0.56 | -0.08 | 0.54 | -0.21 | 0.57 |
| V | 0.02 | -0.11 | -0.14 | -0.05 | -0.17 | 0.01 | -0.22 | -0.23 | -0.16 | 0.16 | -0.17 | 0.60 | 0.13 |
| Zn | -0.40 | -0.12 | 0.03 | 0.40 | 0.12 | -0.13 | 0.01 | 0.42 | 0.06 | 0.44 | 0.14 | -0.51 | 0.76 |
| Y | -0.18 | -0.10 | -0.04 | -0.37 | 0.61 | -0.16 | -0.30 | -0.29 | 0.61 | -0.40 | 0.59 | -0.34 | 0.20 |
| Ce | -0.45 | -0.32 | 0.29 | 0.01 | 0.04 | -0.12 | -0.11 | 0.38 | -0.02 | 0.33 | 0.01 | -0.51 | 0.62 |

Appendix B.4

(Continued) Elemental Correlation Matrix for Bulk Sample Crusts from Marshall Islands
(Hein et al., 1988).

| | Cd | Co | Cr | Cu | Mo | Ni | Pb | Sr | V | Zn | Y | Ce |
|----|-------------|--------------|-------|--------------|-------------|-------------|-------|-------------|-------|-------|------|------|
| Cd | 1.00 | | | | | | | | | | | |
| Co | 0.54 | 1.00 | | | | | | | | | | |
| Cr | -0.15 | -0.07 | 1.00 | | | | | | | | | |
| Cu | -0.01 | -0.57 | -0.08 | 1.00 | | | | | | | | |
| Mo | 0.26 | 0.00 | -0.43 | 0.29 | 1.00 | | | | | | | |
| Ni | 0.67 | 0.15 | -0.22 | 0.50 | 0.46 | 1.00 | | | | | | |
| Pb | 0.39 | 0.58 | -0.02 | -0.51 | 0.09 | 0.01 | 1.00 | | | | | |
| Sr | -0.23 | -0.57 | -0.15 | 0.47 | 0.43 | 0.04 | -0.41 | 1.00 | | | | |
| V | -0.18 | -0.21 | -0.10 | 0.12 | 0.58 | -0.19 | -0.08 | 0.50 | 1.00 | | | |
| Zn | 0.40 | -0.12 | -0.13 | 0.73 | 0.41 | 0.75 | -0.29 | 0.40 | 0.13 | 1.00 | | |
| Y | -0.26 | -0.38 | -0.02 | 0.10 | -0.18 | -0.08 | -0.22 | 0.37 | -0.11 | -0.04 | 1.00 | |
| Ce | 0.34 | 0.06 | -0.14 | 0.31 | 0.02 | 0.45 | 0.20 | 0.11 | -0.31 | 0.46 | 0.20 | 1.00 |

APPENDIX C

Appendix C.1 Factor Loadings of the Crust RD50S1B from Hawaii

| Elements | F1 | F2 | F3 | F4 |
|----------|-------|-------|-------|-------|
| Cr | 0.28 | -0.27 | -0.46 | 0.76 |
| Y | 0.92 | 0.13 | -0.32 | 0.14 |
| Ba | -0.36 | 0.77 | 0.34 | -0.16 |
| La | 0.97 | 0.13 | -0.01 | -0.12 |
| Ce | -0.31 | 0.18 | 0.51 | -0.39 |
| Pr | 0.96 | -0.12 | -0.19 | -0.08 |
| Nd | 0.96 | -0.06 | -0.23 | -0.03 |
| Sm | 0.95 | -0.14 | -0.27 | 0.00 |
| Eu | 0.95 | -0.12 | -0.28 | 0.01 |
| Gd | 0.96 | -0.06 | -0.28 | 0.03 |
| Tb | 0.95 | -0.12 | -0.26 | 0.03 |
| Dy | 0.96 | -0.10 | -0.25 | 0.06 |
| Ho | 0.96 | -0.05 | -0.26 | 0.08 |
| Er | 0.96 | -0.04 | -0.25 | 0.06 |
| Tm | 0.97 | -0.10 | -0.19 | 0.03 |
| Yb | 0.97 | -0.15 | -0.17 | 0.04 |
| Ir | -0.25 | -0.27 | 0.00 | 0.91 |
| Pt | -0.35 | 0.80 | 0.19 | -0.02 |
| Au | -0.22 | -0.23 | 0.05 | 0.93 |
| Pb | -0.27 | -0.60 | 0.56 | 0.13 |
| Bi | -0.42 | 0.27 | 0.70 | -0.22 |
| Th | 0.01 | -0.83 | -0.19 | 0.46 |
| U | -0.08 | -0.82 | 0.50 | -0.16 |
| Al | 0.38 | 0.24 | -0.86 | 0.16 |
| Ca | 0.91 | 0.10 | -0.10 | 0.02 |
| Si | 0.29 | 0.09 | -0.91 | 0.05 |
| P | 0.92 | 0.09 | -0.20 | 0.14 |
| Ti2 | 0.06 | -0.76 | 0.09 | -0.14 |
| Cu | -0.27 | 0.89 | 0.30 | 0.08 |
| Mg | 0.05 | 0.22 | -0.20 | 0.78 |
| Co | -0.24 | -0.79 | 0.37 | 0.30 |
| Fe | -0.15 | 0.63 | -0.12 | -0.25 |
| Mn | -0.45 | -0.09 | 0.85 | -0.13 |
| Ni | -0.41 | 0.06 | 0.77 | 0.37 |
| Sr | -0.22 | 0.02 | 0.86 | -0.39 |
| Zn | -0.38 | 0.53 | 0.63 | 0.02 |
| V | -0.21 | 0.66 | 0.56 | 0.13 |
| CeAN | -0.80 | 0.18 | 0.35 | -0.07 |

Appendix C.2 Factor Loadings of the Crust 6RD08-08 from Kiribati

| Elements | F1 | F2 | F3 | F4 |
|----------|-------|-------|-------|-------|
| Al | -0.21 | -0.28 | 0.04 | -0.70 |
| Si | 0.07 | -0.60 | -0.03 | -0.68 |
| P | 0.00 | 0.67 | 0.68 | -0.28 |
| Cu | 0.19 | 0.65 | 0.14 | 0.63 |
| Mg | 0.10 | 0.02 | -0.16 | 0.90 |
| Co | 0.14 | -0.21 | -0.31 | 0.73 |
| Fe | -0.04 | -0.58 | -0.52 | -0.54 |
| Mn | 0.16 | -0.09 | -0.35 | 0.84 |
| Ni | 0.04 | -0.01 | 0.16 | 0.91 |
| Sr | 0.08 | 0.63 | 0.06 | -0.09 |
| Zn | 0.24 | 0.33 | -0.35 | 0.73 |
| Ti | -0.02 | 0.23 | -0.34 | 0.16 |
| V | 0.10 | -0.49 | -0.32 | 0.01 |
| CeAN | -0.17 | 0.90 | -0.25 | 0.11 |
| Cr | -0.33 | 0.56 | -0.04 | -0.28 |
| Y | 0.13 | 0.06 | 0.96 | -0.11 |
| Ba | 0.34 | 0.74 | -0.19 | 0.35 |
| La | 0.80 | 0.07 | 0.57 | -0.04 |
| Ce | 0.38 | 0.87 | -0.02 | 0.19 |
| Pr | 0.96 | 0.13 | 0.02 | 0.21 |
| Nd | 0.97 | 0.03 | 0.15 | 0.16 |
| Sm | 0.95 | 0.06 | 0.04 | 0.21 |
| Eu | 0.94 | 0.00 | 0.25 | 0.13 |
| Gd | 0.85 | 0.18 | 0.46 | 0.12 |
| Tb | 0.87 | -0.07 | 0.45 | 0.11 |
| Dy | 0.68 | -0.16 | 0.70 | 0.02 |
| Ho | 0.45 | -0.19 | 0.86 | -0.08 |
| Er | 0.34 | -0.19 | 0.90 | -0.12 |
| Tm | 0.30 | -0.21 | 0.90 | -0.14 |
| Yb | 0.27 | -0.23 | 0.90 | -0.18 |
| Ir | -0.11 | 0.49 | 0.40 | -0.34 |
| Pt | 0.16 | 0.88 | -0.23 | 0.06 |
| Au | 0.05 | 0.32 | 0.44 | -0.29 |
| Pb | 0.43 | -0.33 | -0.65 | -0.16 |
| Bi | -0.05 | 0.69 | -0.11 | 0.27 |
| Th | 0.68 | 0.53 | -0.11 | 0.21 |
| U | 0.61 | -0.15 | -0.46 | -0.09 |
| Ca | 0.08 | 0.59 | 0.75 | -0.03 |

Appendix C.3 Factor Loadings of the Crust from Marshall Islands

| Elements | F1 | F2 | F3 | F4 |
|-----------------|-------|-------|-------|-------|
| Si | 0.27 | -0.33 | -0.79 | -0.10 |
| Al | 0.09 | -0.15 | -0.90 | 0.15 |
| Fe | 0.12 | -0.02 | 0.10 | -0.04 |
| Mg | 0.35 | 0.81 | -0.14 | 0.01 |
| Ca | -0.93 | -0.10 | 0.20 | 0.17 |
| Na | 0.18 | 0.44 | 0.19 | -0.45 |
| K | 0.32 | 0.19 | -0.72 | 0.10 |
| Ti | 0.30 | 0.30 | -0.54 | 0.30 |
| P | -0.94 | -0.15 | 0.17 | 0.13 |
| Mn | 0.48 | 0.57 | 0.55 | 0.06 |
| CO ₂ | -0.92 | -0.06 | 0.12 | 0.16 |
| As | 0.69 | -0.36 | 0.19 | -0.37 |
| Ba | -0.09 | 0.01 | 0.06 | 0.92 |
| Cd | 0.15 | 0.73 | 0.27 | -0.09 |
| Co | 0.35 | 0.46 | 0.15 | -0.60 |
| Cr | 0.03 | -0.10 | -0.53 | -0.05 |
| Cu | -0.17 | 0.20 | -0.02 | 0.88 |
| Mo | 0.23 | 0.18 | 0.78 | 0.36 |
| Ni | -0.07 | 0.81 | 0.27 | 0.37 |
| Pb | 0.45 | 0.07 | 0.28 | -0.52 |
| Sr | -0.32 | -0.31 | 0.38 | 0.65 |
| V | 0.44 | -0.33 | 0.44 | 0.35 |
| Zn | -0.03 | 0.53 | 0.13 | 0.77 |
| Y | -0.66 | -0.29 | 0.09 | 0.07 |
| Ce | -0.06 | 0.16 | 0.14 | 0.34 |

Appendix C.4 Factor Loadings of the Crust from Horizon Guyot

| Elements | F1 | F2 | F3 | F4 |
|----------|-------|-------|-------|-------|
| Na | 0.85 | -0.01 | 0.06 | 0.28 |
| Mg | 0.63 | 0.12 | 0.59 | -0.41 |
| Al | 0.03 | -0.71 | 0.35 | 0.17 |
| Si | -0.19 | 0.12 | -0.86 | -0.22 |
| P | -0.05 | -0.29 | 0.09 | 0.93 |
| K | 0.74 | -0.20 | 0.57 | 0.06 |
| Ca | 0.04 | -0.24 | 0.06 | 0.95 |
| Ti | -0.19 | 0.75 | -0.46 | -0.18 |
| Mn | 0.75 | 0.24 | 0.33 | -0.47 |
| Fe | 0.06 | 0.01 | -0.96 | -0.10 |
| Co | 0.21 | 0.63 | 0.50 | -0.11 |
| Ni | 0.40 | 0.08 | 0.82 | -0.30 |
| Cu | 0.21 | 0.77 | 0.34 | -0.35 |
| Zn | 0.86 | 0.06 | 0.24 | 0.02 |
| Ba | 0.85 | -0.02 | -0.10 | -0.22 |
| Pb | 0.61 | -0.63 | -0.24 | 0.31 |

REFERENCES

- Alvarez, R., DeCarlo, E. H., Cowen, J., and Andermann, G. 1990. Micromorphological characteristics of a marine ferromanganese crust. *Marine Geology* 94, 239-249.
- Aplin, A. C. and Cronan, D. S. 1985. Ferromanganese oxide deposits from Central Pacific Ocean. I: Encrustations from the Line Island Archipelago, *Geochim. Cosmochim. Acta*, 49, 427-436.
- Aplin, A. 1984. Rare earth element geochemistry of Central Pacific ferromanganese encrustations. *Earth Planet. Sci. Let.* 71, 13-22.
- Archer, D. E. 1991, Equatorial pacific calcite preservation cycles: Production or Dissolution? *Paleoceanography*, Vol. 6, No. 5, Pages 561-571.
- Balistrieri L. S. and Murray J. W. 1981. The surface chemistry of goethite (α FeOOH) in major ion seawater, *Amer. J. Sci.* 281, 788-806.
- Balistrieri L. S. and Murray J. W. 1982. The surface chemistry of δ MnO₂ in major ion seawater. *Geochim. Cosmochim. Acta*, 46, 1041-1052.
- Balistrieri, L., Brewer, P. G. and Murray, J. W. 1981. Scavenging residence times of trace metals and surface chemistry of sinking particles in the deep ocean. *Deep-Sea Research*. Vol. 28A, pp. 101-121.
- Bertram, M. A. and Cowen, J. P. 1994. Testate rhizopod growth and mineral deposition on experimental substrates from Cross Seamount. *Deep-Sea Research I*, Vol. 41, No. 4, pp 575-601.
- Bruland, K. W. 1983. Trace elements in sea-water. In *Chemical Oceanography*, Vol. 8, Chapter 45, Academic press, 157-220.

Burns, R. G. and Burns, V. M. 1977. Mineralogy. In: G. P. Glasby (Editor), *Marine Manganese Deposits*, Elsevier Oceanography Series, 15, Elsevier, Amsterdam, 185-248.

Byrne, R. H. and Kim, K.-H. 1990. The influence of surface and solution chemistry on rare earth distribution in seawater. *Geochim. Cosmochim. Acta*, 54, 2645-2656.

Cantrell, K. J., and Byrne, R. H. 1987. Rare earth element complexation by carbonate and oxalate ions. *Geochim. Cosmochim. Acta* 51, 597-605.

Cowen, J. P., DeCarlo, E. H., and McGee., D. 1993. Calcareous nannofossil biostratigraphic dating of a ferromanganese crust from Schumann Seamount. *Mar. Geol.*, 115, 289-306.

De Baar H. J. W., Bacon M. P., Brewer P. G. and Bruland K. W. 1985 Rare earth elements in the Pacific and Atlantic Ocean, *Geochim. Cosmochim. Acta*, 49, 1943-1959.

De Carlo, E. H. and McMurtry, G. M. 1992. Rare earth element geochemistry of Fe-Mn deposits from the Hawaiian Archipelago. *Chem. Geol.* 95, 235-250.

DeCarlo, E. H. 1991. Paleoceanographic implication of rare earth element variability in a marine Fe-Mn crust from the Hawaiian Archipelago. *Marine Geology*. 98(2/4), 449-467.

DeCarlo, E. H. and Pruszkowski, E. 1992. Application of laser ablation ICP/MS to the determination of rare earth elements in marine ferromanganese deposits. *Proceedings of Winter Conference on Plasma Spectrochemistry*, January 6-11, 1992, San Diego, California.

DeCarlo, E. H., McMurtry, G. M. and Kim, K. H. 1987a. Geochemistry of ferromanganese crusts from the Hawaiian Archipelago-I. Northern survey areas. *Deep-sea Research*. Vol. 34, No. 3, pp. 441-467.

DeCarlo, E. H., Pennywell, P. A., and Fraley, C. M. 1987b. Geochemistry of ferromanganese Deposits from the Kiribati and Tuvalu Region of West Central Pacific Ocean, *Marine Mining*, 6, 301-321.

Elderfield, H. 1988. The oceanic chemistry of the rare-earth elements. *Phil. Trans. R. Soc. Lon.*, A325, 105-126.

Emerson, S., and D. Archer. 1992. Glacial carbonate dissolution cycles and atmospheric pCO₂: A view from the ocean bottom, *Paleoceanography*, Vol. 7 No. 3, Pages 319-331.

Farrel, J. W., and Prell, W. L. 1989. Climatic change and CaCO₃ preservation: An 800000 year bathymetric reconstruction from the central equatorial pacific ocean, *Paleoceanography*, Vol. 4, Pages 447-466.

Farrel, J. W., and Prell, W. L. 1991. Pacific CaCO₃ preservation and $\delta^{18}\text{O}$ since 4 Ma: Paleoceanic and paleoclimatic implications, *Paleoceanography*, Vol. 6, No. 4, pages 485-498.

Friedrich, G., and Schmitz-Wiechowski, A. 1980. Mineralogy and chemistry of a ferromanganese crust from a deep-sea hill, central Pacific, Valdivia cruise VA 13/2. *Marine Geology*, 37, 71-90.

Glasby, G. P. editor 1977. *Marine manganese deposits*. Elsevier Oceanographic Series, Vol. 15, Elsevier, Amsterdam, 523 pp.

Glasby, G. P., Gwozdz, R., Kunzendorf, H., Friedrich, G. and Thijssen., T. 1987. Distribution of rare earth and minor elements in manganese nodules and sediments from the equatorial and SW Pacific. *Lithos*, 20, 97-113.

Glenn, C. R., and Arthur, M. A. 1988. Petrology and major element geochemistry of Peru margin phosphorites and associated diagenetic minerals: Authigenesis in modern organic-rich sediments, *Mar. Geol.*, 80, 231-267.

Glenn, C., and Arthur, M. A. Resig, J. M. Burnett, W. C. Dean, W. E. and Jahnke, R. A. 1994. Are modern and ancient phosphorites really so different? Proc. 29th Int'l. Congr., Part C, pp. 159-188

Goldberg, E. D. 1954. Marine geochemistry I- Chemical scavengers of the sea. *J. Geol.* 62, 249-265.

Halbach, O., Puteanus, D. and Manheim, F. T. 1984. Platinum concentration in ferromanganese seamount crusts from the Central Pacific. *Naturwissenschaften*, 71: 577-579.

Halbach, P. and Manheim, F. T. 1984. Potential of cobalt and other metals in ferromanganese crusts on seamounts of the Central Pacific Basin. *Mar. Min.*, 4(4): 319-336.

Halbach, P. and Puteanus, D. 1984. The influence of the carbonate dissolution rate on the growth and composition of Co-rich ferromanganese crusts from Central Pacific seamount areas. *Earth Planet. Sci. Lett.*, 68: 73-87.

Halbach, P. 1986. Processes controlling the heavy metal distribution in Pacific ferromanganese nodules and crusts. *Geol. rundsch.*, 75: 235-247.

Halbach, P., Giovanoli, R., and Borstel, von. D. 1982. Geochemical processes controlling the relationship between Co, Mn, and Fe in early diagenetic deep-sea nodules. *Earth Planet Sci. Lett.*, 60, pp 226-236.

Hein, J. R., Bohrsen, W. A., Schulz, M. J., Noble, M., and Clague, D. A. 1992. Variations in the fine-scale composition of a central Pacific ferromanganese crust: Paleoceanographic implications. *Paleoceanography* 7: 63-77.

Hein, J. R., Schulz, M. S., and Kang, J.-K. 1990 Insular and submarine ferromanganese mineralization of the Tonga-Lau region, *Mar. Min.*, 9, 305-354.

Hein, J. R., Schwab, W. C. and Davis, A. S. 1988. Cobalt-and platinum-rich ferromanganese crusts and associated substrate rocks from the Marshall Islands. *Marine Geology*, 78, p. 255-283.

Henderson, P. Editor, 1984. *Rare Earth Element Geochemistry*. Elsevier Developments in Geochemistry 2, Elsevier publishing, Amsterdam, 510pp.

Herbelin, L. A., and Westall, J. C. 1994. A computer program for determination of chemical equilibrium constants from experimental data. Department of Chemistry, Oregon State University, Corvallis, Oregon 97331

Heye, D. 1978. The internal micro-structure of manganese nodules and their relationship to the growth rate. *Mar. Geol.*, 26, M59-M66.

Honeyman, B. D., Balistrieri, L. S., and Murray, J. W. 1988. Oceanic trace metal scavenging: the importance of particle concentration. *Deep Sea Res.*, 35(2), 227-246.

Ingram, B. L., Hein, J. R. and Farmer, G. L. 1990. Age determinations and growth rates of Pacific ferromanganese deposits using strontium isotopes. *Geochim. Cosmochim. Acta*, 54, 1709-1721.

Janin, M. -C. 1987. The imprints of Cenozoic calcareous nannofossils from polymetallic concretions: Biostratigraphic significance for two crusts from the central Pacific. *Ahb. Geol. B. -A.* 39: 121-141.

Janin, M.-C. 1988. Biostratigraphie comparée de nodules et sédiments du pacifique nord-Equatorial. *Bull. Soc. Geol. France*, 8, t. (II) no 3, 373-380.

Kang, J.-K. 1987 Mineralogy and internal structures of a ferromanganese crust from a seamount, central Pacific, *J. Oceanolog. Soc. Korea*, 22, 168-178.

Kennett, J. P. 1982. *Marine Geology*, Prentice-Hall, Englewood Cliffs, N. J., 813pp

Klinkhammer, G. D., and Bender, J, M. L. 1980. The distribution of manganese in the Pacific Ocean. *Earth Planet. Sci. Lett.* 46: 361-384.

Koepfenkastrof, D. and DeCarlo, E. H. 1993. Uptake of rare earth elements from solution by metal oxides. *Env. Sci. and Tech.*, 27 1796-1802.

Koepfenkastrof, D. and DeCarlo, E. H. 1992. Sorption of rare earth elements from seawater onto pure mineral phases: An experimental approach. *Chemical Geology*, 95, 251-263.

Koepfenkastrof, D., DeCarlo, E. H., and Roth, 1991. M. A method to investigate the interaction of rare earth elements with metal oxides in aqueous solution. *J. Radioanalytical and Nuclear chemistry*, 151(2).

Krauskopf, K. B. 1956. Factors controlling the concentrations of thirteen rare metals in seawater. *Geochim. Cosmochim. Acta* 9, 1-32.

Le Suavé, R., Pichoki, C., Pautot, G., Hoffert, M., Orel, Y., Voisset, M., Monti, S., Amosse, J. and Kosakevitch, A. 1989. Geological and mineralogical study of Co-rich ferromanganese crusts from a submerged atoll in the Tuamotu Archipelago (French Polynesia). *Marine Geology* 87: 227-247.

Lee J. -H. and Byrne R. H. 1992. Examination of comparative rare earth elements complexation behavior using linear free-energy relationship. *Geochim. Cosmochim. Acta.*, 56, 1127-1138.

Lee J. -H. and Byrne R. H. 1993. Complexation of trivalent rare earth elements (Ce, Eu, Gd, Tb, Yb) by carbonate ions. *Geochim. Cosmochim. Acta.*, 57, 295-302.

Li, Y.-H. 1981. Ultimate removal mechanisms of elements from the ocean. *Geochim. Cosmochim. Acta* 45, 1659-1664.

Li, Y. H. 1982. Interelement relationship in abyssal Pacific ferromanganese nodules and associated pelagic sediments. *Geochim. Cosmochim. Acta*, 46, pp. 1053-1060.

- Li, Y.-H. 1991. Distribution patterns of the elements in the ocean: A synthesis. *Geochim. Cosmochim. Acta.*, 55, pp. 3223-3240.
- Manheim, F. T. and Lane-Bostwick, C. M. 1988. Cobalt in ferro-manganese crusts as a monitor of hydrothermal discharge on the Pacific sea floor. *Nature*, 335: 59-62.
- Manheim, F. T. and Lane-Bostwick, C. M. 1989. chemical composition of ferromanganese crusts in the world ocean: A review and comprehensive database. USGS open File Report, 200pp.
- Manheim, F. T. and Lane-Bostwick, C. M. 1989. Chemical composition of ferromanganese crusts in the world ocean: A review and comprehensive database. USGS open file report, 200pp.
- Manheim, F. T. 1986. Marine cobalt resources. *Science*, 232, 600-608.
- Martin, J. H. and Knauer, G. A. 1985. The lateral transport of manganese within the north-east Pacific Gyre oxygen minimum. *Nature*, 314, 524-526.
- McMurtry, G. M., VonderHaar, D. L., Eisenhauer, A., Mahoney, J. J., and Yeh, H. W. 1994 Cenozoic accumulation history of a Pacific ferromanganese crust. *Earth Planet. Sci.Lett.* 125: 105-384.
- Moffett, J. 1990. Microbially mediated cerium oxidation in seawater. *Nature*, 345, 421-423.
- Murray, J. W. 1974. The surface chemistry of hydrous manganese dioxide. *J. Coll. Int. Sci.*, 46, 357-371.
- Murray, J. W. 1975a. The interaction of metal ions at the manganese dioxide-solution interface. *Geochim. Cosmochim. Acta*, 39, 505-519.

Murray, J. W. 1975b. The interaction of cobalt with hydrous manganese dioxide. *Geochim. Cosmochim. Acta*, 39, 635-647.

Ostwald, J. 1988. Mineralogy of Groote Eylandt manganese oxides: A review. *Oce Geol. Rev.*, 4, 3-45.

Piegras, D. J. and Jacobsen, S. B. 1992. The behavior of rare earth elements in seawater: Precise determination of variations in the North Pacific water column. *Geochim. Cosmochim. Acta*, 56, 1851-1862.

Piper, D. Z. 1974. Rare earth elements in ferromanganese nodules and other marine phases. *Geochim. Cosmochim. Acta*, 38, 1007-1022.

Puteanus, D. and Halbach, P. 1988. Correlation of Co concentration and growth rate: a method for age determination of ferromanganese crusts. *Chem. geol.* 69: 73-85.

Puteanus, D. and Halbach, P. 1988. Correlation of Co concentration and growth rate: A method for age determination of ferromanganese crusts. *Chem. Geol.*, 69: 73-85.

Stumm, W. and Morgan, J. 1981. *Aquatic Chemistry*. Wiley-Interscience, New York, N. Y., 2nd ed., 780 pp.

Van Andel, T. H., Heath, G. R., and Moore, T. C. 1975. *Cenozoic History and Paleooceanography of the Central Equatorial Pacific Ocean*. GSA Memoir 143, Geological Society of America.

Von Stackelberg, U., Kunzendorf, H., Marchig, V. and Gwodz, R. 1984. Growth history of a large ferromanganese crust from the equatorial north Pacific nodule belt. *Geol. Jb.* A75: 213-235.

VonderHaar, D. L. 1990. *A stratigraphic Interpretation of Selected Fe-Mn Crusts from Schumann Seamount*, Unpublished MS.. thesis, University of Hawaii, Honolulu, 71pp.

Wen, X. Y. and DeCarlo, E. H. 1994. A comparative study of the geochemistry and internal structure of seamount ferromanganese crusts. *EOS*, 74, 78.

Whitfield, M. and Turner, D. R. 1987. Aquatic Surface chemistry: The role of particles in regulating the composition of seawater, Stuman, W.,(Ed), John Wiley, 1987, pp.457-493.

Wright, J., Schrader, H. and Holser, W. T. 1987. Paleoredox variations in ancient oceans recorded by rare earth elements in fossil apatite. *Geochim. Cosmochim. Acta*, 51, 631-644.

Yan, C. Y., and Kroenke, L. W. 1993. A plate tectonic reconstruction of the Southwestern Pacific, 0-100 Ma, proceeding of the Ocean Drilling Program, scientific Results, Vol. 130